AD-A108 588 TORONTO UNIV DOWNSVIEW (ONTARIO) INST FOR AEROSPACE --ETC F/G 20/5
STUDY OF LASER CREATED METAL VAPOUR PLASMAS.(U)
SEP 81 R M MEASURES AFOSR-80-0057

UNCLASSIFIED AFOSR-TR-81-0789 NL

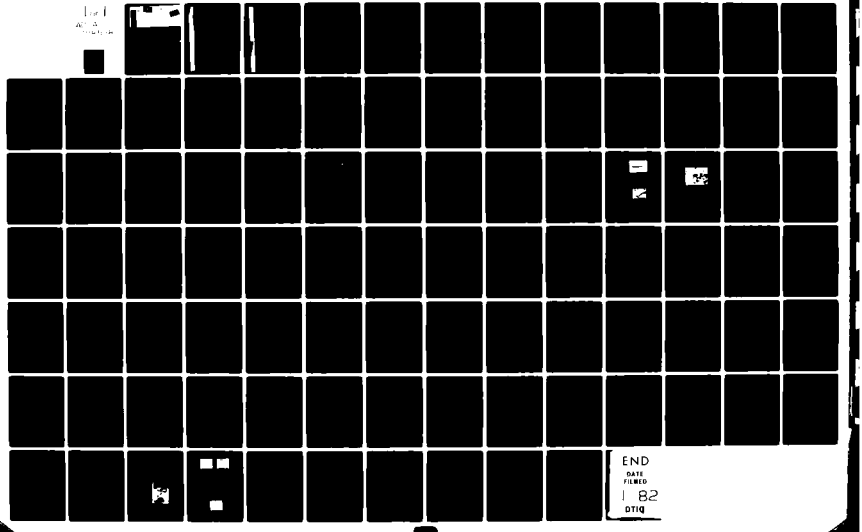

END
DATE FILMED
1 82
DTIC

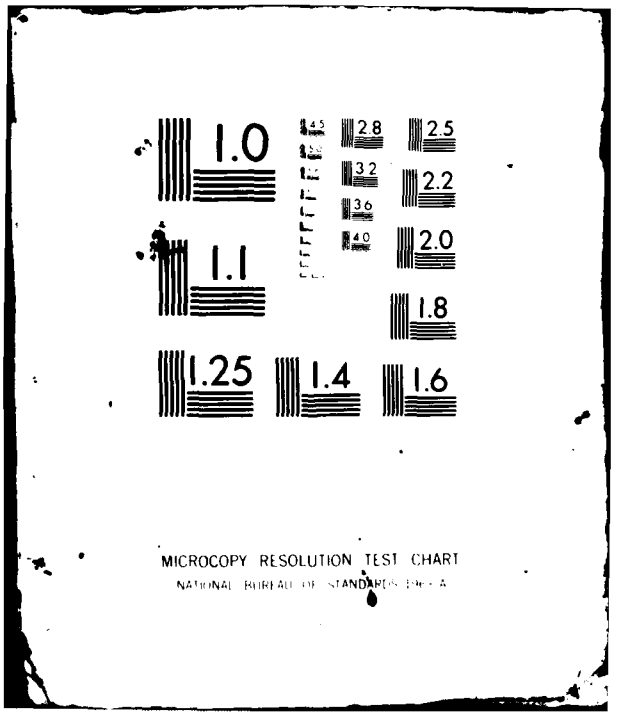
1.0
1.1
1.25
1.4
1.6
1.8
2.0
2.2
2.5
2.8
3.2
3.6
4.0
4.5
MICROCOPY RESOLUTION TEST CHART
NATIONAL BUREAU OF STANDARDS-1963-A

INSTITUTE
FOR
AEROSPACE STUDIES

UNIVERSITY OF TORONTO

AFOSR-TR- 81 -0789

STUDY OF LASER CREATED METAL VAPOUR PLASMAS

ANNUAL TECHNICAL REPORT

(FOR PERIOD ENDING SEPTEMBER 29, 1981)

Prepared by

Dr. R. M. Measures
Professor of Applied Science and Engineering
Institute for Aerospace Studies
University of Toronto
4925 Dufferin Street
Downsview, Ontario, Canada
M3H 5T6

UNCLASSIFIED
SECURITY CLASSIFICATION OF THIS PAGE (When Data Entered)

REPORT DOCUMENTATION PAGE		READ INSTRUCTIONS BEFORE COMPLETING FORM
1. REPORT NUMBER AFOSR-TR- 81 -0789	2. GOVT ACCESSION NO. AD-A108 588	3. RECIPIENT'S CATALOG NUMBER
4. TITLE (and Subtitle) STUDY OF LASER CREATED METAL VAPOUR PLASMAS		5. TYPE OF REPORT & PERIOD COVERED Annual Technical Report (Oct.1/80 - Sept.30/81) 6. PERFORMING ORG. REPORT NUMBER
7. AUTHOR(s) R. M. Measures		8. CONTRACT OR GRANT NUMBER(s) AFOSR 80-0057
9. PERFORMING ORGANIZATION NAME AND ADDRESS University of Toronto, Institute for Aerospace Studies, 4925 Dufferin St., Downsview, Ontario, Canada, M3H 5T6		10. PROGRAM ELEMENT, PROJECT, TASK AREA & WORK UNIT NUMBERS 61102F 2301/A8
11. CONTROLLING OFFICE NAME AND ADDRESS Air Force Office of Scientific Research, /NP Bldg. 410, Bolling Air Force Base, DC 23032 U.S.A.		12. REPORT DATE Sep 1981 13. NUMBER OF PAGES 52
14. MONITORING AGENCY NAME & ADDRESS(if different from Controlling Office)		15. SECURITY CLASS. (of this report) Unclassified 15a. DECLASSIFICATION/DOWNGRADING SCHEDULE

16. DISTRIBUTION STATEMENT (of this Report)

Approved for public release; distribution unlimited.

17. DISTRIBUTION STATEMENT (of the abstract entered in Block 20, if different from Report)

18. SUPPLEMENTARY NOTES

19. KEY WORDS (Continue on reverse side if necessary and identify by block number)

Laser Resonance Saturation, Laser Ionization, Laser Superelastic Heating, Plasma Formation, Ground Level Inversion, Short Wavelength Lasers, Rapid Plasma Heating, Anomalous Laser Absorption, Alkali-Metal Plasmas, Heat Pipe Ovens.

20. ABSTRACT (Continue on reverse side if necessary and identify by block number)

Laser resonance saturation represents a powerful new form of interaction that can lead at high densities to extremely *rapid* and *efficient* coupling of laser energy into both gases and plasmas. We have developed both a comprehensive experimental facility and a theoretical program for studying these interactions in alkali-vapours. Preliminary calculations have suggested that laser resonance saturation could lead to extensive *ground level burnout* of certain kinds of atoms or ions and that this could lead to the creation of a ground level

DD FORM 1 JAN 73 1473

UNCLASSIFIED
SECURITY CLASSIFICATION OF THIS PAGE (When Data Ente

inversion in these species. We believe that this approach could lead to the development of short wavelength lasers of high quantum efficiency.

3

STUDY OF LASER CREATED METAL VAPOUR PLASMAS

ANNUAL TECHNICAL REPORT

(FOR PERIOD ENDING SEPTEMBER 29, 1981)

AFOSR 80-0057

Prepared by

Dr. R. M. Measures
Professor of Applied Science and Engineering
Institute for Aerospace Studies
University of Toronto
4925 Dufferin Street
Downsview, Ontario, Canada
M3H 5T6

Abstract

Laser resonance saturation represents a powerful new form of interaction that can lead at high densities to extremely *rapid* and *efficient* coupling of laser energy into both gases and plasmas. We have developed both a comprehensive experimental facility and a theoretical program for studying these interactions in alkali-vapours. Preliminary calculations have suggested that laser resonance saturation could lead to extensive *ground level burnout* of certain kinds of atoms or ions and that this could lead to the creation of a ground level inversion in these species. We believe that this approach could lead to the development of short wavelength lasers of high quantum efficiency.

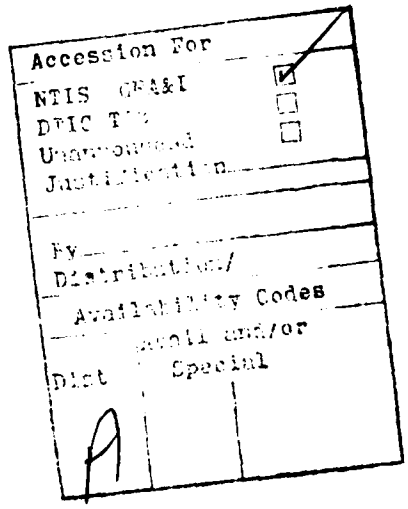

CONTENTS

RESEARCH OBJECTIVES

Laser resonance saturation represents a new technique for rapidly and efficiently coupling laser energy into a suitable gas or plasma. As such it could have considerable application potential. Our primary research objective is to study this new kind of interaction in order to gain a better understanding of its capabilities.

We feel that laser resonance saturation offers a new approach towards the development of relatively efficient short wavelength lasers. This approach is based on rapidly *burning out* the ground level population of a suitable ionic species within a plasma to the point where it becomes possible to create a *ground level population inversion* and thereby a short wavelength laser with a high quantum efficiency. Much of our future research will be directed at investigating various aspects of this application of *laser interactions based on resonance saturation*, LIBORS.

STATUS OF RESEARCH

The consequences of laser saturation of a resonance transition within an atom or ion depend critically upon the length of time saturation is maintained. If the laser locks the ground and resonance level populations together for a period that is short compared to the lifetime of the resonance level, then the primary effect is a burst of intensified spontaneous emission. The author was the first to recognize the diagnostic potential of this so called *momentary* laser saturation[1,2] and subsequently also pointed out the highly perturbative aspect of *extended* laser saturation.[3] The word *extended* in this context relates to the fact that the laser locks the resonance and ground level populations in the ratio of their respective degeneracies for a time that is very long compared to the lifetime of the resonance level. Under these circumstances considerable ionization and heating are possible.[4]

During the past year we have continued our study of laser resonance saturation, including both the diagnostic and ionizational aspects. In this section we shall present only the highlights of our recent work that has been (or is about to be) published. Copies of these papers are appended to this report. A more complete description of ongoing work is also provided.

ABLATION PLASMA STUDIES

As we have indicated *laser selective excitation spectroscopy* involves the momentary locking of the population of two atomic levels in the ratio of their respective degeneracies by an intense pulse of suitably tuned laser radiation. The subsequent burst of *intensified spontaneous emission*, ISE, from the overpopulated level represents a spectroscopic signal that is both spatially and temporally resolved. This powerful diagnostic technique has been used in a variety of applications, including: atomic lifetime measurements,[5-7] trace element analysis,[8,9] single atom detection,[10-13] combustion and flame studies,[14-17] neutral hydrogen measurements in Tokamaks[18,19] and fusion plasma impurity diagnostics.[20,21] Ablation of a solid is central to many of the approaches towards attaining very short wavelength laser action. It is to be expected that a detailed knowledge of the density ratio of consecutive ionization stages in these rapidly expanding plasmas will be of value if these methods are to be optimized. We have recently shown that laser selective excitation spectroscopy can provide this information with both spatial and temporal resolution.

In a *proof of principle* experiment we have used two short pulse, appropriately tuned, dye lasers to produce bursts of *intensified spontaneous emission* (ISE) on one resonance line from each of the two stages of ionization of interest. The experimental arrangement is portrayed in figures 1 and 2. The results (see Appendix A) indicate that an *ionization freeze-out* at about 0.1% ionization was attained in strontium 2 μsec after the moment of laser ablation. This observation was made about 1 cm above the ablation target.

LASER IONIZATION BASED ON RESONANCE SATURATION

Our current program includes both a theoretical and experimental study of the consequences of extended laser resonance saturation. Our recent theoretical work has involved: (i) the formulation of a simple model of LIBORS, (ii) a comparison of the results predicted by this simple model with those obtained from our comprehensive LIBORS computer code,* and (iii) a study of the influence of molecular nitrogen upon the ionization and heating

*Our LIBORS computer code treats the laser pumped species as a 20 energy level system and takes account of all of the radiative-collisional processes. It solves the subsequent set of rate equations in conjunction with the energy equations of the free electrons, the neutral and the ion species. The code provides the temporal variation in: the population of each level, the free electron density, the ion and electron temperatures and the absorbed laser power density.

associated with laser resonance saturation. Our experimental program has included: (i) some preliminary observations of the plasma emission created through LIBORS, and (ii) the measurement of an anomalous absorption of the laser pulse energy. Currently, we are assembling a new and much improved facility for undertaking a more definitive series of experiments aimed at strengthening our understanding of this new form of laser interaction in order that we may explore some of its potential applications.

LIBORS *Simple Model*

Although we have developed a fairly comprehensive computer code for simulating the laser interactions resulting from resonance saturation, we have felt that it should be possible to formulate a relatively simple model to describe LIBORS. During the past year we have successfully completed this task. The advantages of this simple model are: (i) it yields closed form solutions for the temporal growth of the free electron density, (ii) it is not limited to one alkali metal, but can readily be extended to study the ionization behaviour of most elements having relatively low lying energy states, and (iii) it provides considerable physical insight into the relative importance of the major interactions.

In this simple model the ionization is perceived to proceed in three stages, once the resonance transition has been saturated: (i) *seed ionization* creates an initial pool of electrons that are free to gain energy through *superelastic collisions*, (ii) these *hot* electrons are then capable of directly *ionizing the resonance level atoms* and populating the intermediate levels which are subsequently *photoionized*, (iii) finally direct *electron impact ionization* of this intermediate level population leads to a very rapid and near complete *ionization burnout* phase - see figure 3.

A detailed description of this simple LIBORS model is provided in the form of two papers that have recently been published.[4,22] Copies of these papers are appended as Appendices B and C. Consequently, we shall not describe the simple model or its solutions in this section. However, we should point out that the paper presented as Appendix B deals with a simpler version of the model that does not take continuity into account. Although this leads to a singularity in the solution for the free electron density at burnout, it nevertheless provides a reasonable prediction of the time to achieve ionization burnout (> 95% ionization) as seen by the comparison with the full LIBORS code for sodium. This results from the very fast rate of ionization in this last phase of ionization, see figure 7 of Appendix B.

The model presented as Appendix C takes account of continuity but yields somewhat more complex solutions for the temporal growth of the free electron density. These solutions are found to be in excellent agreement with the predictions of our full LIBORS computer code. This agreement can be seen to extend over a dynamic range of six orders of magnitude in figure 4, where the initial sodium atom density was assumed to be 10^{16} cm^{-3} and the laser irradiance was 10^{6} W cm^{-2}. We have also applied this simple model to most of the alkali metals and have predicted the *time for ionization burnout* (> 95% ionization) over a wide range of densities and laser irradiances, see Table 1 of Appendix C. Figure 5 clearly reveals that this ionization time is expected to be close to 100 nsec (to within ± 15%) for most of the alkali-metal vapours, if the initial atom density is 10^{16} cm^{-3} and the laser irradiance is 10^{6} W cm^{-2}.

We should also mention that in this paper (Appendix C) we have shown that if allowance is made for the spatial and temporal nature of the laser pulse, the *apparent (i.e., observed) ionization time* is found to be approximately twice that for the step-like, uniform laser pulse assumed in both the LIBORS code and earlier version of the simple model. In this comparison the peak irradiance of the realistic laser pulse was set equal to that of the step-like pulse. It should be noted that figure 6 and Table II of Appendix C were incorrect and the Erratum presented here as Appendix D should be substituted.

Since rapid cooling of a plasma represents one approach to achieving a population inversion we have considered the impact of a background density of molecular nitrogen on LIBORS. Our initial study has indicated that the *ionization time* of those solutions for which the intermediate phase dominates the ionization time (i.e., S1 solutions in the nomenclature of Appendix B) are likely to be quite sensitive to the presence of molecular nitrogen, under conditions of low laser irradiance. This can physically be understood by reference to figure 3 and figure 6. For S1 solutions, the *ionization burnout time* can be approximately expressed in the form

$$\tau_B \cong \frac{1}{I} \ln(N_e^{**}/N_e^{*}) \qquad (1)$$

Under conditions of low laser irradiance, i.e.,

$$F << N_2 K_{2c}/\sigma_{max}^{(1)} \qquad (2)$$

the *intermediate ionization rate coefficient,*

$$I \cong N_2 K_{2c} + \frac{F}{K_{2c}} \sum_{m \geq 3} K_{2m} \sigma_{mc}^{(1)} \qquad (3)$$

where N_2 is the saturated resonance state population density and can be written as $\frac{3}{4} N_o$ for sodium where N_o is the original atom density,

K_{2c} is the electron collisional ionization rate coefficient for the resonance state $|2\rangle$,

K_{2m} is the electron collisional rate coefficient between the intermediate state $|m\rangle$ and $|2\rangle$,

$\sigma_{mc}^{(1)}$ is the single photon ionization cross section for state m, and

$\sigma_{max}^{(1)}$ is the maximum value of this cross section,

F is the laser photon flux density ($F = \int I^{\ell}(\nu) d\nu/h\nu$),

N_e^{**} represents the critical free electron density for which the burnout rate of ionization equals the intermediate rate of ionization and in a like manner,

N_e^{*} represents the characteristic electron density for which the intermediate ionization rate equals the seed ionization rate, see Appendix B.

In general for SI solutions $N_e^{**}/N_e^{*} \cong 100$ and given (2), equations (1) and (3) indicate that τ_B is inversely proportional to K_{2c} and will consequently depend strongly upon the free electron temperature. The low laser irradiance criterion for sodium indicates that this situation will apply for $I^{\ell} \lesssim 10^6$ W cm^{-2}. For much higher values of laser irradiance free electron creation during the intermediate phase will predominantly arise through collisional excitation to the intermediate levels which are subsequently photoionized. Under these circumstances τ_B will be less sensitive to T_e.

Influence of Molecular Gas (N_2) on LIBORS

The presence of an appreciable background density of molecular nitrogen will not only aid in rapidly cooling the plasma, it will also impede the expansion and have a detrimental effect upon the degree of ground level burnout achieved. In the case of resonance saturation of alkali metal atoms, the typical energy involved is low enough (few eV) that only vibrational and rotational modes of N_2 need to be considered. Under these conditions a set of vibrational-rate equations need to be solved in conjunction

with the normal set of LIBORS equations and an amended electron energy equation. If we assume that only a small fraction of the nitrogen molecules are vibrationally excited we can avoid having to solve the set of vibrational rate equations and can write the electron energy equation in the form

$$\frac{3}{2} k \frac{dT_e}{dt} = \begin{matrix}\text{LIBORS terms} \\ \text{(see Eq. 5 of} \\ \text{Appendix B)}\end{matrix} - n_o \sum_{w>o} \langle \sigma v \rangle_{ow} \Delta E_{wo} \qquad (4)$$

where n_o is the total nitrogen density, $\langle \sigma v \rangle_{ow}$ the collision rate coefficient for excitation from the ground vibrational state to one with w-vibrational quanta. ΔE_{wo} is the corresponding energy jump.

Solution of this equation will yield a lower value of T_e than would be expected in reality and will consequently lead to a conservative estimate for the lengthening of the ionization time. It should also be noted that $\langle \sigma v \rangle_{ow}$ decreases as w increases and so in our preliminary work we have summed to w = 4 in equation (4). These rates were numerically evaluated from the cross-sectional data available in the literature.[23] The subsequent vibrational cooling term in equation (4) is dependent upon the electron temperature and is fitted by an expression of the form $n_o A T_e^B \exp(C T_e)$ in our LIBORS code, where $A = 1.315 \times 10^{-35}$, $B = 7.341$ and $C = -7.32 \times 10^{-4}$.

The results of our analysis reveal that if the alkali percentage seeding drops below about 0.5% substantial cooling results which in turn lead to a marked increase in the time to achieve maximum ionization - and furthermore, full ionization (> 95%) can no longer be attained; see figures 7 and 8. A paper describing this work more fully has just been accepted for publication in the Journal of Applied Physics and a copy is appended to this report as Appendix E.

Experimental Facility and Preliminary Results

Our first LIBORS experimental facility included: a Phase-R Model DL-2100A flashlamp pumped dye laser, a specially designed and built crossed heat pipe (Heat-cross), an energy meter, two photodiodes, two cameras and two Heath monochromators with accompanying photomultipliers. A schematic of the experimental arrangement is presented as figure 9. The Heat-cross oven used to contain the sodium vapour has four windows. These provided access for the laser beam and enabled us to evaluate the absorption of the laser pulse after transmission through the column of sodium vapour, the length

of which was about 40 cm and determined by the position of the water cooling coils and the argon buffer gas pressure. Observations of any laser induced emission or laser scattered radiation can be made through the other pair of windows. Rhodamine 6G in ethanol was used in the dye laser to provide output energy pulses that ranged between 100 and 400 mJ. The spectral width of the dye laser was narrowed to about 0.06 nm by the inclusion of a one to two intracavity beam expander and a grating.

A 50 cm focal length lens was used to slightly focus the laser beam within the Heat-cross oven, attaining a diameter of about 0.50 cm at the centre. The resulting luminous.plasma column, as photographed by Camera C1, is dramatically illustrated in figure 10. Both the intensity and diameter of this plasma channel was observed to decrease with progressive detuning of the laser, disappearing completely when the laser was detuned by about 1 nm to the long wavelength side of the 589 nm resonance line.

Figure 11 displays both the incident laser pulse (from PD1) and a 4 nm band of emission centred about 406 nm - which is close to the edge of the radiative recombination continuum to the 3p resonance levels. It is evident that the continuum radiation has a much shorter rise time than the laser pulse, but a very much slower decay time. The long decay time for the emission is consistent with recombination of the plasma channel. The delayed, short rise time for the emission is in general agreement with the LIBORS concept where extremely rapid ionization burnout is predicted after some onset period.

Unfortunately, substantial absorption of the laser pulse occurs at the vapour pressures of interest. This means that our present experimental arrangement is unsatisfactory because the energy and even the shape (and more important the onset time) of the laser pulse is in fact unknown at the observation region. This makes it very difficult to relate the emission results attained to date to our theory. Consequently, we have designed and built a new kind of alkali oven that will provide us with far superior optical access. Indeed, with this oven we should be able to observe the region where the laser pulse is incident upon the alkali vapour.

Anomalous Absorption of Laser Energy

In another series of preliminary experiments the laser was tuned to the 589 nm resonance line of sodium and the energy absorbed in transmission through a 40 cm column of sodium vapour was measured by a pair of photodiodes.

These were calibrated against an energy meter so that the shape and energy of both the incident and transmitted laser pulses were monitored. The variation in the absorbed energy as a function of the incident laser energy was thereby evaluated.

We were able to demonstrate that the laser energy absorbed can be understood in terms of simple radiation transport for low values of laser irradiance. However, *anomalous absorption* is observed to arise for increasing values of incident laser energy. We have been able to show that this additional absorption of energy does not have its origin in either two photon ionization or laser induced Penning ionization of the large population of resonance state atoms.

We believe that this anomalous absorption results from the development of an appreciable density of free electrons (primarily through associative ionization) which are then able to extract a significant amount of energy from the laser beam through superelastic collision quenching of the laser maintained resonance state population. This interaction, in effect, heats the free electrons and enables them to produce further ionization and excitation. We view these observations as representing our first (albeit indirect) evidence of superelastic electron heating induced through laser resonance saturation.

This work was recently published[24] and a copy of the paper is appended as Appendix F. However, in this analysis we had assumed that the resonance state population can be regarded as being in equilibrium with the radiation field of the laser beam, i.e.,

$$N_2(z,t) = \frac{GN_o\phi(z,t)}{1 + \phi(z,t)} \qquad (5)$$

where $G \equiv g/(1+g)$, g representing the resonance to ground level degeneracy ratio,

N_o represents the original (prior to laser excitation) ground level density of the vapour,

$\phi(z,t)\{\equiv F(z,t)/F_s\}$ represents the normalized laser photon flux density where $F(z,t)$ represents the laser photon flux density, and

F_s represents the saturated photon flux density.[24]

This led to a simple solution of the radiative transfer equation of the form

$$\phi(z,t) + \ell n\{\phi(z,t)\} = \phi(o,t) + \ell n\{\phi(o,t)\} - GN_o\sigma^{\ell}z \qquad (6)$$

where σ^{ℓ} is the appropriate absorption cross section (Appendix F).

Recently, we have checked the validity of equation (5) by solving the pair of coupled radiative-population rate equations [(9) and (10) of Appendix F] directly and comparing the results with that obtained using the approximation represented by equation (5). It was found that the complete solution yielded a form of *pulse sharpening* for just the leading edge of the laser pulse but otherwise made little difference to the conclusions reached in Appendix F.

Development of New LIBORS Facility

In order to avoid the difficulties encountered with our earlier experimental setup, we have constructed a new facility that includes a more powerful flashlamp pumped dye laser, a new design of oven for the sodium vapour, and a more comprehensive diagnostic arrangement. A photograph of this facility is presented as figure 12 and a schematic diagram which is helpful for understanding the photograph is presented as figure 13.

An important feature of the new oven, which is in the form of a heat sandwich rather than the crossed heat pipe used previously, is its 360° optical access. This will enable observations to be made of the entire alkali vapour region, including the transition zones between the cool buffer gas and the alkali vapour. This avoids the uncertainties associated with having the laser pulse traverse an appreciable column of alkali vapour before reaching the observation zone - a serious drawback of the crossed heat pipe design.

The new laser has been found to have at least five times the energy of our earlier system and should enable us to undertake experiments at relatively high densities (10^{16} - 10^{17} cm^{-3}). We shortly intend to commence a definitive series of experiments that will be designed to test and strengthen our theoretical understanding of the complex sequence of interactions that arise when a resonance transition is saturated for an extended period of time. These will include:

(i) determining the ionization burnout time and evaluating its dependence upon: the initial atom density of the laser pumped species, the peak laser irradiance (assuming a reproducible pulse shape) and the wavelength of the laser radiation;

(ii) studying the influence of a molecular background gas (nitrogen) on this dependence;

(iii) measuring the temporal, spatial and spectral characteristics of the laser pulse before and after transmission through the alkali vapour.

The ionization burnout time will be determined from the temporal behaviour of the plasma emission and *Stark measurements* on selected emission lines. In particular a number of spectral lines and a segment of the recombination continuum will be monitored with a dual photodetection system, comprising two monochromator-photomultiplier assemblies, and a common collection optics package, see figure 13. The temporal structure of the laser pulse before and after transmission through the alkali-vapour column will be monitored, as in our preliminary experiment, by a calibrated pair of photodiodes. In addition we plan to use a *reticon* (photodiode array) to measure either the spatial structure of the laser beam or its spectral profile (using an etalon arrangement, see figure 13) before and after transmission through the vapour.

Stark Measurements

The *peak electron density* and the time of its occurrence will be evaluated from measurements of the *Stark profile* of selected spectral lines. An example of the Stark profiles,[25] for one possible line in sodium, corresponding to several electron densities is presented in figure 14. A measurement of the ratio of the intensity within the two spectral intervals shown in figure 14 should reveal the temporal variation of the electron density through the burnout phase. The sensitivity of such measurements to uncertainty in the electron temperature can be gauged by reference to figure 15 where this intensity ratio is plotted as a function of the electron density for three values of the electron temperature that encompass the likely range of temperatures expected during the burnout phase. Indeed, an uncertainty of 100% in the electron temperature is expected to lead to only a 20% error in the electron density measurement at about 10^{16} cm^{-3}. Clearly, operation at higher densities will provide an improvement in the accuracy of such measurements.

The experimental arrangement for this undertaking will involve imaging the exit slit of a SPEX monochromator onto the face of a three channel fiber optic array, see figure 13. An appropriate choice of tuning, exit slit opening and optics will then ensure that the two outer fiber optic bundles sample the spectral profile in accordance with figure 14. Use of all three channels should lead to better accuracy and might enable us to extend the measurements to lower values of electron density.

Ground Level Burnout Calculation

Of considerable importance to the application of laser resonance saturation to the development of short wavelength lasers is the degree of ground level burnout that can be attained. Clearly, the greater the reduction in the ground level population the easier it will be to create a ground level population inversion. In order to gain some insight into what might be attainable through laser resonance saturation we have undertaken an extended computer run of our LIBORS code. The result is presented as figure 16 where it can be seen that sodium vapour at 10^{17} cm^{-3} will burn to over 99.7% ionization within 100 nsec when subjected to laser irradiance of 10^{8} Wcm^{-2}. Indeed, after 150.7 nsec the percentage of ionization was found to reach 99.78% while the electron temperature attained 19,432 K. Furthermore, the ground level population burnt out to a value of 9.49×10^{12} cm^{-3} corresponding to a *ground level burnout factor*, α ($\equiv N_1/N_e$) of 9.49×10^{-5} which is very close to the value expected on the basis of LTE (local thermodynamic equilibrium) and laser saturation, i.e.,

$$\alpha^{LTE} = \frac{N_o}{gS(kT_e)} = \frac{N_o \times 10^{-21} e^{-3.04/kT_e}}{3x(kT_e)^{3/2}} \qquad (7)$$

We assume here that

$$\alpha \equiv \frac{N_1}{N_e} = \frac{N_2}{gN_e} \qquad (8)$$

under conditions of laser saturation and if LTE prevails, then

$$N_2 = N_e^{\,2}/S(kT_e) \qquad (9)$$

where N_e is the free electron density and

$$S(kT_e) \cong 6 \times 10^{21} (kT_e)^{3/2} \frac{Z^+(kT_e)}{g_2} e^{-E_{c2}/kT_e} \qquad (10)$$

if kT_e and the resonance level ionization energy, E_{c2}, are in (eV). In the case of sodium the ion partition function, $Z^+(kT_e) \cong 1$, over the range of temperatures of interest.

It is quite apparent that LTE may be assumed to hold (at least for $N_e > 10^{16}$ cm^{-3}) during the period of ground level burnout and so we have undertaken a calculation aimed at determining the *limiting value* for the ground level burnout factor α.

In this calculation we assume that a plasma comprising almost entirely of ions of charge q is irradiated with intense laser radiation tuned to saturate the ground to resonance transition of the ion of charge q. This leads to a burnout of the q-ions and the creation of ions of charge q+1. If LTE is assumed to prevail we can write a modified Saha equation of the form

$$S(T_e) \cong \frac{N_e N^{q+1}}{N_2^q} = 6.03\times10^{21}(kT_e)^{3/2}\frac{Z^{q+1}(kT_e)}{g_2^q} e^{-\{E_{c2}^q-\Delta E_q\}/kT_e} \quad (11)$$

where N^{q+1} represents the density of ions of charge q+1,

N_2^q represents the density of ions of charge q in the laser pumped resonance state,

$Z^{q+1}(kT_e)$ represents the partition function of the ions of charge q+1,

g_2^q represents the degeneracy of the resonance level of the ion of charge q,

E_{c2}^q represents the ionization energy of the resonance level of the ion of charge q,

ΔE_q represents the ionization depression for the ions of charge q, and

kT_e represents the mean thermal energy of the free electrons in (eV).

Continuity of mass leads to the relation

$$N^{q+1} + N^q \cong N_o^q \quad (12)$$

where N_o^q represents the original density of ions of charge q. Continuity of charge requires that

$$N_e \cong (q+1)N^{q+1} + qN^q \quad (13)$$

Furthermore,

$$N^q = \sum_{n\geq 1} N_n^q = N_1^q + N_2^q + \sum_{n>2} N_n^q \quad (14)$$

Under conditions of laser saturation of the resonance transition,

$$N_2^q = \frac{g_2^q}{g_1^q} N_1^q = g^q N_1^q \quad (15)$$

If (15) is used in (14) we can write

$$N^q = \frac{N_2^q}{G}\left\{1 + G \sum_{n>2} g_n^q e^{-E_{n2}^q/kT_e}\right\}$$

or

$$N^q = N_2^q P(T_e)/G \tag{16}$$

where

$$G \equiv g^q/(1+g^q) \tag{17}$$

If (12) is used in (13) to eliminate N^{q+1} and (16) is used for N^q, then we can write

$$N_e = [N_o^q - N_2^q P(T_e)/G](q+1) + qN_2^q P(T_e)/G$$

or

$$N_2^q = G[(q+1)N_o^q - N_e]/P(T_e) \tag{18}$$

If we also use (16) in (12)

$$N^{q+1} = N_o^q - N_2^q P(T_e)/G \tag{19}$$

Using (18) and (19) in (11) yields

$$\frac{N_e[N_o^q - N_2^q P(T_e)/G]P(T_e)}{G[(q+1)N_o^q - N_e]} = S(T_e)$$

or with a little algebraic manipulation and elimination of N_2^q through use of (18) we arrive at a simple quadratic relation for N_e, i.e.,

$$N_e^2 + bN_e - d = 0 \tag{20}$$

where

$$b = GS(T_e)/P(T_e) - qN_o^q \tag{21}$$

and

$$d = G(q+1)N_o^q S(T_e)/P(T_e) \tag{22}$$

Equation (20) has two solutions, one of which is negative since $\{b^2+4d\}^{\frac{1}{2}} > b$ and has no physical interpretation. The other can be expressed in the form

$$N_e = [\{b^2 + 4d\}^{\frac{1}{2}} - b]/2 \qquad (23)$$

It is evident from (21), (22) and (23) that N_e can be evaluated once the electron temperature is known.

In order to determine the limiting value of the electron temperature we consider the *energy balance* of the system. If we neglect gradient effects then an energy balance will arise when the volume rate of laser energy deposition (through superelastic heating) just equals the volume rate of radiation loss from the plasma. The primary contributions to this radiation energy loss will arise from line radiation from the excited states within both ions and recombination radiation in the ion of charge q. We shall assume that bremsstrahlung loss is negligible and that inverse bremsstrahlung heating by the laser radiation is also negligible. At the high densities of interest in this work, *radiation trapping* may be quite significant - this would in fact reduce the energy loss and allow the temperature to rise even higher than expected by neglecting this effect. Our radiation loss is likely to yield a pessimistic value for the ground level burnout achievable. On the other hand, oscillator strength information for the q+1 ion tends to be rather sparse so that our radiation loss may not be as complete as we would like.

Finally, there is the matter of thermal conduction loss from a plasma of finite dimensions - this will be dominated by electron conduction in most instances. If we assume that the plasma is cylindrical in nature (being formed along the laser beam) with radius a and that the lateral gradient is likely to be much more severe than the axial gradient then the energy balance equation can be expressed in the form

$$N_e N_2^q K_{21}^q E_{21}^q = \sum_{n>1} N_n^q \sum_{m<n} A_{nm}^q E_{nm}^q + N_e N^{q+1} \sum_{n\geq 1} \beta_n^q E_{cn}^q + \sum_{n>1} N_n^{q+1} \sum_{m<n} A_{nm}^{q+1} E_{nm}^{q+1}$$

$$+ \frac{2}{a} K_e \left\{ \frac{\partial T_e}{\partial r} \right\}_{r=a} + N_e N_1^q K_{12}^q E_{21}^q \qquad (24)$$

where the electron thermal conductivity,[26] $K_e \cong 0.284\ T_e^{5/2}/\ell n\Lambda$ ($Wcm^{-1}\ T^{-1}$), T_e is in eV and $\ell n\Delta \cong 3$ for the range of conditions of interest. β_n^q represents

the radiative recombination rate coefficient for level n of the ion of charge q, K_{21}^q is the superelastic collision rate coefficient, E_{nm}^q is the q-ion energy difference between levels n and m and A_{nm}^q represents the Einstein spontaneous transition probability for the nm transition in the ion of charge q. If we assume LTE holds then we can use

$$N_n^q = N_2^q \frac{g_n^q e^{-E_{n2}^q/kT_e}}{g_2^q} \qquad \text{(for } n > 2\text{)} \qquad (25)$$

and

$$N_n^{q+1} = \frac{N^{q+1} g_n^{q+1} e^{-E_{n1}^{q+1}/kT_e}}{Z^{q+1}(T_e)} \qquad \text{(for } n > 1\text{)} \qquad (26)$$

in the energy balance equation. Under these circumstances equation (24) becomes an equation in terms of N_e and T_e. However, we saw from equation (23) that N_e can be written in terms of T_e. Consequently, the elimination of N_e between equations (23) and (24) leads to a complex transcendental equation for T_e. This can be written in the form

$$S_H(T_e) = L_R(T_e) + L_c(T_e) \qquad (27)$$

where $S_H(T_e)$ represents the volume *net* rate of heating through *superelastic collisions*, i.e., $S_H \approx N_e N_2^q K_{21}^q E_{21}^q [1 - e^{-E_{21}^q/kT_e}]$, under LTE conditions,

$L_R(T_e)$ represents the volume rate of cooling through *radiation loss*

$L_c(T_e)$ represents the volume rate of cooling through *conduction loss*.

If we assume that the temperature of the plasma column drops to zero at the boundary, then we can approximate the radial gradient in (27) by T_e/a. $S_H(T_e)$, $L_R(T_e)$ and $\{L_R(T_e) + L_c(T_e)\}$ are then evaluated and plotted as a function of T_e for the case of sodium vapour with $N_o = 10^{17}$ cm^{-3} in figure 17. Two temperatures can be determined from the crossover points of these curves. T_e^R represents the radiative balance temperature and T_e^{C+R} the radiative-conduction balance temperature for the superelastically heated plasma. T_e^{C+R} probably represents a more likely temperature for determining the limiting value of the *ground level burnout* factor α^{C+R}. Both T_e^{C+R} and T_e^R are plotted as a function of sodium density, N_o, in figure 18.

The general definition of the GLB factor takes the form

$$\alpha \equiv N_1^q / N^{q+1} \qquad (28)$$

Under conditions of laser saturation, we can write

$$\alpha = \frac{N_2^q}{g^q N^{q+1}} \tag{29}$$

which can be calculated in terms of N_o^q and T_e from equations (18) and (19). In the case of sodium we have used both T_e^R and T_e^{C+R} to determine the GLB factor and the results are also plotted in figure 18. If only radiation losses are considered it is apparent that the lower the density the lower the GLB factor attained. With the inclusion of thermal conduction losses it is evident that there exist an optimum density for minimizing α and in the case of sodium we see that

$$\alpha_{min}^{C+R} \cong 6.6 \times 10^{-5}$$

for

$$N_o \cong 2 \times 10^{17} \text{ cm}^{-3}$$

As might be expected from equation (24) and indicated in figure 17 the radiation losses from the species being pumped decreases with increasing temperature and in the absence of other losses the laser might well be expected to literally burn the species out of existence. In reality, radiation loss from the next stage of ionization increases with increasing temperature above some critical temperature, witness the sudden rise in the radiation loss above 2 eV in figure 17. The greater the ionization energy (or more properly the resonance state energy) of the next ionization stage the higher will be the onset temperature for significant radiation loss from this ion and in the absence of other losses (e.g., conduction loss) the smaller the GLB factor attained. For each of the ions (i.e., B_eII, BIII or CIV) suggested in our proposed approach towards the development of a short wavelength laser there is a significant jump in the ionization energy for the next ionization stage and so in all probability it will again be conduction losses that limit the temperature and degree of GLB attained. We shall obviously have to study this subject in much greater depth and attempt to confirm experimentally our predictions on GLB.

ACKNOWLEDGEMENTS

The excellent theoretical and experimental contributions of Paul Cardinal, Peter Wizinowich, Silvester Wong, Greg Schinn, John Bird, Mark Cappelli and Randy Kissack are gratefully appreciated. This work has been supported by the U.S. AFOSR under grant No. 80-0057A. Additional support has been provided by the Sandia Laboratory under Contract No. 49-2859A, and by the Natural Science and Engineering Research Council of Canada.

REFERENCES

1. R. M. Measures, J. Appl. Phys. 39, 5232-5245 (1968).
2. R. M. Measures, The Phys. of Fluids, 13, 1889-1890 (1970).
3. R. M. Measures, JQRST, 10, 107-125 (1970).
4. R. M. Measures and P. G. Cardinal, Physical Review A, 23, 804-815 (1981).
5. R. M. Measures, N. Drewell and H. S. Kwong, Phys. Rev. A, 16, 1093-1097 (1977).
6. H. S. Kwong and R. M. Measures, Appl. Optics, 19, 1025-1027 (1980).
7. W. Gornik, D. Kaiser, W. Lange, H. H. Radloff and H. Schulz, Appl. Phys., 1, 285-286 (1973).
8. R. M. Measures and H. S. Kwong, Appl. Optics, 18, 281-286 (1979).
9. H. S. Kwong and R. M. Measures, Analytical Chemistry, 51, 428-432 (1979).
10. V. I. Balykin, V. S. Letokhov, V. I. Mishin and V. A. Semchishen, JETP Lett., 26, 359-360 (1977).
11. G. S. Hurst, M. G. Payne, S. D. Kramer and J. P. Young, Reviews of Modern Physics, 51, 167-819 (1979).
12. J. A. Gelbwachs, C. F. Klein and J. E. Wassel, Appl. Phys. Lett., 30, 489 (1977).
13. J. A. Gelbwachs, C. F. Klein and J. E. Wassel, IEEE I. Quantum Electron, QE-14, 121 (1978).
14. J. W. Daily, Appl. Optics, (a) 16, 568-571 (1977); (b) 17, 1610 (1978).
15. R. P. Lucht and N. M. Lauendeau, Appl. Optics, 18, 856-860 (1979).
16. J. W. Hosch and E. H. Piepmeier, Appl. Spectrosc., 32, 444-446 (1978).
17. N. Omenetto, Ed., "Analytical Laser Spectroscopy" (Wiley, New York, 1979).
18. D. W. Koopman, T. J. McIlrath and V. P. Myerscough, JQSRT, 19, 555-567 (1978).
19. R. Hess and F. Burrell, JQSRT, 21, 23-33 (1979).
20. K. G. Muller and M. Stania, J. Appl. Phys., 49, 5801-5805 (1978).
21. C. H. Muller, III, and K. H. Burrell, "Impurity Measurements on ISX-B by Use of Laser Saturation Spectroscopy", Paper 7P19, Bull. Am. Phys. Soc., 25, 977 (1980).
22. R. M. Measures, P. G. Cardinal, G. W. Schinn, J. Appl. Phys. 52, 1269-1277 (1981)
23. J. F. Clarke and M. McChesney, "Dynamics of Relaxing Gases", Butterworth Inc., Boston, (1976).
24. R. M. Measures, P. L. Wizinowich and P. G. Cardinal, J. Appl. Phys. 51, 3622-3628 (1980).

25. H. R. Griem, "Spectral Line Broadening by Plasmas" (Academic Press, New York, 1974).

26. S.Glasstone and R. H. Lovberg, "Controlled Thermonuclear Reactions" (Van Nostrand Co., New York, 1960).

CUMULATIVE CHRONOLOGICAL LIST OF PUBLICATIONS (1976-PRESENT)

1. R. M. Measures, S. K. Wong, P. G. Cardinal, "The Influence of Molecular Nitrogen Upon Plasma Channel Formation by Laser Resonance Saturation", Accepted for J. Appl. Physics, Feb. 1982.
2. M. R. Arnfield and R. M. Measures, "Ion to Neutral Atom Measurements within an Ablation Plasma Through Laser Selective Excitation Spectroscopy", Physical Review A, 24, 535-539, 1981.
3. R. M. Measures, P. G. Cardinal and G. W. Schinn, "Theoretical Model of Laser Ionization of Alkali Vapours Based on Resonance Saturation", J. Appl. Phys., 52, 1269-1277, 1981.
4. P. G. Cardinal, P. L. Wizinowich and R. M. Measures, "Anomalous Laser Energy Absorption Associated with Resonance Saturation", J. Quant. Spectrosc. Radiant. Transfer, 25, 537=545, 1981.
5. R. M. Measures and P. G. Cardinal, "Laser Ionization Based on Resonance Saturation - A Simple Model Description", Physical Review A, 23, 804-815, 1981.
6. R. M. Measures, P. L. Wizinowich, P. G. Cardinal, "Fast and Efficient Plasma Heating Through Superelastic Laser Energy Conversion", J. Appl. Phys., 51, 3622-3628, 1980.
7. H. S. Kwong and R. M. Measures, "Lifetime Measurements on Atoms in Compounds Embedded in Matrices Using Laser Selective Excitation and Ablation Dynamics", Appl. Optics, 19, 1025-1027, 1980.
8. R. M. Measures, N. Drewell, P. Cardinal, "Electron-and Ion-Beam Transportation Channel Formation by Laser Ionization Based on Resonance Saturation - LIBORS", J. Appl. Phys. 50, 2622-2669, 1979.
9. R. M. Measures, N. Drewell, P. Cardinal, "Laser Interaction Based on Resonance Saturation (LIBORS): An Alternative to Inverse Bremsstrahlung for Coupling Laser Energy into a Plasma", Appl. Optics, 18, 1824-1827, 1979.
10. H. S. Kwong, R. M. Measures, "Trace Element Laser Microprobe Having High Sensitivity and Freedom from Chemical Matrix Effects", Analytical Chemistry, 51, 428-432, 1979.
11. R. M. Measures, H. S. Kwong, "Development of a Trace Element Analyser Based on Laser Ablation and Selective Excited Radiation - TABLASER", Appl. Optics, 18, 281-285, 1979.
12. R. M. Measures, N. Drewell, P. Cardinal, "Superelastic Laser Energy Conversion (SELEC)", Radiation Energy Conversion in Space (Ed. K. W. Billman), Vol. 61 of Progress in Astronautics and Aeronautics, 1978.

13. R. M. Measures, "PROBE - Profile Resolution Obtained by Excitation", Applied Spectroscopy, 32, 381-388, 1978.

14. R. M. Measures, "PROBE - A New Technique for Measuring the Density Profile of a Specific Constituent Using Counter Propagating Laser Pulses", Appl. Optics, 16, 3016-3026, 1977.

15. R. M. Measures, N. Drewell, H. S. Kwong, "Atomic Lifetime Measurement Obtained by Use of Laser Ablation and Selective Excitation Spectroscopy", Phys. Rev. A, 16, 1093-1097, 1977.

16. R. M. Measures, "Efficient Laser Ionization of Sodium Vapor - A Possible Explanation Based on Superelastic Collisions and Reduced Ionization Potential", J. Appl. Phys., Vol. 48, 2673-2675, 1977.

17. R. M. Measures, "LIDAR Equation Analysis - Allowing for Target Lifetime Laser Pulse Duration and Detector Integration Period", Appl. Optics, Vol. 16, 1092-1103, 1977.

Book

R. M. Measures, "Analytical Use of Lasers in Remote Sensing", Chapter 6 of Analytical Laser Spectroscopy (Ed. N. Omenetto), J. Wiley Publications, 1979.

PROFESSIONAL PERSONNEL

Principal Investigator:

Dr. R. M. Measures (Professor of Applied Science and Engineering)

Research Assistants:

P. G. Cardinal (Ph.D. Student)

R. S. Kissack (Ph.D. Student)

S. K. Wong (Ph.D. Student)

J. C. Bird (M.A.Sc. Student)

M. A. Cappelli (M.A.Sc. Student)

H. Herchen (M.A.Sc. Student)

G. W. Schinn (M.A.Sc. Student)

INTERACTIONS

Two papers were presented at the IEEE International Conference on Plasma Science, Santa Fe, New Mexico, May 18-20, 1981. They were:

1. R. M. Measures and P. G. Cardinal, "The Application of Laser Resonance Saturation to the Development of Efficient Short-Wavelength Lasers".
2. R. M. Measures, S. K. Wong and P. G. Cardinal, "Ion Beam-Laser Ionization Guide Channel Formation in the Presence of Nitrogen".

We also presented a paper at the Am. Phys. Soc. Plasma Div. Meeting, San Diego, Nov. 10-15, 1980, Paper 8E9, read:

3. R. M. Measures and P. G. Cardinal, "Rapid Ionization and Heating Through Laser Resonance Saturation".

NEW DISCOVERIES STEMMING FROM RESEARCH

Saturation of an atomic transition by the intense radiation field of a suitably tuned laser represents an important kind of interaction with potential applications in many areas. The consequences of laser resonance saturation and the subsequent applications stemming from this interaction depend to a very large extent upon the period of saturation. If the resonance to ground level populations are only momentarily locked (in the ratio of respective degeneracies) the principal effect is a burst of intensified spontaneous emission, on the other hand an extended period of saturation (lasting for very much longer than the resonance lifetime) can lead to extensive perturbation of the medium. Indeed, almost total ionization and very rapid heating can arise if the superelastic collision time is very short compared to the duration of the laser pulse.

The author was the first to recognize the importance of this interaction (see references 1, 2, 3) and many of its possible areas of application. Subsequent work in the author's laboratory and elsewhere have proven that laser resonance saturation does represent a significant form of interaction between laser radiation and atomic vapours or plasmas.

The combination of laser ablation and selective excitation spectroscopy (LASES) represents a new approach at evaluating fundamental atomic quantities, such as: radiative lifetimes, branching ratios, transition probabilities and selected collision cross-sections. A preliminary paper on this subject was published in Physical Review in 1977; see publication Nos. 7 and 15. The LASES technique, as well as being convenient and accurate, is particularly well suited for measurements on short lived, highly ionized species created by laser ablation. Furthermore, the LASES approach is versatile and can use multiphoton or stepwise excitation as the means of generating the bursts of intensified emission.

As a spin-off of this work we have also shown that the LASES concept can also form the basis of a new form of trace element laser microprobe called a TABLASER; see publication Nos. 10 and 11.

More recently, we have demonstrated in a proof of principle experiment that laser selective excitation spectroscopy can be used to directly measure with both spatial and temporal resolution the ion to neutral atom density ratio in a rapidly expanding ablation plasma, see publication No. 2.

Currently, our efforts are concentrating upon obtaining a better understanding of the consequences of extended laser resonance saturation (see

publication Nos. 1, 3, 4, 5 and 6) and in particular we are starting to study the way in which this very efficient and fast method of coupling laser energy into a plasma could be used in the development of new and efficient short wavelength lasers.

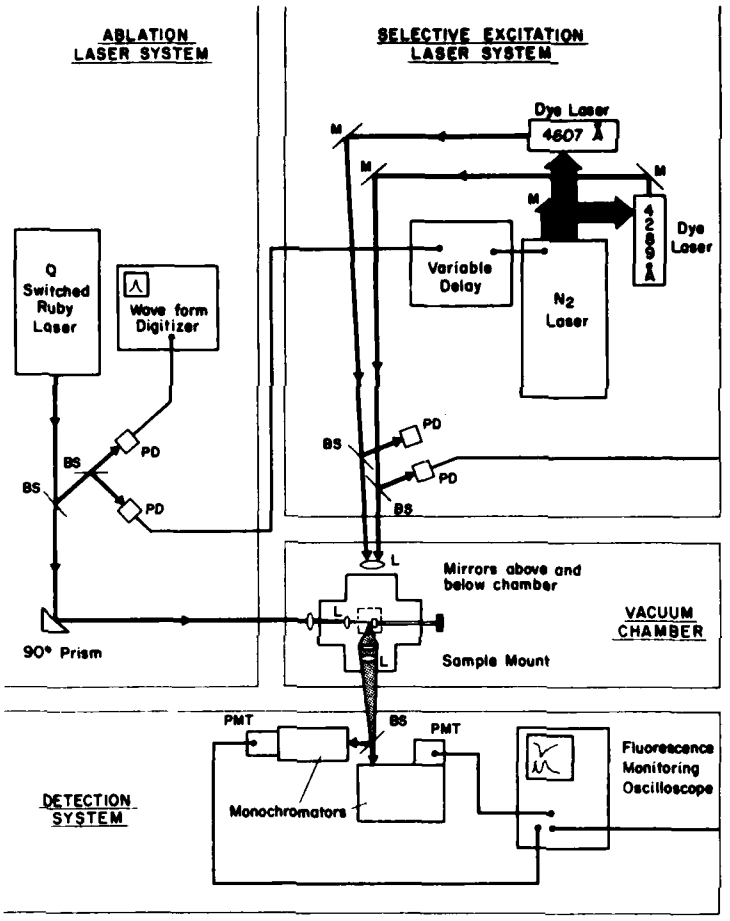
ABLATION LASER SYSTEM
SELECTIVE EXCITATION LASER SYSTEM
Dye Laser 4607 Å
M
M
M
M
4289 Å
Dye Laser
Variable Delay
N2 Laser
Q Switched Ruby Laser
Wave form Digitizer
PD
BS
PD
BS
PD
BS
PD
BS
L
Mirrors above and below chamber
VACUUM CHAMBER
L
L
90° Prism
Sample Mount
PMT
BS
PMT
Fluorescence Monitoring Oscilloscope
DETECTION SYSTEM
Monochromators

FIG. 1

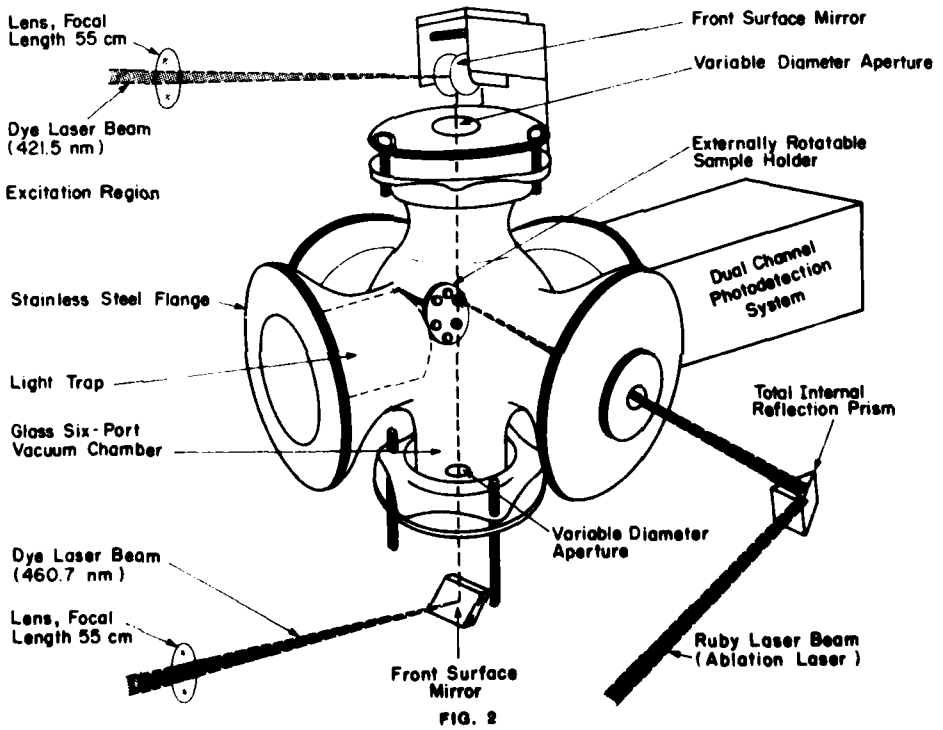
Lens, Focal Length 55 cm
Dye Laser Beam (421.5 nm)
Excitation Region
Stainless Steel Flange
Light Trap
Glass Six-Port Vacuum Chamber
Dye Laser Beam (460.7 nm)
Lens, Focal Length 55 cm
Front Surface Mirror
Variable Diameter Aperture
Externally Rotatable Sample Holder
Dual Channel Photodetection System
Total Internal Reflection Prism
Variable Diameter Aperture
Ruby Laser Beam (Ablation Laser)
Front Surface Mirror

FIG. 2

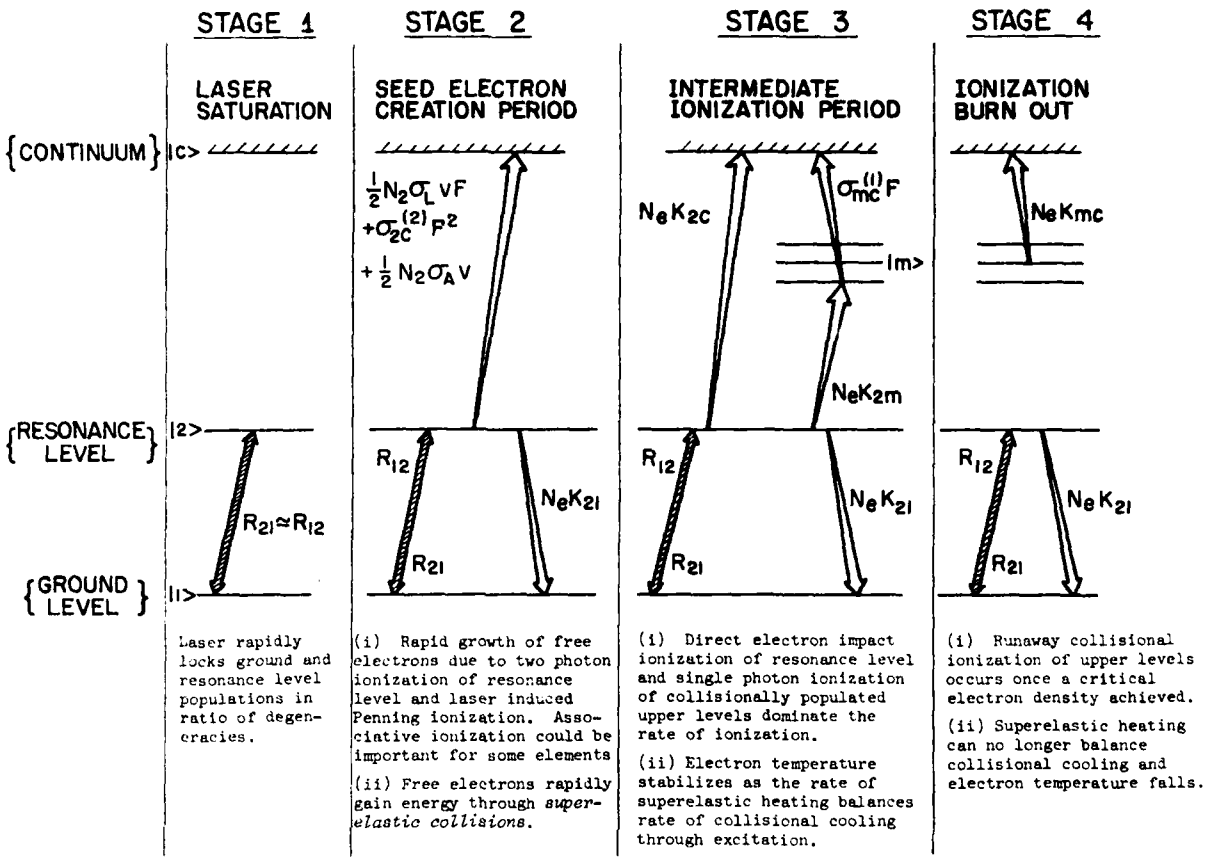

FIG. 3 Four Stages of LIBORS

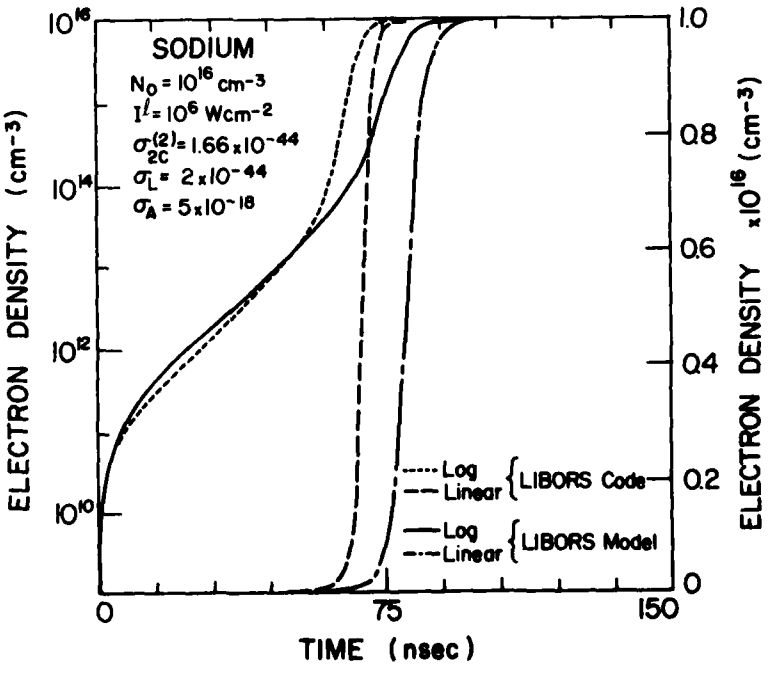

FIG. 4

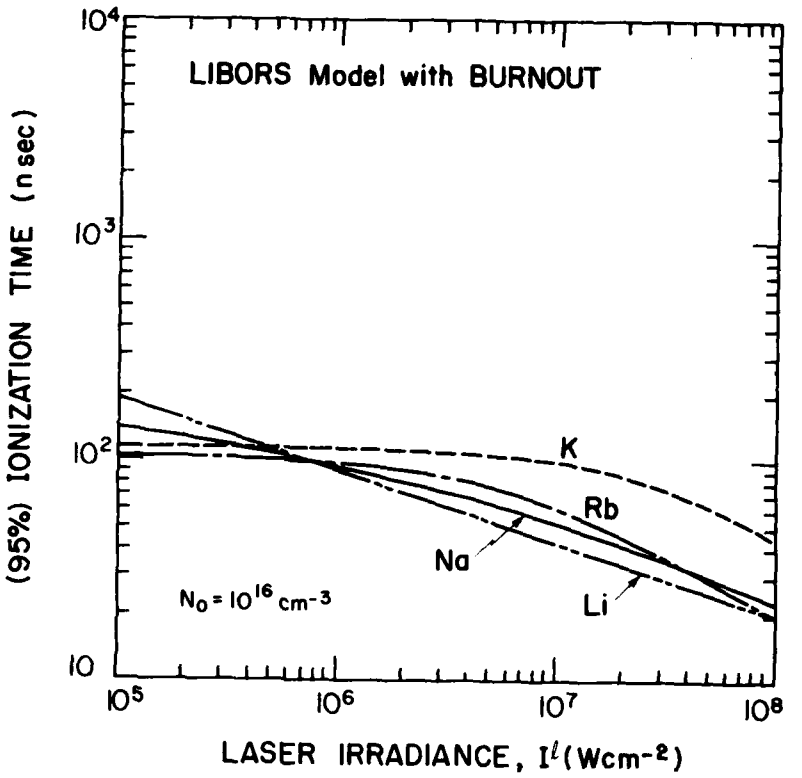
LIBORS Model with BURNOUT
(95%) IONIZATION TIME (n sec)
10^4
10^3
10^2
10
K
Rb
Na
Li
$N_0 = 10^{16}$ cm^{-3}
10^5
10^6
10^7
10^8
LASER IRRADIANCE, I^{ℓ} (Wcm^{-2})

FIG. 5

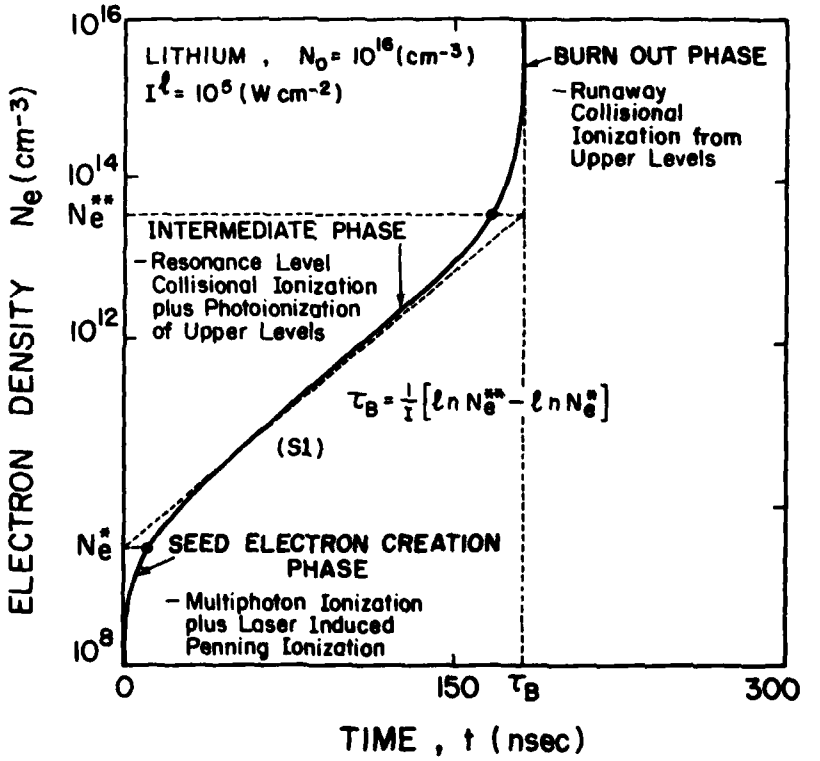
LITHIUM , $N_0 = 10^{16}$ (cm^{-3})
$I^{\ell} = 10^5$ (W cm^{-2})
BURN OUT PHASE
– Runaway Collisional Ionization from Upper Levels
INTERMEDIATE PHASE
– Resonance Level Collisional Ionization plus Photoionization of Upper Levels
$\tau_B = \frac{1}{I}\left[\ell n N_e^{**} - \ell n N_e^{*}\right]$
(S1)
SEED ELECTRON CREATION PHASE
– Multiphoton Ionization plus Laser Induced Penning Ionization
ELECTRON DENSITY N_e (cm^{-3})
10^{16}
10^{14}
N_e^{**}
10^{12}
N_e^{*}
10^8
0
150
τ_B
300
TIME , t (nsec)

FIG. 6

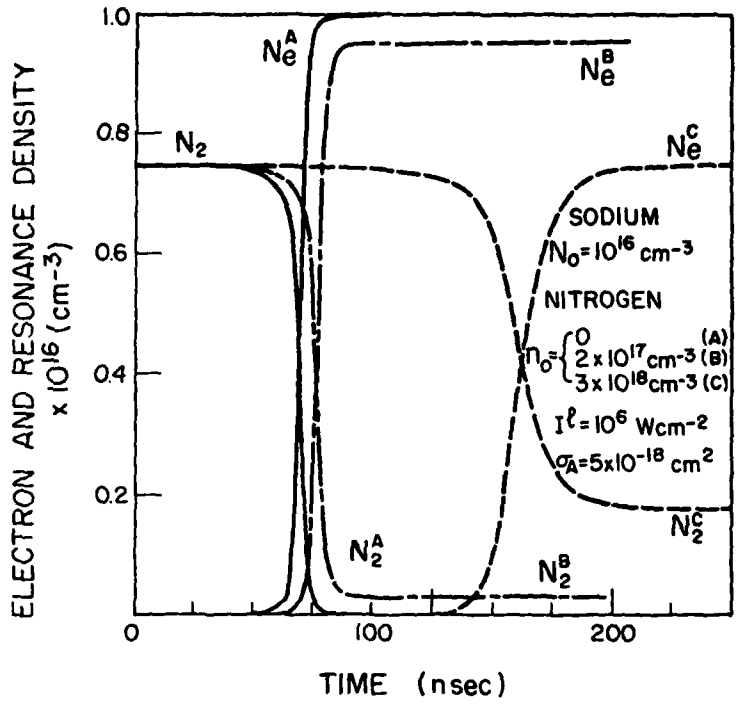
ELECTRON AND RESONANCE DENSITY
x 10^16 (cm^-3)
1.0
0.8
0.6
0.4
0.2
0
100
200
TIME (nsec)
N_e^A
N_e^B
N_e^C
N_2
N_2^A
N_2^B
N_2^C
SODIUM
N_o = 10^16 cm^-3
NITROGEN
n_o = 0 (A)
2 x 10^17 cm^-3 (B)
3 x 10^18 cm^-3 (C)
I ℓ = 10^6 Wcm^-2
σ_A = 5x10^-18 cm^2

FIG. 7

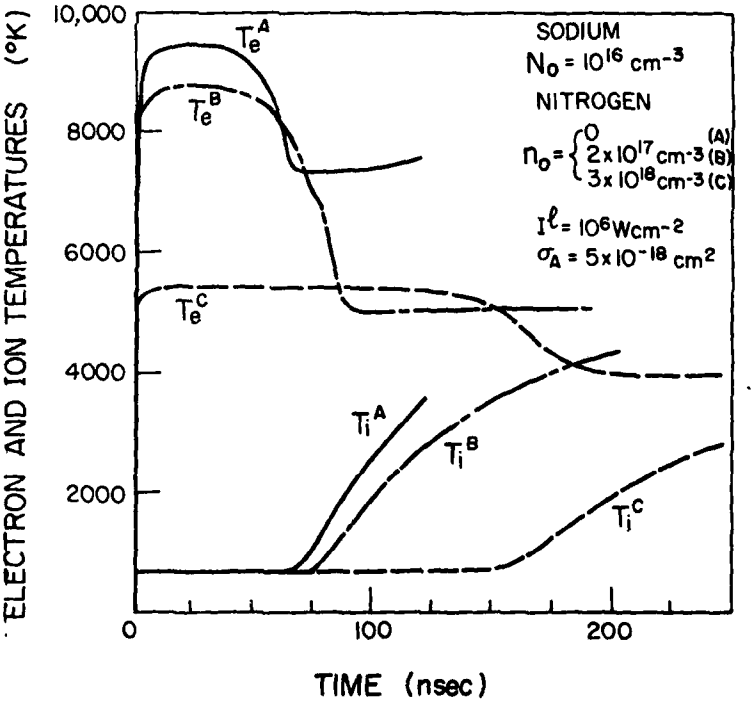
ELECTRON AND ION TEMPERATURES (°K)
10,000
8000
6000
4000
2000
0
100
200
TIME (nsec)
T_e^A
T_e^B
T_e^C
T_i^A
T_i^B
T_i^C
SODIUM
N_o = 10^16 cm^-3
NITROGEN
n_o = 0 (A)
2 x 10^17 cm^-3 (B)
3 x 10^18 cm^-3 (C)
I ℓ = 10^6 Wcm^-2
σ_A = 5 x 10^-18 cm^2

FIG. 8

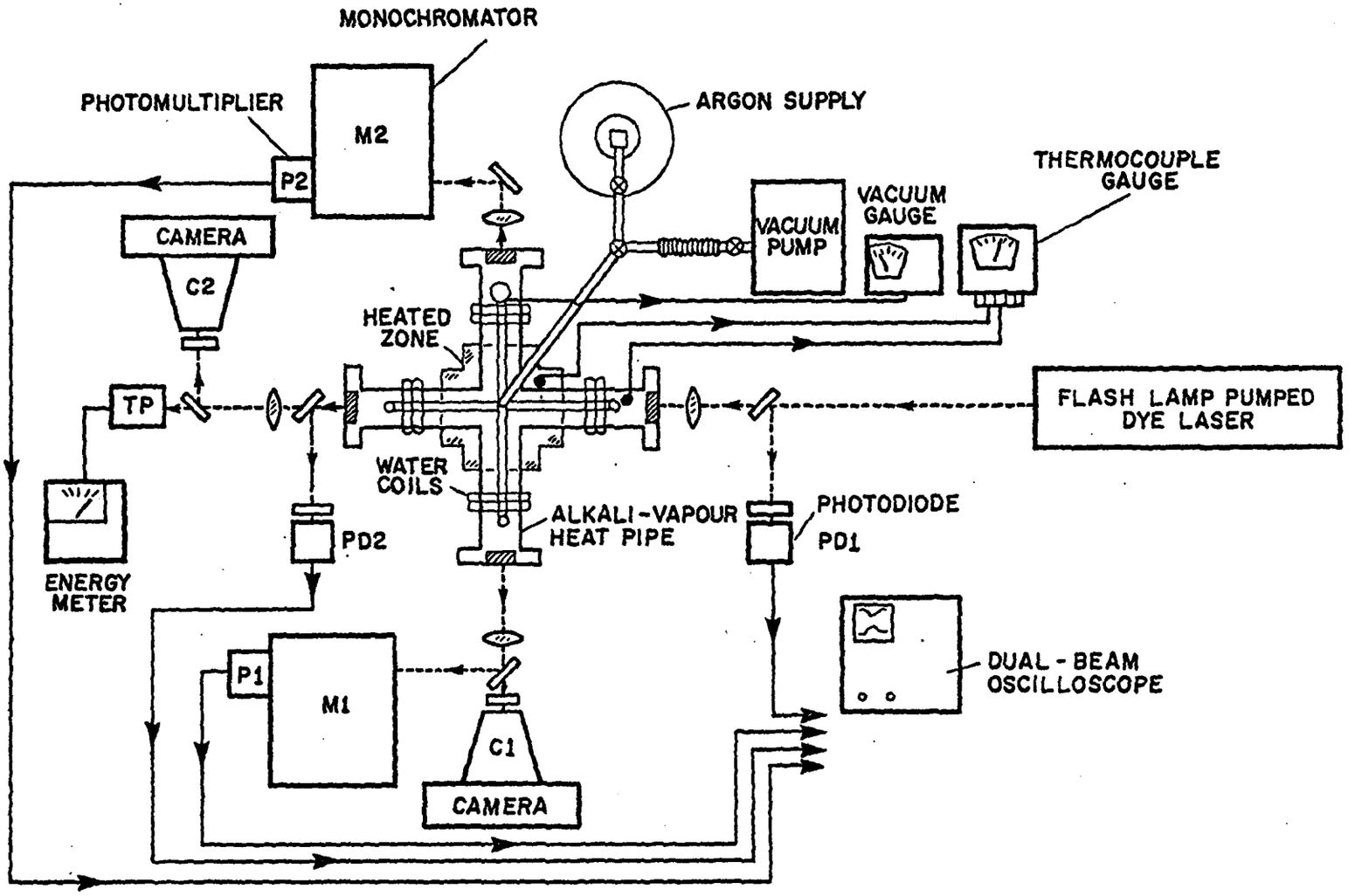

FIG. 9 LIBORS FACILITY

LIBORS created *plasma channel* in sodium vapour ($10^{16}cm^{-3}$) when laser tuned to the 589 nm resonance line and photographed through side port of crossed heat pipe. The incident laser energy was 205 mJ.

FIG. 10

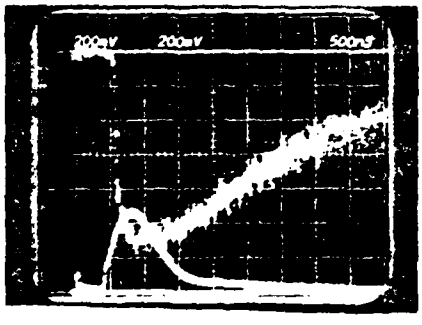

Lower trace is from PD1 and represents incident laser pulse. Upper trace corresponds to the inverted photomultiplier signal at 406 nm (corresponding to 4 nm band of radiative recombination continuum from sodium plasma).

FIG. 11

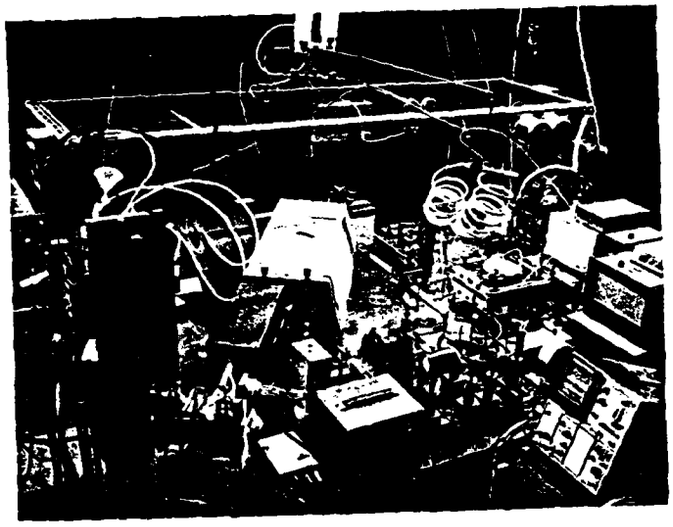

LIBORS Experimental Facility

FIG. 12

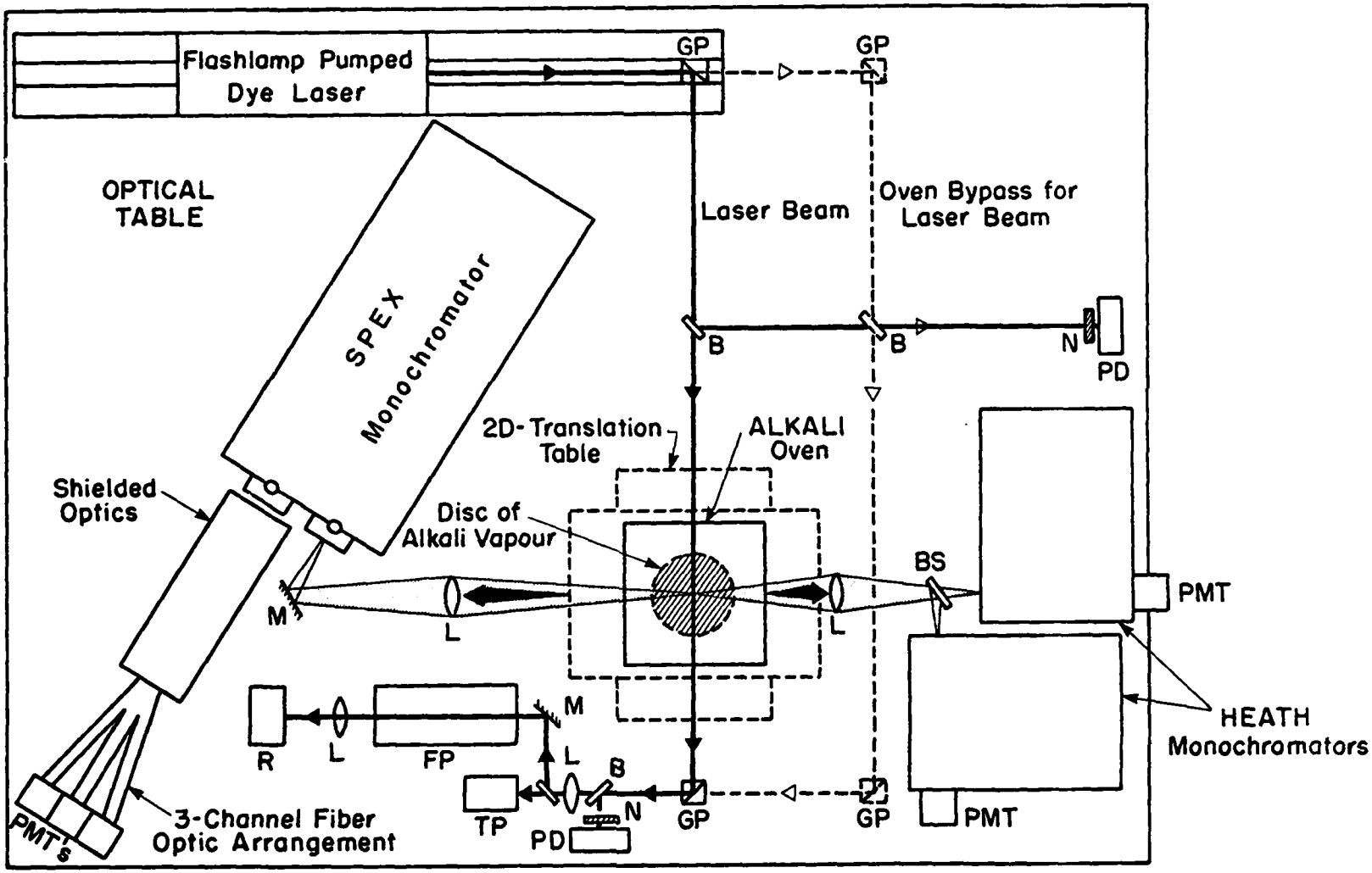

Schematic of LIBORS Experimental Facility

FIG. 13

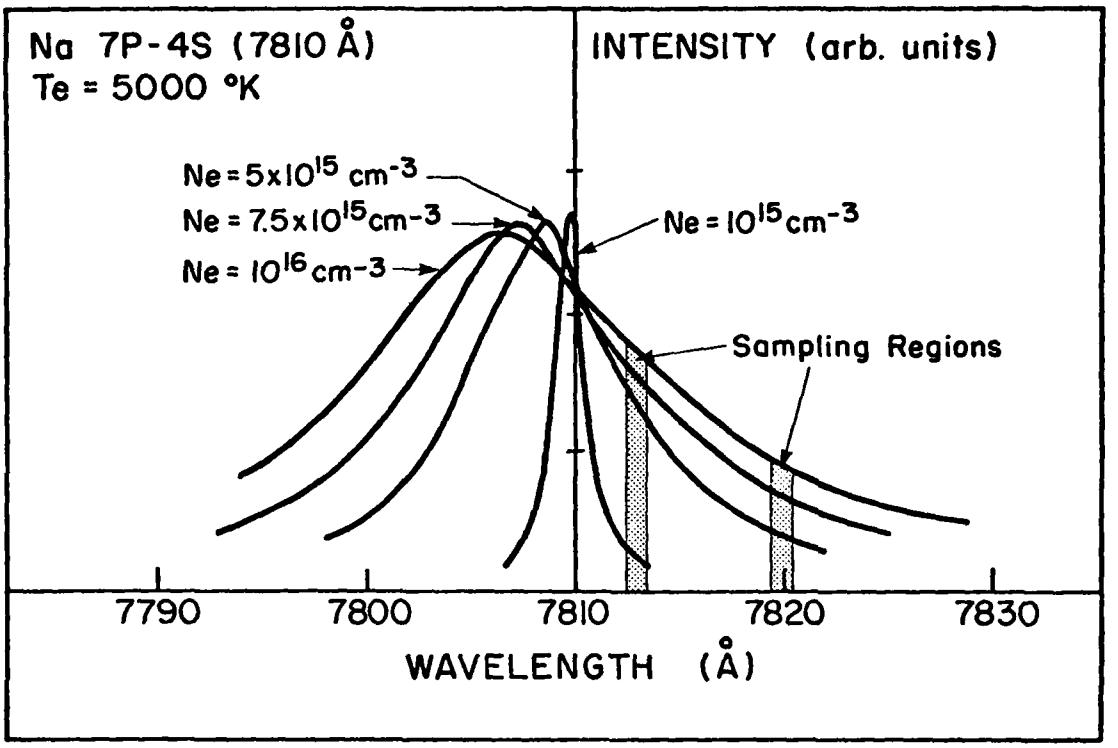

Stark Profiles for Sodium Plasma

FIG. 14

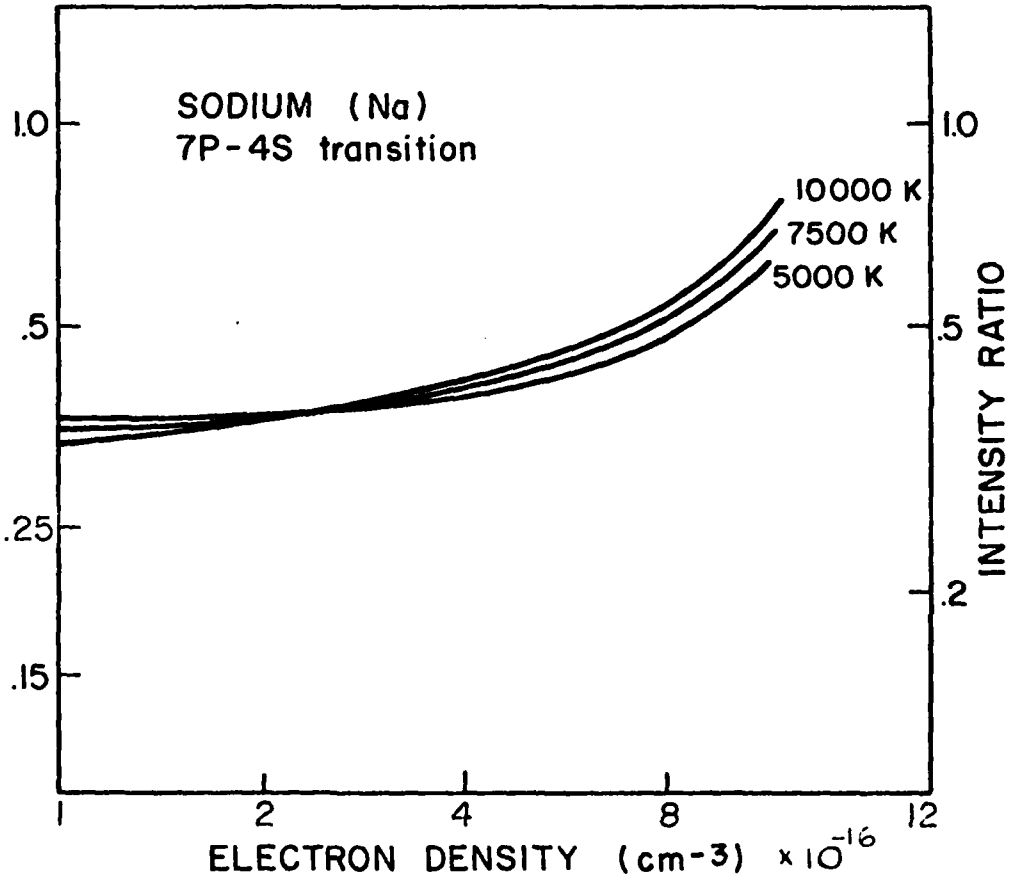

FIG. 15 Variation of Profile Intensity Ratio with Electron Density

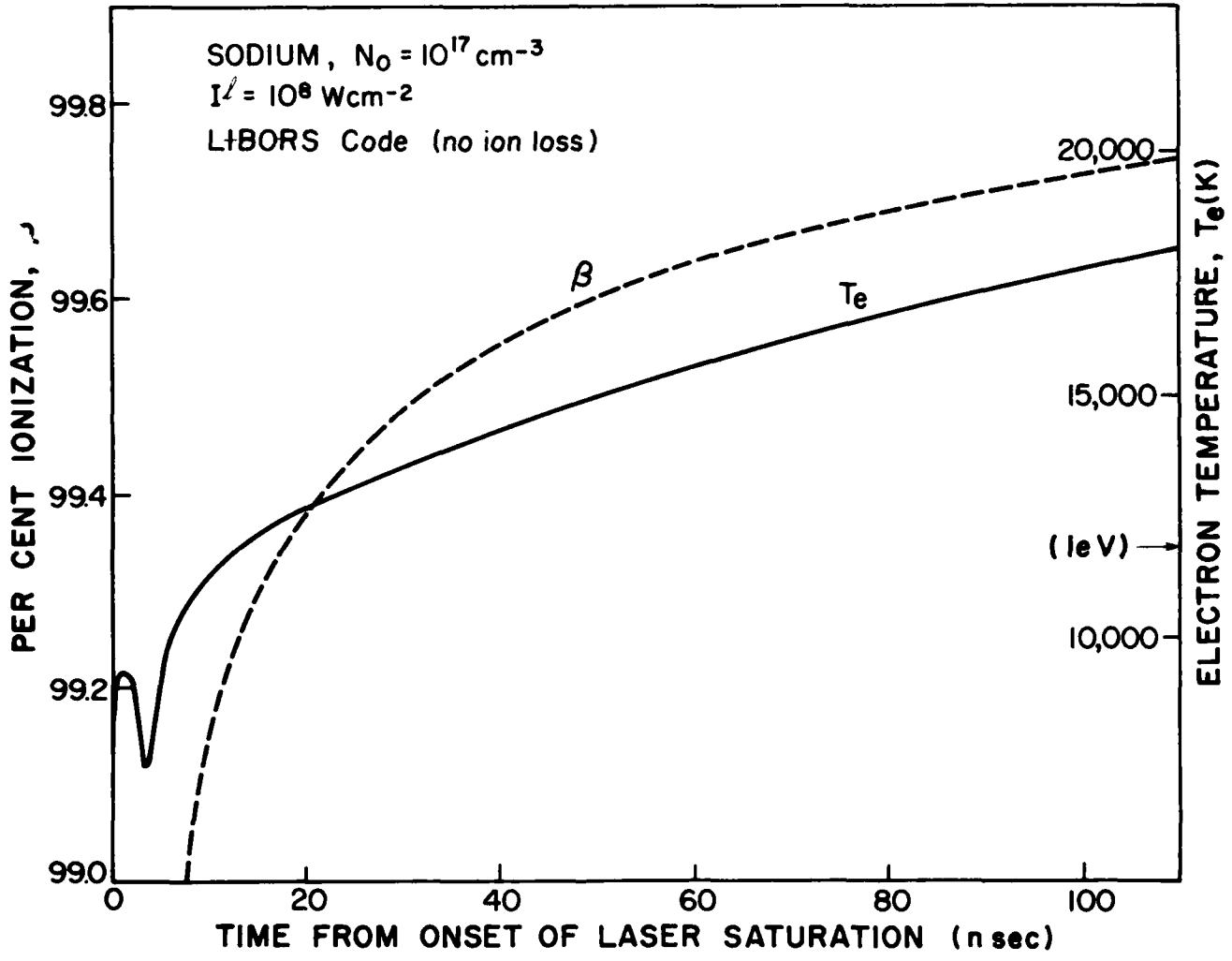
SODIUM, $N_0 = 10^{17}\,cm^{-3}$
$I^{\ell} = 10^{8}\,Wcm^{-2}$
LIBORS Code (no ion loss)
β
Te
99.8
99.6
99.4
99.2
99.0
PER CENT IONIZATION, β
20,000
15,000
(1eV)
10,000
ELECTRON TEMPERATURE, Te(K)
0
20
40
60
80
100
TIME FROM ONSET OF LASER SATURATION (n sec)

FIG. 16

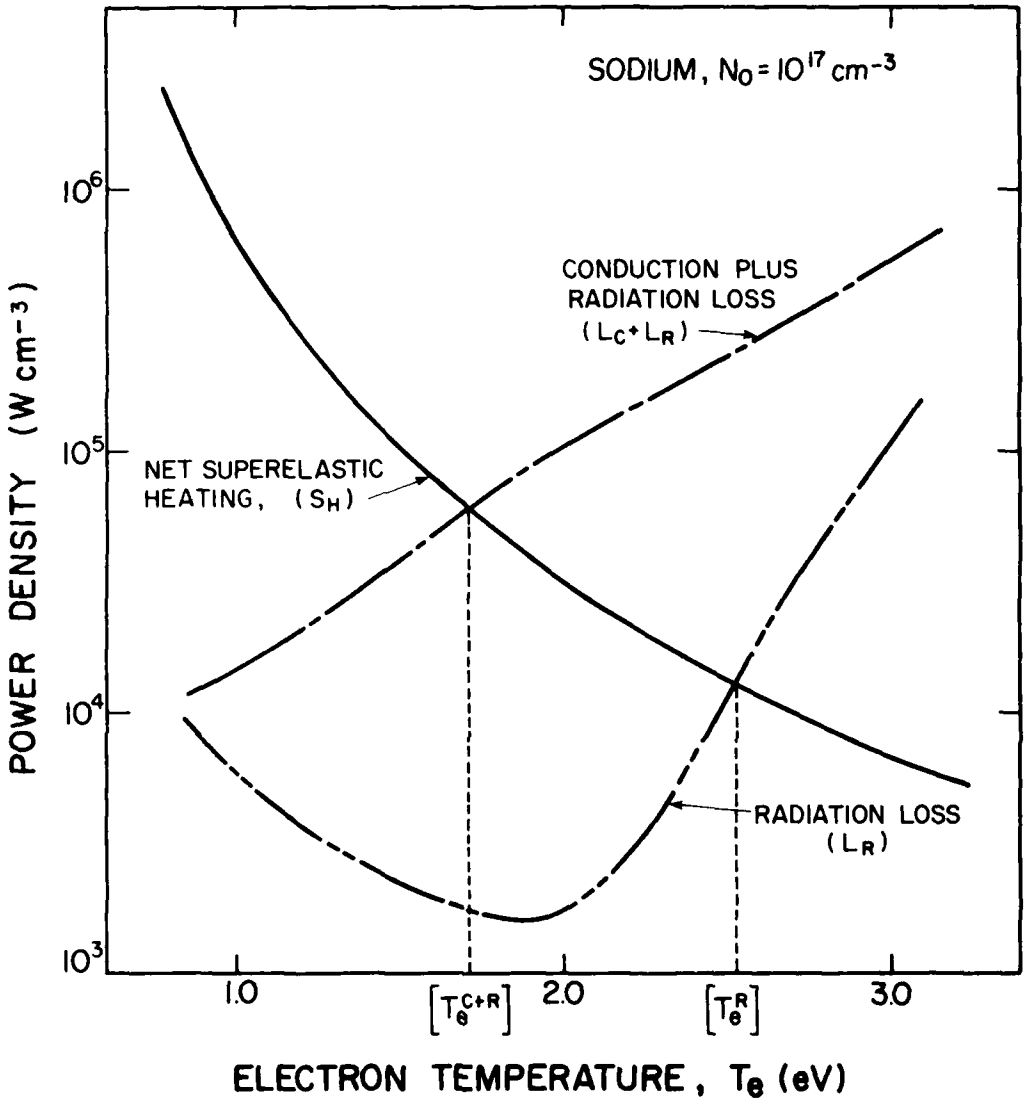
SODIUM, $N_0 = 10^{17}\ cm^{-3}$
CONDUCTION PLUS RADIATION LOSS ($L_C + L_R$)
NET SUPERELASTIC HEATING, (S_H)
RADIATION LOSS (L_R)
POWER DENSITY (W cm^{-3})
10^6
10^5
10^4
10^3
1.0
$[T_e^{C+R}]$
2.0
$[T_e^R]$
3.0
ELECTRON TEMPERATURE, T_e (eV)

FIG. 17

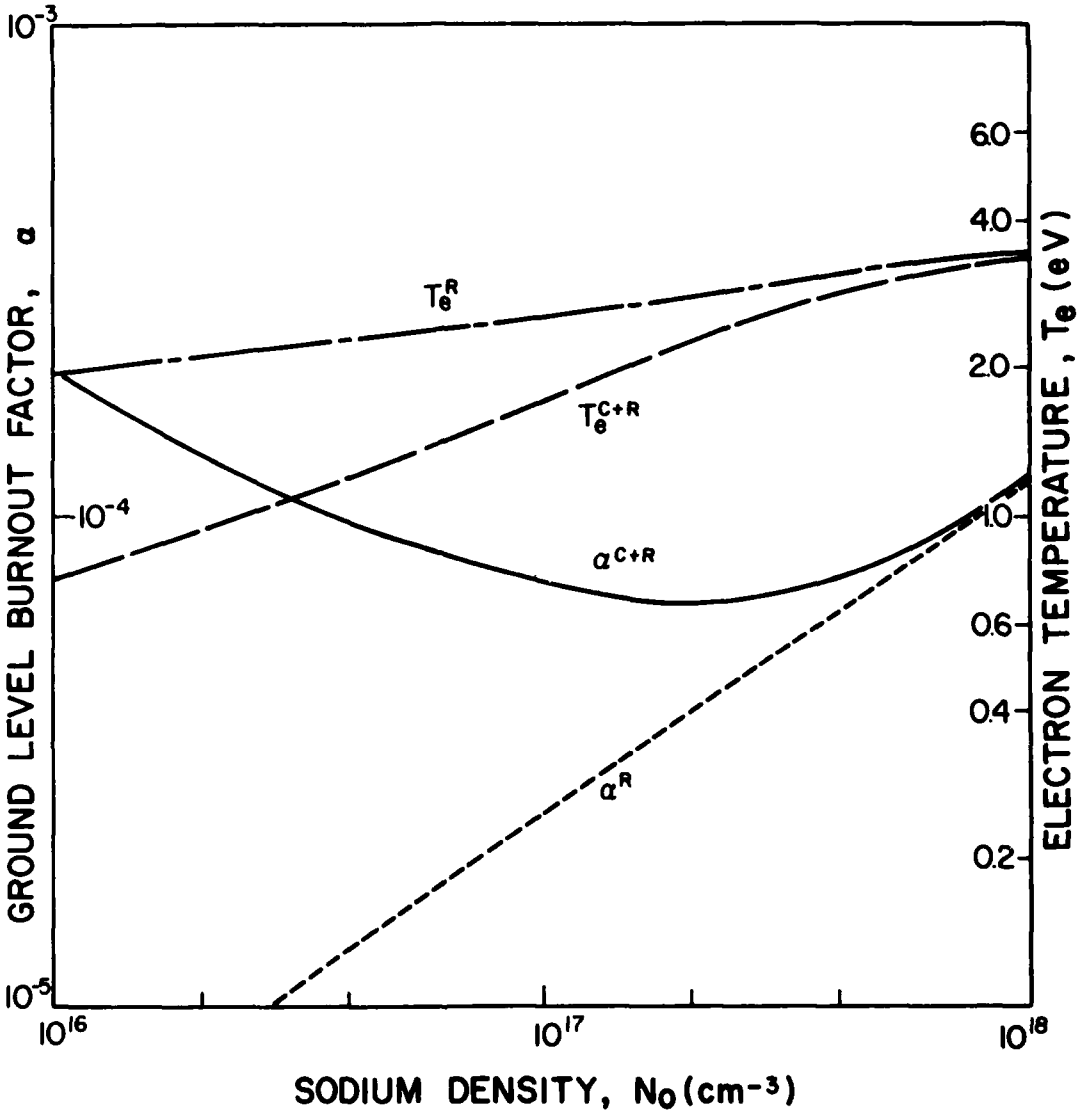
10^{-3}
10^{-4}
10^{-5}
GROUND LEVEL BURNOUT FACTOR, α
6.0
4.0
2.0
1.0
0.6
0.4
0.2
ELECTRON TEMPERATURE, T_e (eV)
T_e^R
T_e^{C+R}
α^{C+R}
α^R
10^{16}
10^{17}
10^{18}
SODIUM DENSITY, N_0 (cm^{-3})

FIG. 18

Appendix A

PHYSICAL REVIEW A VOLUME 24, NUMBER 1 JULY 1981

Ion–to–neutral-atom measurements within an ablation plasma through laser selective-excitation spectroscopy

M. R. Arnfield and R. M. Measures

Institute for Aerospace Studies, University of Toronto, 4925 Dufferin Street, Downsview, Ontario, M3H 5T6, Canada

(Received 29 December 1980; revised manuscript 9 March 1981)

A direct measurement of the ion–to–neutral-atom density ratio has been made in a rapidly expanding ablation plasma by means of laser selective-excitation spectroscopy. Evidence of an ionization freeze out at a degree of ionization of about 0.1% is presented.

INTRODUCTION

Laser selective-excitation spectroscopy (often referred to as laser saturation spectroscopy in the literature) involves momentarily locking the population of two atomic levels in the ratio of their degeneracies by an intense pulse of laser radiation, as first suggested by Measures.[1-3] The subsequent burst of *intensified spontaneous emission* from the overpopulated level represents a spectroscopic signal that is both spatially and temporally resolved. This powerful diagnostic technique has been used in a wide range of applications, that include (i) atomic lifetime measurements,[3-6] (ii) trace element analysis,[7,8] (iii) single-atom detection,[9-12] (iv) combustion and flame studies,[13-16] (v) neutral-hydrogen measurements in Tokamaks,[17,18] and (vi) fusion-plasma–impurity diagnostics.[19,20] A broad review of time-resolved laser-fluorescence spectroscopy has been written by Gauthier and Delpeck.[21]

Laser ablation of a solid is central to many diverse areas of endeavour including laser fusion,[22] x-ray–laser development,[23-25] trace-element analysis,[7,8,27] ion-beam generation,[28] and laser sputtering.[29] In addition, some interest has recently been shown in using laser vaporization of thin metal films for chemical kinetic studies.[29,30] Although there have been several investigations of the ablated material, some concerned with the electrons and ions,[31,32] others with the neutrals,[33,34] these measurements were either spatially or temporally integrated.

In the present paper we demonstrate that laser selective-excitation spectroscopy can provide a direct means of evaluating, with spatial and temporal resolution, the density ratio of two consecutive stages of ionization in a rapidly expanding ablation plasma. This diagnostic approach uses two short pulse, appropriately tuned lasers to produce a burst of *intensified spontaneous emission* (ISE) on one resonance line from each of the two stages of ionization of the species of interest.

THEORETICAL BASIS OF MEASUREMENTS

In accordance with the basic ideas of *selective-excitation spectroscopy*[1] the resonance–to–ground-level population ratio, for an ensemble of atoms excited by a steplike pulse of laser radiation tuned to the resonance transition, approaches the corresponding degeneracy ratio (equivalent to an effective infinite-temperature distribution) once the rate of stimulated emission plus absorption dominates the decay rate of the resonance level (in the absence of laser radiation). This requirement for *saturation of the transition* can be expressed in the form

$$(1+g)R_{21} \gg 1/\tau_2 , \tag{1}$$

where the rate of stimulated emission

$$R_{21} = B_{21} \int I^{l}(\nu)\mathfrak{L}_{21}(\nu)d\nu/4\pi , \tag{2}$$

$I^{l}(\nu)$ is the laser spectral irradiance, $\mathfrak{L}_{21}(\nu)$ is the resonance transition profile function, B_{21} is the Milne stimulated emission coefficient for the resonance transition, g is the ratio of the resonance to ground level degeneracies, and τ_2 is the resonance level lifetime in the absence of laser radiation.

In the case of broad-band laser radiation, this criterion for saturation can be expressed in the form

$$I^{l}(\nu) \gg I_s , \tag{3}$$

where the *saturated spectral irradiance*

$$I_s = \frac{8\pi h\nu^3}{c^2(1+g)}\left(\frac{\tau_2^{\mathrm{rad}}}{\tau_2}\right). \tag{4}$$

Here, h is Planck's constant, ν is the laser (i.e., resonance transition) frequency, c is the velocity of light, and τ_2^{rad} is the radiative lifetime of the resonance transition.

For a steplike laser pulse the resonance–to–ground-level population ratio N_2/N_1 approaches the degeneracy ratio g with an exponential time constant[1]

$$\tau_s = [(1+g)R_{21}]^{-1}. \tag{5}$$

Consequently, saturation is only achieved if the laser pulse duration $\tau^l \gg \tau_s$. For an experimental broad-band fast-rising laser pulse, saturation can be expected if: (i) the half-maximum duration of the laser pulse $\tau^l_{1/2} \gg \tau^p_s$, where

$$\tau^p_s = [(1+g)R^p_{21}]^{-1} \tag{6}$$

and R^p_{21} is the peak stimulated emission rate; and (ii) the peak laser irradiance $I^l_p \gg I_s \Delta\nu^l$, where $\Delta\nu^l$ is the laser bandwidth. Saturation of the resonance transition implies that $N_2 = GN_0$, where $G \equiv g/(1+g)$ and N_0 is the original (prior to laser irradiation) ground-level atom density, provided the laser pulse duration does not exceed the time for collisional excitation or multiphoton ionization of the resonance population. Recent theoretical[35] and experimental work[36] has clearly demonstrated that laser saturation of a resonance transition for an extended period can lead to appreciable perturbation (ionization) of the laser pumped species.

Under conditions of momentary laser saturation of an atomic resonance transition the peak intensified spontaneous-emission signal is directly proportional to the ground-state population of the laser irradiation N_0, viz.,

$$S_p = GN_0 A_{21} V \frac{\Delta\Omega}{4\pi} D, \tag{7}$$

where S_p represents the peak in the ISE signal obtained from the photodetector, A_{21} represents the Einstein transition probability of the observed transition, V represents the volume of excitation that is viewed by the receiving optics of the photodetector, $\Delta\Omega$ represents the acceptance solid angle of the receiving optics, and D represents the photodetector and receiving optics spectral sensitivity factor. This includes factors such as the spectral transmission factor for the receiving optics and monochromator, the photocathode quantum efficiency at the wavelength of the observed ISE, and the electronic gain of the dynode chain of the photomultiplier.

When two lasers are used to momentarily saturate, a resonance transition in the first ionized state (II) and one in the neutral atom (I) of a given species, the corresponding ISE peak signal ratio

$$\frac{S^{II}_p}{S^{I}_p} = \frac{G^{II}N^{II}_0 A^{II}_{21} D^{II}}{G^{I}N^{I}_0 A^{I}_{21} D^{I}} \tag{8}$$

can be seen to be directly proportional to the ratio of the ion to the neutral density ratio of the species of interest. The degree of ionization of the species $\alpha \simeq N^{II}_0/(N^{I}_0 + N_e)$, but for $\alpha \leq 1\%$ we can see that $\alpha \simeq N^{II}_0/N^{I}_0$. Equation (8) is valid provided the laser beams excite a common volume and that the receiver optics is common to both photodetectors. In general, the other quantities on the right-hand side of Eq. (8) can be calculated from knowledge of the transitions or evaluated by calibration, providing radiation trapping is negligible for both ISE signals.

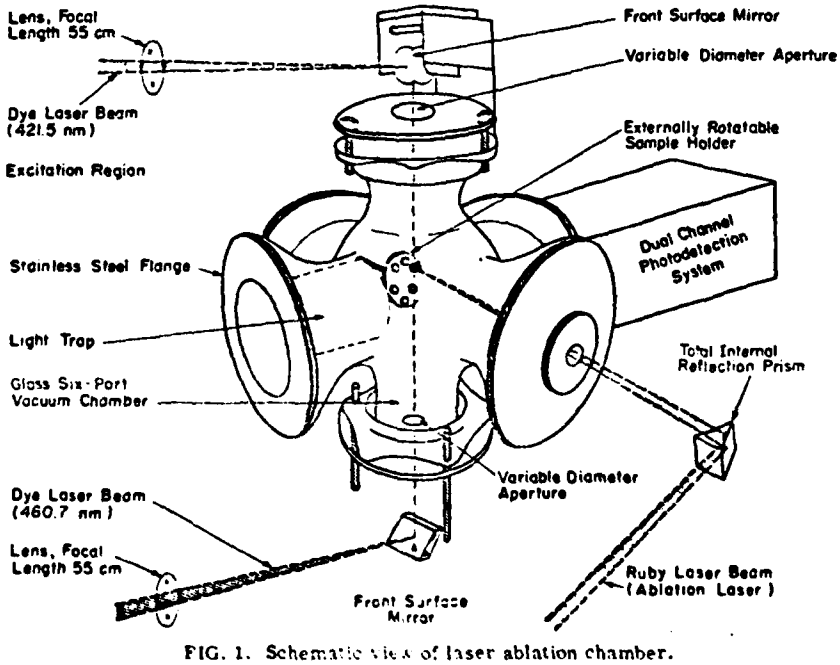

FIG. 1. Schematic view of laser ablation chamber.

EXPERIMENTAL FACILITY AND MEASUREMENTS

Our facility for undertaking these measurements comprise two nitrogen-laser–pumped dye lasers of the Hansch design[37] (excluding the etalon), a dual-wavelength photodetection system, and a low-pressure ablation chamber that has six optical ports and a rotatable multisample target (see Fig. 1) that allows us to change the target during an experiment without breaking the system's vacuum. A Q-switched ruby laser is used to create the ablation plasma. An RCA 8575 PMT and a SPEX 1700 monochromator are used in one channel, while an RCA 4526 PMT and a Jobin-Yvon H20 monochromator are used in the other channel. The background pressure in the chamber during the experiments was less than 10^{-4} torr.

Strontium was selected for this work since both the neutral and singly ionized form possesses resonance line wavelengths that conveniently fell within the operating range of our dye lasers. An example of the two intensified spontaneous emission signals generated about 1 cm out from the target surface and about 1 μsec from the moment of ablation is presented as Fig. 2. The upper trace corresponds to the ISE signal from the strontium atoms at 460.7 nm corresponding to Sr I ($^1P_1 - {}^1S_0$) while the lower trace corresponds to the ISE signal from the strontium ions at 421.6 nm corresponding to Sr II ($^2P_{1/2} - {}^2S_{1/2}$). The first pulse (not clearly seen) on the lower trace arises from a photodiode that monitors one of the dye lasers.

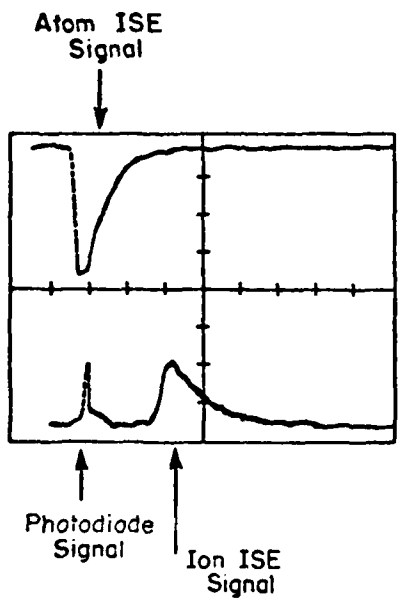

FIG. 2. Laser-intensified spontaneous-emission signals arising from an ablation plasma (1.2 μsec after ablation). The upper trace corresponds to the ISE signal from strontium atoms (at 460.7 nm) while the lower trace corresponds to the ISE signal from strontium ions (at 421.6 nm). The first pulse on the lower trace arises from a photodiode that monitors one of the dye lasers. Time scales are 20 nsec/division.

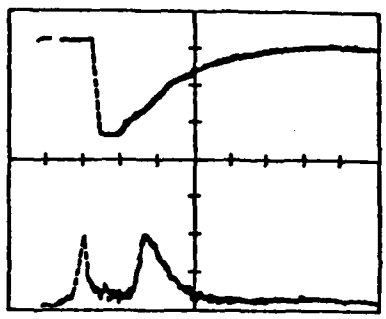

FIG. 3. Laser-intensified spontaneous-emission signals arising from an ablation plasma (1.2 μsec after ablation). The upper trace corresponds to the ISE signal from strontium atoms (at 460.7 nm) while the lower trace corresponds to the ISE signal from strontium ions (at 421.6 nm). The first pulse on the lower trace arises from a photodiode that monitors one of the dye lasers. Time scales are 20 nsec/division. N.B. The longer decay of the atom ISE signal relative to Fig. 2 arises from radiation trapping as density of strontium is higher in this experiment.

In our preliminary experiments radiation trapping of the atom ISE signal was quite apparent since the radiative lifetime of the $^1P_1$ level of Sr I was known[38,39] to be about 5 nsec which was close to an order of magnitude smaller than the observed decay time for the 460.7-nm ISE signal as seen in Fig. 3. In order to eliminate the problem of radiation trapping, the strontium doping of the target material was reduced from 10% to below 1%. This had the unfortunate effect of also reducing the already weak ion ISE signal. To compensate for this the diameter of the 421.5-nm laser beam was increased from 0.25 to 0.8 mm, an effective increase in the excitation volume of close to a factor of 10. (The PMT used on the ion ISE signal was also changed from a degraded RCA 31034 to a new RCA 8575.) A comparison of Fig. 3 with Fig. 2 clearly reveals the elimination of radiation trapping on the atom 460.7-nm ISE signal in the latter work (Fig. 2). The residual difference between the observed decay time and the known radiative lifetime can be accounted for in terms of the finite duration of the laser pulse (about 5 nsec) and the combined temporal response time of the RCA 4526 PMT and the Tektronix 8744 oscilloscope.

The temporal variation in the degree of ionization of the strontium in the ablation plasma (at

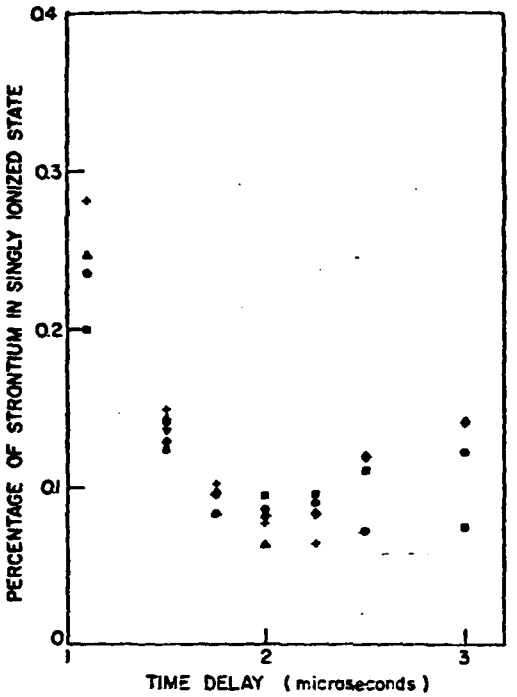

FIG. 4. The percentage of singly ionized strontium (to neutral strontium) as a function of time from the moment of ablation and at about 1 cm from the target as evaluated from the ratio of peak ISE signals from SR II and Sr I.

about 1 cm from the target surface) as determined from the ion to neutral ISE signal ratio is presented as Fig. 4. The lower limit of the time scale (about 1 μsec) was determined by the fixed delay in firing the nitrogen laser with respect to a photodiode signal from the ruby laser pulse. The upper limit was given by the weakness of the ion ISE signal. The relationship between the ISE peak signal ratio S_p^{II}/S_p^{I} and the ion to neutral density ratio (prior to laser irradiation) is given in our experiments by the expression

$$\frac{N_0^{II}}{N_0^{I}} = 2.3\times10^{-3}\frac{S_p^{II}}{S_p^{I}}. \qquad (9)$$

In the case of our experiments, the saturated spectral irradiance equation (4) is estimated to be about 10^{-9} W cm^{-2} Hz^{-1} for each of the transitions (assuming negligible collision quenching), while the laser bandwidth is close to 7×10^{10} Hz. Consequently, saturation requires that the peak laser irradiance greatly exceeds 70 W cm^{-2}. Indeed, since the duration of the laser pulses was only 5 nsec, we would expect that a peak laser irradiance of closer to 10^3 W cm^{-2} is probably required to ensure that saturation is achieved within the period of laser excitation.

Unfortunately, the dye-laser power available to us was limited (by the output of the N_2 laser) and it was found that when the ion-dye-laser area was increased it led to only marginal saturation. The consequences of this were that the ion ISE signal had a stronger dependence on the laser irradiance than it would if true saturation occurred. Thus not only did the ion ISE signal vary as a result of the shot-to-shot irreproducibility of the dye laser, it was also vulnerable to some extent to the further shot-to-shot variation associated with attenuation of the dye-laser pulse in propagating through the ablation plasma. These effects contributed to the spread in the data presented in Fig. 4. An additional source of shot-to-shot variation was structure in the expanding plasma.

Previous work on this facility[7] has revealed that laser scattering from ablation generated particulates should not constitute a source of signal in these experiments due to the judicious choice of the space-time window of observation. It is quite clear that if a more powerful N_2 laser were available and a few other improvements made on our facility (such as better collection optics and better photomultipliers) substantial improvements in accuracy could be achieved. Nevertheless, it is apparent from our measurements that *ionization freeze-out*[31] occurs in our system at about 0.1% ionization in strontium. This represents the first such measurement of its kind and constitutes a reasonable *proof of principle* that laser selective-excitation spectroscopy can be applied to such transient ionization measurements. If the more powerful N_2 laser could also be fired closer in time to the moment of ablation a more comprehensive time history should be attainable.

This work was supported by US/AFOSR under Grant No. 80-0057 and the Natural Science and Engineering Research Council of Canada.

[1]R. M. Measures, J. Appl. Phys. 39, 5232 (1965).
[2]R. M. Measures, Phys. Fluids 13, 1889 (1970).
[3]R. M. Measures and A. B. Rodrigo, Appl. Phys. Lett. 20, 102 (1972).
[4]R. M. Measures, N. Drewell, and H. S. Kwong, Phys. Rev. A 16, 1093 (1977).
[5]H. S. Kwong and R. M. Measures, Appl. Opt. 19, 1025 (1980).
[6]W. Gornik, D. Kaiser, W. Lange, H. H. Radloff, and H. Schulz, Appl. Phys. 1, 265 (1973).
[7]R. M. Measures and H. S. Kwong, Appl. Opt. 18, 281 (1979).

[8]H. S. Kwong and R. M. Measures, Anal. Chem. 51, 428 (1979).
[9]V. I. Balykin, V. S. Letokhov, V. I. Mishin, and V. A. Semchishen, Zh. Eksp. Teor. Fiz. Pis'ma Red 26, 492 (1977) [JETP Lett. 26, 357 (1977)].
[10]G. S. Hurst, M. G. Payne, S. D. Kramer, and J. P. Young, Rev. Mod. Phys. 51, 167 (1979).
[11]J. A. Gelbwachs, C. F. Klein, and J. E. Wassel, Appl. Phys. Lett. 30, 489 (1977).
[12]J. A. Gelbwachs, C. F. Klein, and J. E. Wassel, IEEE I. Quantum Electron QE-14, 121 1978.
[13]J. W. Daily, Appl. Opt. 16, 568 (1977); 17, 1610 (1978).
[14]R. P. Lucht and N. M. Lauendeau, Appl. Opt. 18, 856 (1979).
[15]J. W. Hosch and E. H. Piepmeier, Appl. Spectrosc. 32, 444 (1978).
[16]*Analytical Laser Spectroscopy* edited by N. Omenetto (Wiley, New York, 1979).
[17]D. W. Koopman, T. J. McIlrath, and V. P. Myerscough, J. Quant. Spectrosc. Radiat. Transfer 19, 555 (1978).
[18]R. Hess and F. Burrell, J. Quant. Spectrosc. Radiat. Transfer 21, 23 (1979).
[19]K. G. Muller and M. Stania, J. Appl. Phys. 49, 5501 (1978).
[20]C. H. Muller III and K. H. Burrell, Bull. Am. Phys. Soc. 25, 977 (1980).
[21]J. C. Gauthier and J F. Delpech, Advances Electron. Electron Phys. 46, 131 (1978).
[22]H. Motz, *The Physics of Laser Fusion* (Academic, New York, 1979).
[23]L. I. Gudzenko and L. A. Shelepin, Zh. Eksp. Teor. Fiz. 45, 1445 (1963) [Sov. Phys.—JETP 18, 998 (1964)].
[24]J. M. Geen and W. T. Silfvast, Appl. Phys. Lett. 28, 253 (1976).
[25]R. W. Waynant and R. C. Elton, Proc. IEEE 64, 1059 (1976).
[26]W. W. Jones and A. W. Ali, Appl. Phys. Lett. 26, 450 (1975).
[27]K. Laqua, *Analytical Laser Spectroscopy*, edited by N. Omenetto (Wiley, New York, 1979), Chap. 2.
[28]R. H. Hughes, R. J. Anderson, C. K. Manka, M. R. Carruth, L. G. Gray, and J. P. Rosenfeld, J. Appl. Phys. 51, 4088 (1980).
[29]B. G. Wicks, S. P. Tang, and J. F. Friichtenicht, Laser Focus 70, 1979.
[30]J. F. Friichtenicht, Rev. Sci. Instrum. 45, 51 (1974).
[31]P. T. Rumsby and J. W. M. Paul, Plasma Phys. 16, 247 (1974).
[32]A. Raven and O. Willi, Phys. Rev. Lett. 43, 278 (1979).
[33]A. T. Prengel, J. Dehaven, E. J. Johnson, and P. Davidevits, J. Appl. Phys. 48, 3551 (1977).
[34]J. R. Greig and R. E. Pechacek, J. Appl. Phys. 48, 596 (1977).
[35]R. M. Measures and P. G. Cardinal, Phys. Rev. A 23, 804 (1981).
[36]T. B. Lucatorto and T. J. McIlrath, Phys. Rev. Lett. 37, 428 (1976).
[37]T. W. Hansch, Appl. Opt. 11, 895 (1972).
[38]F. M. Kelly, T. K. Koh, and M. S. Mathur, Can. J. Phys. 52, 795 (1974).
[39]N. M. Erdevdi and L. L. Shimon, Opt. Spectrosc. 40, 443 (1976).

Appendix B

PHYSICAL REVIEW A VOLUME 23, NUMBER 2 FEBRUARY 1981

Laser ionization based on resonance saturation—a simple model description

R. M. Measures and P. G. Cardinal
Institute for Aerospace Studies, University of Toronto, 4925 Dufferin Street, Downsview, Ontario M3H 5T6, Canada
(Received 21 March 1980)

We have developed a simple physical model of *laser ionization based on resonance saturation* that involves the most important collisional and radiative interactions, yet lends itself to analytical solutions that enable the time history of the free electron density to be evaluated. We have been able to demonstrate that in the case of sodium the predictions of this simple model are within 15% of the values calculated by our extensive LIBORS computer code. The model has also been used to estimate the ionization time for each of the alkali metals over a wide range of conditions. These results are found to be consistent with several experimental observations.

INTRODUCTION

Laser-induced ionization is of considerable interest both from the standpoint of understanding the mechanisms involved and from attempts to exploit these interactions in a diverse range of applications. During the last few years there has grown a considerable body of experimental evidence to indicate that intense illumination of a resonance transition of an atomic vapor in the density range (10^{13}–10^{17} cm^{-3}) leads to substantial excitation and ionization.[1–8] Indeed, the degree of ionization achieved has been found to approach 100% if the duration of the laser pulse greatly exceeds the lifetime of the resonance state.[1–3]

Although at low densities (below 10^{13} cm^{-3}) multiphoton processes tend to dominate the ionization, for densities above 10^{13} cm^{-3} collisional effects start to play an important role and significant levels of excitation and ionization can be achieved for quite low values of laser irradiance.[6–8] Lucatorto and McIlrath[1,2] were the first to demonstrate that if laser radiation of relatively modest power density (~10^{6} W cm^{-2}) were tuned to the resonance line of an alkali metal vapor (density 10^{15}–10^{16} cm^{-3}), almost complete ionization resulted in a remarkably short period—far shorter than could be accounted for in terms of any multiphoton or atom-atom collisional process.[9] The validity of these results has been substantiated by similar experimental work of Skinner[3] and *Young et al.*[4] The explanation for this efficient and rapid new method of ionization can be found in a much earlier paper devoted to laser enhancement of ionization for MHD power generation.[10] In that paper one of the present authors had proposed that under conditions of laser saturation of a resonance transition, the energy of any free electrons would be rapidly increased by superelastic collision quenching of the overpopulated resonance level. Subsequently, the rate of ionization would be dramatically enhanced, not only as a result of the increased electron temperature, but also by virtue of the fact that the laser-maintained resonance-state population constitutes a substantial pool of atoms (roughly $\frac{1}{2}$) having an ionization energy that is reduced by the laser-photon energy.

In experiments where there is essentially no initial ionization, multiphoton ionization,[9,11] laser-induced Penning ionization,[4] or associative ionization[12] could liberate the "seed" electrons required for the above mechanism. Although associative ionization has been found to have very large cross sections for high-lying Rydberg states,[13] an effective value of around 10^{-17} cm^2 seems to be more appropriate[12,14] for alkali resonance transitions. In spite of this small cross section, Cardinal[15] has shown that associative ionization would dominate the initial-rate of ionization in the experimental work with sodium of Lucatorto and McIlrath.[1,2]

We have developed a fairly comprehensive code for studying laser ionization based on resonance saturation (LIBORS). This code treats the laser-excited atom as a 20-energy-level system and solves the subsequent set of energy and population rate equations by a fourth-order Runge-Kutta technique. A detailed description of the code is presented elsewhere[15–18] and will not be repeated here. It will suffice to mention that the code evaluates the temporal behavior of (i) each of the 20-atomic-level populations, (ii) the free electron density, (iii) the free electron temperature, (iv) the ion and neutral temperatures, (v) the laser power absorbed per unit volume, and (vi) the power radiated per second per unit volume as a result of radiative recombination to the resonance level, assuming a steplike laser pulse.

The results of our computer simulations for sodium are consistent with the experimental observations of Lucatorto and McIlrath[1] and suggest that LIBORS might be ideal for creating the plasma guide channels that are deemed to be

necessary for transportation of electron or ion beams to the fuel pellet of future particle-beam fusion reactors.[17] We have also shown that the concepts of *superelastic laser-energy conversion* (SELEC) could, under certain conditions, have several advantages over inverse bremsstrahlung as a means of coupling laser energy into a plasma or an un-ionized gaseous medium. In the event that SELEC is applied to a strong transition within a suitable ionic species, extremely rapid rates of plasma heating can be achieved[19]—a feature that is quite conducive to the development of short-wavelength lasers. Indeed, in the case of a boron III plasma, we predict[19] that a heating rate in excess of 10^{13} K sec^{-1} could be attained with a laser irradiance of close to 10^8 W cm^{-2}.

The purpose of the present paper is to reveal a relatively simple physical model of LIBORS that lends itself to an analytical expression for the temporal growth of ionization, yet retains almost all of the important interactions. This model allows us to predict the ionization time under a wide range of conditions and is very helpful in providing a physical interpretation of the more comprehensive LIBORS code results. Of particular significance is the fact that this simple model enables us to quickly and inexpensively extend our ionization time estimates to other elements. Several examples are provided which are found to be consistent with experimental observations. In the case of solium our simple-model ionization-time predictions have been found to agree to within 15% of our full LIBORS code results.

In passing, we feel obliged to comment on the term saturation, as used in the above context. Recently, some confusion has been displayed in the literature[20-22] regarding the attainment and meaning of saturation. In particular, several workers have suggested that their experiments have failed to demonstrate saturation of the laser-induced fluorescence (or intensified spontaneous emission) even at high values of laser irradiance. In the context of the present paper, saturation is taken to mean that the resonance to ground-level population densities are locked in the ratio of their degeneracies by the laser fields. This concept was first enunciated by Measures.[23] Recently, Salter *et al.*[24] have demonstrated that this condition can in fact apply, even though the laser-induced fluorescence fails to saturate at the corresponding laser irradiance. Salter[22] has attributed this failure to observe saturation to radiation trapping. However, Rodrigo and Measures[25] and Daily[26] have provided an alternative explanation of this effect in terms of the laser beam's radial profile and the spatially averaged signal. Some combination of these mechanisms might in fact be needed to adequately account for this anomalous observation.

LIBORS SIMPLE-MODEL FORMULATION

We shall consider the case of a homogeneous, single-constituent, atomic gaseous medium suddenly irradiated with an intense pulse of laser radiation that is tuned to one of the electronic resonance transitions. Although the interaction of this radiation field with the atoms is most accurately treated through use of the density-matrix approach, a rate equation analysis is reasonably reliable[27] if the bandwidth of the laser radiation is large compared to the Rabi frequency $|\Omega_r|$. In the case of a strong transition, $|\Omega_r| \approx 10^8\sqrt{I}$ rad sec^{-1}, where I W cm^{-2} is the frequency-averaged laser irradiance, and a rate equation analysis will be reasonable for most laser-ionization experiments (where the typical laser line width $\gtrsim$0.05 nm) up to a laser irradiance of about 10^8 W cm^{-2}.

Rapid collisional dephasing also improves the reliability of the rate equation analysis. Under conditions of resonance collisional broadening, the dephasing time can be less than, or of the order of, 1 nsec for the densities of interest according to McIlrath and Carlsten.[28]

The model we shall develop is particularly appropriate to atoms with low-lying resonance states, such as the alkali metals. For this class of atoms, $2E_{21} < E_{c1} \lesssim 3E_{21}$, where E_{21} represents the energy difference between the ground and the laser-excited resonance state (and is consequently equal to the laser-photon energy $h\nu$) and E_{c1} represents the ionization energy of the ground state. If the laser radiation is assumed to be suddenly applied at $t = 0$, then the subsequent chain of events can be viewed as proceeding in the four stages indicated in Fig. 1.

According to Measures[23] the resonance to ground-state population densities are locked in the ratio of their degeneracies, *viz.*, $N_2/N_1 \approx g_2/g_1 \equiv g$, in a characteristic time $\tau_R \approx [(1+g)R_{21}]^{-1}$, provided $I^1(\nu) \gg I_s(\nu)$ in the case of broadband laser radiation. $R_{21}[\equiv B_{21}\int I^1(\nu)\mathfrak{L}(\nu)d\nu/4\pi]$ represents the stimulated emission-rate coefficient for the resonance transition. B_{21} represents the appropriate Milne coefficient and $\mathfrak{L}(\nu)$ the corresponding line-profile function. $I^1(\nu)$ represents the laser spectral irradiance and $I_s(\nu)$ is the saturated spectral irradiance, given by

$$I_s(\nu) = \frac{8\pi h\nu^3}{c^2(1+g)}\left(\frac{\tau_2^{\mathrm{RAD}}}{\tau_2}\right),$$

where $\tau_2^{\mathrm{RAD}}(\equiv A_{21}^{-1})$ and τ_2 is the resonance-state lifetime. A_{21} is the resonance transition Einstein

probability. Invariably, τ_R is very short (much less than 1 nsec for the typical laser fields under consideration) compared to any other process and we assign laser saturation to stage 1.

Once the large pool of resonance-state atoms is created, several kinds of interactions give rise to a linear growth of the free-electron density associated with stage 2. The most important of these are

(i) two-photon ionization of the resonance level:

$$A^* + 2h\nu \rightarrow A^+ + e + \mathrm{KE}\ ,$$

(ii) laser-induced Penning ionization:

$$A^* + A^* + h\nu \rightarrow A + A^+ + e + \mathrm{KE}\ ,$$

and

(iii) associative ionization:

$$A^* + A^* \rightarrow A_2^+ + e + \mathrm{KE}\ .$$

A^* represents a laser-excited resonance-state atom, A^+ the ionic species, and A a ground-state atom of the same species. A_2^+ represents the dimer ion. In the case of the alkali metals, Geltman,[9] de Jong and van der Valk,[12] and Klucharev *et al.*[14] have provided the relevant cross sections. The appropriate rate of ionization during stage 2 can be expressed in the form

$$\left.\frac{dN_e}{dt}\right|_{\text{stage 2}} \approx N_2\sigma_{2c}^{(2)}F^2 + \tfrac{1}{2}N_2^2\sigma_L v F + \tfrac{1}{2}N_2^2\sigma_A v\ , \qquad (1)$$

where $\sigma_{2c}^{(2)}$ (cm^4 sec) is the two-photon, resonance-state, ionization-rate coefficient, σ_L (cm^3 sec) is the laser-induced Penning ionization-rate coefficient, σ_A (cm^2) is the effective associative ionization cross section (allowing for the energy defect of the interaction[14]), v (cm sec^{-1}) is the mean atom velocity, and F (photons cm^{-2} sec^{-1}) represents the laser photon flux density, i.e., $F = \int I^1(\nu)d\nu/h\nu$.

The electrons created by these initial processes rapidly gain energy through superelastic collision quenching of the laser sustained resonance-state population, as first suggested by Measures.[10]

In stage 3, the free-electron temperature[29] is viewed as stabilizing as a result of a balance between the rate of superelastic heating and excitation cooling. This will be considered in more detail later. These electrons now give rise to an exponential growth in the free-electron density due to both direct collisional ionization of the resonance level and single photon-laser ionization of the collisionally populated intermediate levels.

Finally, in stage 4, runaway collisional ionization of the intermediate levels occurs once a critical electron density is achieved. This process leads to the ionization burnout that results in almost complete ionization of the laser pumped species. Our full LIBORS computer code[15-18] indicates that during this rapid burnout phase, superelastic

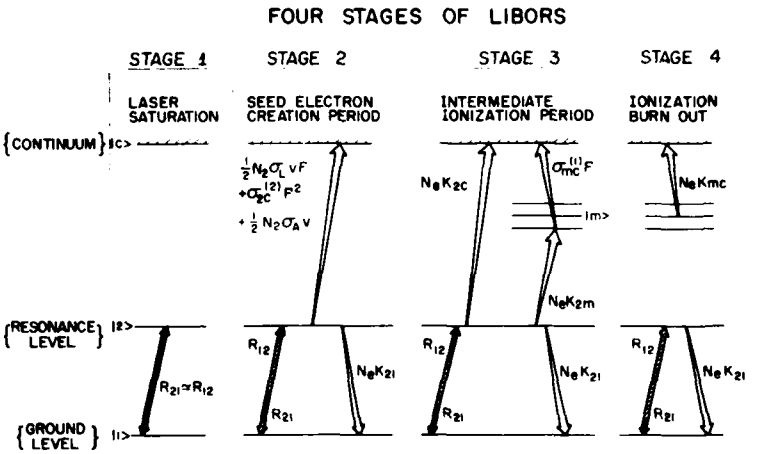

FIG. 1. Four stages of LIBORS. Stage 1: Laser rapidly locks ground and resonance-level populations in ratio of degeneracies. Stage 2: (i) Rapid growth of free electrons due to two-photon ionization of resonance level and laser-induced Penning ionization. Associative ionization is important for some elements. (ii) Free electrons rapidly gain energy through superelastic collisions. Stage 3: (i) Direct electron-impact ionization of resonance level and single-photon ionization of collisionally populated upper levels dominate the rate of ionization. (ii) Electron temperature stabilizes as the rate of superelastic heating balances rate of collisional cooling through excitation. Stage 4: (i) Runaway collisional ionization of upper levels occurs once a critical electron density is achieved. (ii) Superelastic heating can no longer balance collisional cooling and the electron temperature falls.

heating is unable to maintain the free-electron temperature and a sudden drop in the temperature is expected.

In order to obtain an analytical solution for the ionization time from our LIBORS simple model, we shall assume that the free-electron temperature stabilizes and remains constant throughout both stages 3 and 4. Some justification for this assumption can be found in the following argument. During the linear growth period (stage 2), the dominant ionization processes are independent of the free-electron temperature. This is fortunate because it is questionable whether the electron energy distribution could be characterized by a temperature during this period.[29]

The appropriate energy equation for the free electrons takes the form

$$\frac{d}{dt}(N_e\epsilon_e) = N_2N_eK_{21}E_{21} + (2E_{21} - E_{c2})N_2\sigma_{2c}^{(2)}F^2 + \sum_{m>m^*}(E_{21} - E_{cm})N_m\sigma_{mc}^{(1)}F$$
$$+ \tfrac{1}{2}(2E_{21} - E_{c2})N_2^2\sigma_L vF + \tfrac{1}{2}(2E_{21} - E_A)N_2^2\sigma_A v - N_e\sum_{m\geq 1}N_mK_{mc}E_{cm}$$
$$- N_eC - N_e^2H_{ei} - N_eN_aH_{ea} + N_e^3\sum_{m\geq 1}K_{cm}E_{cm} - N_e^2\epsilon_e\sum_{m\geq 1}\beta(m), \quad (2)$$

where $\epsilon_e(J)$ represents the mean translation energy of a free electron, K_{mn} ($cm^3\,sec^{-1}$) represents the rate coefficient for an electron collision induced transition from level m to n,[15] K_{mc} ($cm^3\,sec^{-1}$) represents the rate coefficient for an electron collision induced ionization transition from level m,[15] K_{cm} ($cm^6\,sec^{-1}$) represents the three-body recombination coefficient,[15] $\sigma_{mc}^{(2)}$ (cm^2) represents the single-photon ionization cross section[30] for level m, and the sum extends over all levels $m > m^*$ for which ionization by a single laser photon can be achieved, N_m (cm^{-3}) represents the number density of atoms in the m energy state, C represents the loss of energy per electron due to the net collisionally induced upward movement of bound electrons (exclusive of the resonance superelastic term)

$$C = \sum_{n\geq 1}\sum_{m>n}(N_nK_{nm} - N_mK_{mn})E_{mn} - N_2K_{21}E_{21}, \quad (3)$$

E_{mn} (J) represents the energy separation between levels m and n, E_{cn} (J) represents the ionization energy of level n, E_A (J) represents the energy required for the associative ionization of two laser-excited atoms, H_{ei} ($J\,cm^3\,sec^{-1}$) represents the rate of elastic energy transfer to ions through Coulomb scattering collisions,[17] N_a (cm^{-3}) represents the total neutral atom density, H_{ea} ($J\,cm^3\,sec^{-1}$) represents the rate of elastic energy coupling between the free electrons and the neutral atoms.[17] β ($cm^3\,sec^{-1}$) represents the rate of radiative recombination to level m. Equation (2) can be divided into two equations, one for the rate of growth of the free electron density

$$\tfrac{1}{2}kT_e\frac{dN_e}{dt} = \tfrac{3}{2}kT_e\left(N_2\sigma_{2c}^{(2)}F^2 + \tfrac{1}{2}N_2^2v(\sigma_A + \sigma_LF) + \sum_{m>m^*}N_m\sigma_{mc}^{(1)}F + N_e\sum_{m\geq 1}N_mK_{mc} - N_e^2\sum_{m\geq 1}[N_eK_{cm} + \beta(m)]\right), \quad (4)$$

where T_e (K) represents the free-electron temperature (*viz.*, $\epsilon_e = \frac{3}{2}kT_e$), and the other for the variation of the free-electron temperature,

$$N_e\frac{d}{dt}(\tfrac{3}{2}kT_e) = N_eN_2K_{21}E_{21} + (2E_{21} - E_{c2} - \tfrac{3}{2}kT_e)(N_2\sigma_{2c}^{(2)}F^2 + \tfrac{1}{2}N_2^2\sigma_L vF)$$
$$+ \tfrac{1}{2}(2E_{21} - E_A - \tfrac{3}{2}kT_e)N_2^2\sigma_A v + N_e^3\sum_{m\geq 1}K_{cm}(E_{cm} + \tfrac{3}{2}kT_e)$$
$$- N_e\sum_{m\geq 1}N_mK_{mc}(E_{cm} + \tfrac{3}{2}kT_e) + \sum_{m>m^*}(E_{21} - E_{cm} - \tfrac{3}{2}kT_e)N_m\sigma_{mc}^{(1)}F - N_eC - N_e^2H_{ei} - N_eN_aH_{ea}. \quad (5)$$

Considerable simplification of these equations can be achieved if we restrict our time of interest to the interval for which the degree of ionization is less than a few percent. This will incur only a small loss of accuracy in predicting the ionization time as the ionization proceeds from a few percent to almost total ionization in a very small fraction of the total time for full ionization, due to the very fast rate of ionization achieved in stage 4—the runaway region—a result confirmed

by our LIBORS code which does not make these simplifications.

Under these conditions we can write for the alkali metal vapors, where $2E_{21} \lesssim E_{c1} \lesssim 3E_{21}$, the rate of ionization in the form

$$\frac{dN_e}{dt} \simeq N_2[\sigma_{2c}^{(2)}F^2 + \tfrac{1}{2}N_2F(\sigma_A + \sigma_L F) + N_e K_{2c}] + \sum_{m>3} N_m(\sigma_{mc}^{(1)}F + N_e K_{mc}). \quad (6)$$

The first term on the right-hand side of Eq. (5) represents the superelastic heating rate and it is possible to show that for times $\gtrsim \Delta E/(N_2 K_{21} E_{21})$, where $\Delta E \simeq 2E_{21} - E_{c2} - \frac{3}{2}kT_e$, this superelastic heating term will dominate the heating terms associated with the seed creation processes. For the alkali metals, this characteristic time is very short compared to the ionization time (at 10^{17} cm^{-3}, it is typically less than about 1 nsec). The gain in energy due to single-photon ionization and the loss in energy from direct-impact ionization of the resonance level are also neglected in comparison to the superelastic heating and excitation cooling terms in Eq. (5). Under these circumstances the free-electron energy equation, during stage 3 can be reasonably well expressed in the form

$$\frac{d}{dt}(\tfrac{3}{2}kT_e) \simeq N_2 K_{21} E_{21} - N_1 K_{12} E_{21} - N_2 \sum_{m>2} K_{2m} E_{m2}. \quad (7)$$

The first term on the right-hand side of Eq. (7) represents the superelastic heating rate per electron, while the subsequent terms represent the cooling rate per electron associated with the dominant collisional excitation processes. The sum over m in the last term extends over the group of intermediate levels that are rapidly populated by *hot* electrons and depopulated by single-photon laser ionization.

Using electron collision-rate coefficients that are based upon Seaton cross sections,[11] Eq. (7) yields under conditions of laser saturation, a transcendental equation for the *steady-state superelastic temperature*,

$$T_e^s \simeq \frac{E_{32}\, k}{\ln(\exp(-\epsilon_1/kT_e^s) + g\, f_{12}/\sum_{m>2} f_{2m}\exp(-\epsilon_m/kT_e^s))}, \quad (8)$$

where $\epsilon_m = E_{m2} - E_{32}$ and $f_{1m} = f_{1m}\bar{G}_{1m}$. f_{1m} represents the absorption oscillator strength for the $1m$ transition and $\bar{G}_{1m}$ the relevant Gaunt factor averaged over a Maxwellian velocity distribution. This equation can be solved by an iterative procedure, or, in light of the logarithmic nature of the denominator and the fact that $E_{m2} \simeq E_{12}$ (in the model), it can be approximated by the expression

$$T_e^s \simeq \frac{E_{32}\, k}{\ln\left(1 + g\sum_{m>2} \frac{f_{2m}}{f_{12}}\right)}, \quad (9)$$

where we have also assumed $\bar{G}_{1m} \simeq 1$. This value of the free-electron temperature is then used to compute the various collision-rate coefficients.

The relevant intermediate-level population-rate equation can be expressed in the form

$$dN_m/dt = N_2 N_e K_{2m} - N_m(\sigma_{mc}^{(1)}F + A_m^{\dagger} + N_e K_{mc}), \quad (10)$$

where $A_m^{\dagger} = A_{ms}\Lambda_{ms}$ represents the radiation-trapped Einstein transition probability for the ms transition, s can correspond to either the ground or resonance level, Λ_{ms} is the Holstein escape factor,[12] and

$$K_{mc} = K_{mc} + \sum_{n\neq m} K_{mn}. \quad (11)$$

We have assumed that in light of the large population of the resonance-state atoms (due to laser saturation), $N_2 N_e K_{2m}$ will dominate any other rate of population of level m from other levels. This may not be strictly true for closely spaced adjacent levels, but such terms only serve to rapidly equilibrate the population within the manifold of intermediate states. If we introduce

$$P_m = \sigma_{mc}^{(1)}F \quad (12)$$

and set

$$\rho_m = P_m + A_m^{\dagger}, \quad (13)$$

then over a significant fraction of the ionization time

$$\rho_m \gg N_e K_{mc}. \quad (14)$$

Under these circumstances, Eq. (10) has a solution of the form

$$N_m(t) = N_2 K_{2m}\exp(-\rho_m t)\int^t N_e(t')\exp(\rho_m t')dt' \quad (15)$$

if the vapor is assumed to be unexcited prior to laser irradiation, i.e., $N_m(0) = 0$. F, N_2, and K_{2m} are also taken to be constant over the period of interest.

The constancy of N_2 over an appreciable fraction of the time to ionize is quite reasonable on the grounds that the upper levels ($m > 3$) only become significantly populated just prior to ionization burnburnout (stage 4). In fact, if we use the saturation condition, we can write $N_2 \simeq GN_0$, where $G = g(1+g)^{-1}$ and N_0 represents the initial atom density. The time independence of K_{2m} is based upon our previous assumption of a stabilized temperature

during the intermediate phase (stage 3) and F has been set to be constant by our assertion of a step-like laser pulse. The viability of these assumptions will become apparent later when we review the LIBORS computer-code results.

It is apparent that substitution of Eq. (15) into the ionization equation yields a polynomial expansion in N_e on the right-hand side of Eq. (6). At the earliest times from the moment of laser saturation, i.e., stage 2, the free-electron-density growth rate is expected to be independent of N_e, while an exponential growth is to be expected during the subsequent period, stage 3. This suggests that a first approximation to the free-electron density can be expressed in the form

$$N_e(t) \simeq N_{e0}[\exp(\beta t) - 1]. \tag{16}$$

This gives a linear growth for $\beta t \ll 1$ and an exponential growth for $\beta t \gtrsim 1$. N_{e0} can be taken to be the seed electron density for which N_e departs significantly from a linear growth.

Substituting Eq. (16) into Eq. (15) yields

$$N_m(t) = \frac{N_2 K_{2m} N_e(t)}{\beta + \rho_m}\left[1 - \frac{\beta}{\rho_m}\left(\frac{1 - \exp(-\rho_m t)}{\exp(\beta t) - 1}\right)\right]. \tag{17}$$

For times sufficiently great for relaxation of the intermediate-level populations, we obtain an approximation relation of the form

$$N_m(t) \simeq \frac{N_2 K_{2m} N_e(t)}{\beta + \rho_m}, \tag{18}$$

provided

$$t > (1/\beta)\ln(1 + \beta/\rho_m). \tag{19}$$

In many instances this is more restrictive a condition than necessary. Further discussion of this will be provided later. If Eq. (18) is used in Eq. (6) to eliminate N_m we arrive at a simple form of the ionization equation,

$$dN_e/dt = S + IN_e + BN_e^2, \tag{20}$$

where we have introduced

$$S \equiv N_2[\sigma_{2c}^{(2)}F^2 + \tfrac{1}{2}N_2 t(\sigma_A + \sigma_L F)] \tag{21}$$

as the seed-ionization rate,

$$I = N_2\left(K_{2c} + \sum_{m\geq 3}\frac{K_{2m}P_m}{(\beta + \rho_m)}\right) \tag{22}$$

as the intermediate ionization-rate coefficient, and

$$B = N_2 \sum_{m\geq 3}\frac{K_{2m}K_{mc}}{(\beta + \rho_m)} \tag{23}$$

as the burnout-ionization-rate coefficient.

We see that we can now define

$$N_e^{**} \equiv I/B \tag{24}$$

as the critical electron density at which the burnout rate of ionization equals the intermediate rate of ionization. In a like manner we can also define

$$N_e^{*} \equiv S/I \tag{25}$$

as the characteristic electron density for which the intermediate ionization rate equals the seed-ionization rate. It is apparent from a comparison of Eq. (16) with Eq. (20) that we can identify β with I and N_{e0} with N_e^*. In which case we can write

$$I = N_2\left(K_{2c} + \sum_{m\geq 3}\frac{K_{2m}P_m}{(I + \rho_m)}\right) \tag{26}$$

and

$$B = N_2 \sum_{m\geq 3}\frac{K_{2c}K_{mc}}{(I + \rho_m)}. \tag{27}$$

I can be evaluated in an iterative manner by substituting $\rho_m = \rho_{max} = \rho$ into Eq. (26) and obtaining a first approximation of the form

$$I \simeq \tfrac{1}{2}(\kappa - \rho) + \tfrac{1}{2}\left[(\kappa - \rho)^2 + 4\left(\kappa\rho + N_2\sum_{m\geq 3}K_{2m}P_m\right)\right]^{1/2}, \tag{28}$$

where $\kappa = N_2 K_{2c}$. If this first approximation is then reintroduced into the right-hand side of Eq. (26), we have found that in almost all cases I is within 1% of the correct (limiting) value.

The *simple-model* **LIBORS** ionization [Eq. (20)] has two forms of analytical solution depending upon the relative values of S, I, and B. If $I^2 < 4SB$, which is equivalent to $N_e^{**} < N_e^*$, then ionization proceeds directly from stage 2 to stage 4—that is to say, seed ionization leads directly to runaway ionization. The solution to Eq. (20) under these circumstances takes the form

$$t = \frac{2}{a}\left[\tan^{-1}\left(\frac{2BN_e + I}{a}\right) - \tan^{-1}\left(\frac{I}{a}\right)\right], \tag{29}$$

where

$$a \equiv (4SB - I^2)^{1/2} \tag{30}$$

This class of solution is indicative of a very high rate of seed ionization and we shall refer to this as an S3 solution.

If $I^2 > 4SB$, which is equivalent to $N_e^{**} > N_e^*$, stage 3 ionization will play some role in separating stage 2 from stage 4—that is to say intermediate ionization is significant in increasing the free-electron density to the point where runaway ionization occurs. The solution of the ionization Eq. (20) under these circumstances takes the form

$$t = \frac{1}{A}\ln\left[\left(\frac{N_e + R_1}{N_e + R_2}\right)\frac{R_2}{R_1}\right], \tag{31}$$

where

$$A \equiv (I^2 - 4SB)^{1/2}, \tag{32}$$

$$R_1 \equiv \left(\frac{I-A}{2B}\right), \tag{33}$$

$$R_2 \equiv \left(\frac{I+A}{2B}\right). \tag{34}$$

If, however, $I^2 \gg 4SB$ (i.e., $N_e^{**} \gg N_e^*$), then the intermediate processes play a major role in determining the ionization burnout time τ_B. We shall discriminate between solutions that arise when $100SB \gtrsim I^2 \gtrsim 4SB$ and those that apply when $I^2 > 100SB$, by designating the former as S2 solutions and the latter as S1 solutions.

The ionization burnout time for $I^2 > 4SB$ solutions takes the form

$$\tau_B \simeq \frac{1}{A} \ln\left[\left(\frac{N_0 + R_1}{N_0 + R_2}\right)\frac{R_2}{R_1}\right]. \tag{35}$$

However, for S1 solutions, where $I^2 > 100SB$ (or $N_e^{**} \gtrsim 100N_e^*$) we can approximate this by the expression

$$\tau_B \simeq \frac{1}{I} \ln\left(\frac{N_e^{**}}{N_e^*}\right). \tag{36}$$

This relation lends itself to the pictorial interpretation presented as Fig. 2.

For intermediate levels having zero single-photon ionization cross section at the laser wavelength, we have used the *minimum photoionization cross* section in Eq. (18) since collision coupling between adjacent levels plays a role, as stated earlier, in equilibrating adjacent levels. We have also found that in some instances, particularly *S3 solutions*, Eq. (18) grossly overestimates the intermediate-level populations at times corresponding to $\tau_B/3$, as seen from a comparison of N_m obtained by Eqs. (17) and (18). Under these circumstances we have assumed that the intermediate-level populations do not contribute to the intermediate ionization stage and reassign $I = N_2 K_{2c}$.

In the limit of $I^2 \ll 4SB$, the ionization burnout time

$$\tau_B \simeq \frac{\pi}{2\sqrt{SB}}. \tag{37}$$

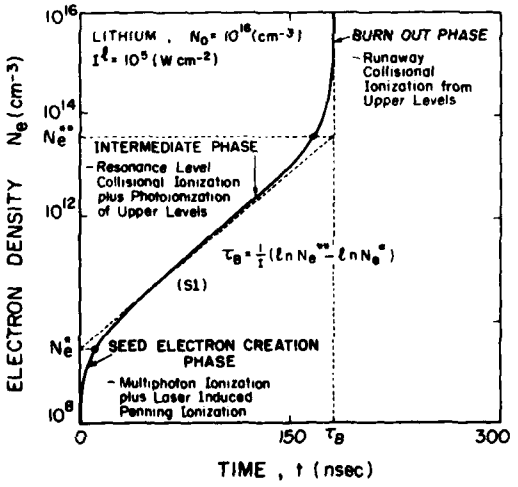

FIG. 2. The three distinct phases (stages 2 to 4 of Fig. 1) of laser ionization based on resonance saturation are indicated in this graph of electron density against time.

LIBORS SIMPLE-MODEL RESULTS FOR ALKALI METALS

In this section we present some representative results of the LIBORS simple-model calculations. The relevant cross sections and parameters required for this analysis are presented for each of the alkali metals in Table I. The type of solution obtained and the appropriate ionization burnout time for each element are also displayed under a wide range of densities and values of laser irradiance. A clear pattern is readily discernible. In the case of lithium all solutions are of the S1 type, which means that the intermediate processes are always important—at least for $10^{15} \lesssim N_0 \lesssim 10^{17}$ (cm^{-3}) and $10^5 \lesssim I \lesssim 10^6$ ($W\,cm^{-2}$) ranges under consideration. S1 solutions are interpreted to mean that the intermediate processes play a dominant role and this appears to be particularly true where associative ionization is absent. The predicted high value of T_e^s is also important.

S1 solutions are also found for sodium under most of these conditions. Reference to Table I shows that for sodium, T_e^s is slightly higher and σ_4 is slightly lower than for the remaining alkali metals (*viz.*, K, Rb, and Cs).

At the other end of the periodic table, cesium has predominantly S3 solutions. This is not surprising in light of the predicted low value of T_e^s and relatively high value of σ_4. It is also apparent that potassium and rubidium have S3 solutions at the highest laser powers. In the case of rubidium this can be understood in terms of the high cross sections for both two-photon resonance ionization and laser-induced Penning ionization.

A representative set of ionization curves is presented in Fig. 3. The original density was assumed to be 10^{15} (cm^{-3}) for each of the elements and the laser irradiance was taken as 10^{6} ($W\,cm^{-2}$). It is interesting to note that the predicted ionization burnout times for both lithium and sodium are shorter than for potassium and cesium, even though the seed-ionization rates for potassium and cesium are greater. This illustrates that a strong intermediate ionization process can compensate for a lower seed-ionization rate.

TABLE I. Basic parameters, ionization times, and types of LIBORS solutions for alkali metals.[a] S1: $I^2 > 100BS$, S2: $I^2 \geq 4BS$, and S3: $I^2 < 4BS$.

	Li	Na	K	Rb	Cs
E_{21} (eV)	1.85	2.10	1.62	1.58	1.43
T_e^s (K)	11 442	8433	7757	8036	4163
σ_A (cm^2)	0	3.26×10^{-18}	1.27×10^{-17}	1.22×10^{-17}	2.19×10^{-17}
(at $N_0 = 10^{16}$)					
σ_L (cm^4 sec)	9.1×10^{-44}	2.0×10^{-44}	1.2×10^{-43}	9.6×10^{-43}	4.5×10^{-42}
$\sigma_{2c}^{(2)}$ (cm^4 sec)	2.2×10^{-48}	1.7×10^{-49}	2.9×10^{-49}	7.7×10^{-48}	5.8×10^{-48}
$\sigma_{\max}^{(1)}$ (cm^2)	1.0×10^{-17}	2.9×10^{-18}	2.3×10^{-18}	8.2×10^{-19}	4.5×10^{-19}
A_{m2})[b] (sec^{-1})	3.5×10^{7}	2.4×10^{7}	2.9×10^{7}	9.8×10^{6}	9.8×10^{6}
$\langle K_{mc}\rangle$ (cm^3 sec^{-1})	2.5×10^{-7}	1.78×10^{-7}	1.5×10^{-7}	1.6×10^{-7}	3.4×10^{-8}
$\langle K_{2m}\rangle$ (cm^3 sec^{-1})	1.73×10^{-8}	3.62×10^{-8}	8.3×10^{-8}	1.26×10^{-7}	1.42×10^{-7}
N_0 (cm^{-3}) / I^l (W cm^{-2})	Ionization time, τ_B (nsec), and class of solution				
10^{15} / 10^5	1060 (S1)	837 (S1)	994 (S2)	976 (S2)	2740 (S3)
10^{15} / 10^6	479 (S1)	435 (S1)	905 (S2)	762 (S2)	1940 (S2)
10^{15} / 10^7	251 (S1)	204 (S1)	595 (S2)	222 (S3)	294 (S3)
10^{15} / 10^8	124 (S1)	93.0 (S1)	131 (S3)	27.2 (S3)	31.8 (S3)
10^{16} / 10^5	180 (S1)	124 (S1)	92.3 (S2)	87.3 (S2)	171 (S3)
10^{16} / 10^6	84.7 (S1)	80.3 (S1)	91.3 (S2)	81.4 (S2)	138 (S3)
10^{16} / 10^7	38.4 (S1)	41.3 (S1)	82.1 (S2)	44.4 (S3)	55.7 (S3)
10^{16} / 10^8	18.8 (S1)	17.0 (S1)	32.5 (S3)	8.04 (S3)	9.29 (S3)
10^{17} / 10^5	23.2 (S1)	13.9 (S2)	8.56 (S2)	7.63 (S2)	10.6 (S3)
10^{17} / 10^6	13.6 (S1)	11.8 (S2)	8.46 (S2)	7.30 (S2)	9.42 (S3)
10^{17} / 10^7	6.39 (S1)	7.63 (S1)	7.83 (S2)	5.46 (S2)	5.50 (S3)
10^{17} / 10^8	2.84 (S1)	3.60 (S1)	4.88 (S3)	1.89 (S3)	1.78 (S3)

[a] The "intermediate levels" used correspond to the next four levels that are optically connected to the resonance level.

[b] The results presented in this table assume radiation trapping with a scale length of 0.1 cm.

In Fig. 4 we plot the variation of the ionization burnout time against the laser irradiance for an initial atom density of 10^{16} cm^{-3} for all of the alkali metals considered (Li through to Cs). It is clear that in the case of potassium, rubidium, and cesium, the laser dependence of the ionization burnout time τ_B is weak at the lower values of laser irradiance. This can be understood in terms of the dominance of associative ionization. Then at the higher values of laser irradiance the influence of laser-induced Penning ionization (and to a lesser extent two-photon ionization) becomes apparent by the rapid fall in τ_B with I^l.

On the other hand, the variation of τ_B with I^l for lithium and sodium can be seen to be much more consistent. This is reasonable in light of the fact that both these elements have lower values of σ_A and σ_L and are controlled much more by the intermediate stage of ionization. In Fig. 5 we have plotted the variation of the ionization burnout time against the initial atom density at a given laser irradiance of 10^{6} (W cm^{-2}) for each of the alkali metals. From this figure it is clear that full ionization is expected for both lithium and sodium under the experimental conditions of the work by Lucatorto and McIlrath.[1,2] They operated with a laser-pulse duration of about 500 nsec, a peak irradiance of about 10^{6} (W cm^{-2}) and densities 6×10^{15} (cm^{-3}) and 10^{16} (cm^{-3}) for lithium and sodium, respectively. On the other hand, appreciable

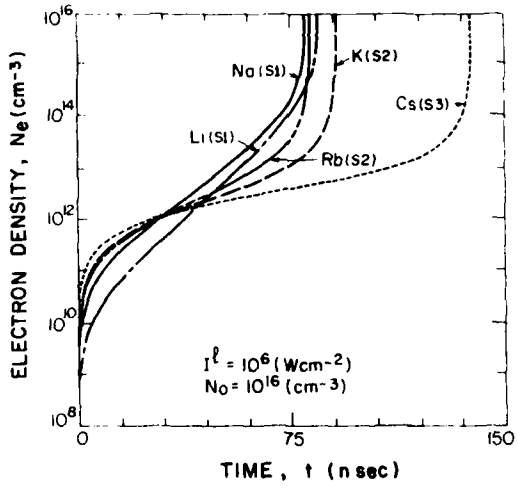

FIG. 3. Ionization time histories for each of the alkali metals as predicted by the LIBORS simple model. The initial number density, N_0 10^{16} cm^{-3}, and the laser irradiance I^{l} · 10^{6} W cm^{-2}.

ionization would not be expected under the experimental conditions of Salter *et al.*[23]

The ionization times predicted in Table I assume that radiation trapping is present and corresponds to a saturating laser-beam radius of 0.1 cm.

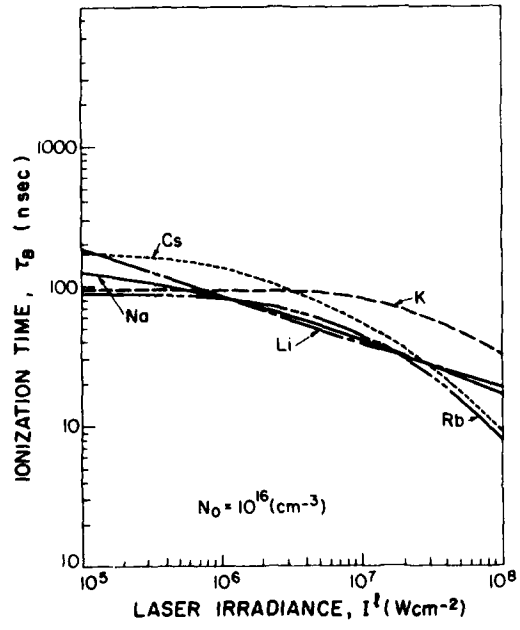

FIG. 4. The variation of the ionization burnout time τ_B, with laser irradiance for each of the alkali metals at an initial density of 10^{16} cm^{-3} as predicted by the LIBORS simple model.

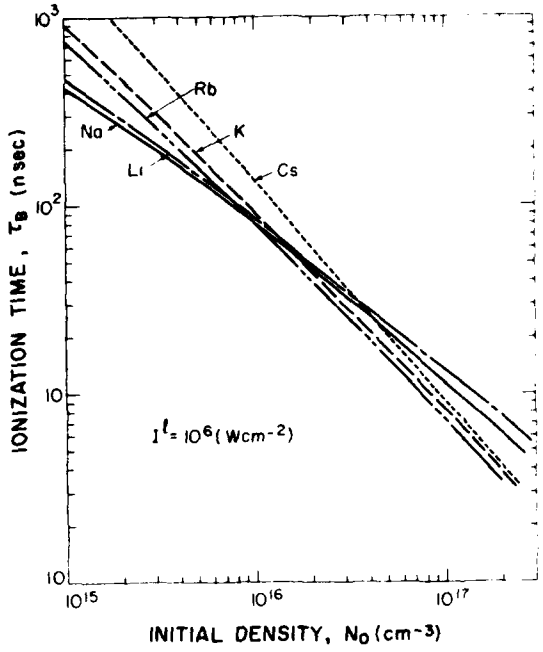

FIG. 5. The variation of the ionization burnout time τ_B, with initial density at a laser irradiance of 10^{6} W cm^{-2} for each of the alkali metals as predicted by the LIBORS simple model.

Although this is quite reasonable, we have considered the influence of neglecting radiation trapping. As might be expected the importance of radiation trapping is less pronounced at high values of density and laser irradiance. This can be seen by reference to Table II, where the ionization times are recalculated assuming "no radiation trapping". The differences in the ionization curves *with* and *without radiation trapping* are illustrated for sodium at an initial density of 10^{1} (cm^{-3}) in Fig. 6.

Although we have attempted to take account of all of the important collisional-radiative processes, ionization resulting from the collision of two excited atoms, where one is in the resonance state and the other is in an intermediate state has not been included in the work presented in this paper. Such collisions could have a large cross section[33,34] and could be fitted into our model, increasing the intermediate ionization-rate coefficient I, and slightly decreasing the burnout rate coefficient B. Our reason for not including them at this time lies in a lack of reliable cross-section data.

Nevertheless, we have undertaken a preliminary parametric study using a range of possible cross sections in the case of cesium. Our results suggest that the ionization time could be considerably

TABLE II. Ionization times (nsec) and types of LIBORS solution for each of the alkali metals assuming no radiation trapping.

N_0 (cm^{-3})	I^l (Wcm^{-2})	Li	Na	K	Rb	Cs
10^{15}	10^5	2430 (S1)	1970 (S1)	1720 (S1)	1240 (S1)	6440 (S3)
10^{15}	10^6	809 (S1)	755 (S1)	1670 (S1)	985 (S1)	3340 (S2)
10^{15}	10^7	288 (S1)	250 (S1)	1160 (S2)	342 (S2)	764 (S3)
10^{15}	10^8	131 (S1)	97.2 (S1)	300 (S3)	50.3 (S3)	82.8 (S3)
10^{16}	10^5	229 (S1)	159 (S1)	112 (S2)	92.0 (S2)	255 (S3)
10^{16}	10^6	101 (S1)	94.3 (S1)	110 (S2)	85.5 (S2)	196 (S3)
10^{16}	10^7	40.7 (S1)	44.0 (S1)	94.3 (S2)	48.3 (S2)	75.9 (S3)
10^{16}	10^8	18.9 (S1)	17.5 (S1)	41.5 (S3)	9.00 (S3)	12.7 (S3)
10^{17}	10^5	24.0 (S1)	14.6 (S2)	8.77 (S2)	7.65 (S2)	12.2 (S3)
10^{17}	10^6	14.0 (S2)	12.2 (S2)	8.70 (S2)	7.35 (S2)	10.8 (S3)
10^{17}	10^7	6.49 (S1)	7.75 (S1)	8.09 (S2)	5.52 (S2)	6.11 (S3)
10^{17}	10^8	2.86 (S1)	3.64 (S1)	5.05 (S3)	1.92 (S3)	1.96 (S3)

shorter than we currently predict for cross sections of about 10^{-14} (cm^2) and under these circumstances most of the ionization curves switch from S3 to S1 solutions.

SIMPLE-MODEL COMPARISON WITH LIBORS COMPUTER-CODE RESULTS

As a further check on the reliability of our simple model of LIBORS, we have compared the ionization burnout times predicted by the simple model with that of our extensive computer code.[15–18] This comparison has, at the moment, been restricted to sodium due to the cost and time involved in running the code for a different alkali. The results, as evident in Fig. 7, are very encouraging for they indicate that over the range of densities and laser irradiances of interest in the present work excellent agreement (≤15%) is obtained. Furthermore, there is also excellent agreement in the detailed features of the ionization time histories. This can be gauged by comparing the N_e curve in Fig. 8 with the corresponding ionization curve for sodium in Fig. 6. Both display the same shape and have changes of slope at about the same values of N_e.

It is also worth pointing out that the LIBORS computer-code results, as shown in Fig. 8, confirm that our basic assumptions regarding the constancy of N_2 and T_e over the major portion of

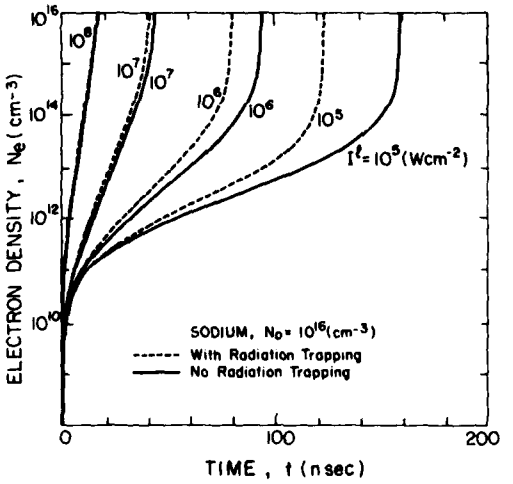

FIG. 6. Ionization curves for sodium *with* and *without* radiation trapping, as predicted by the LIBORS simple model.

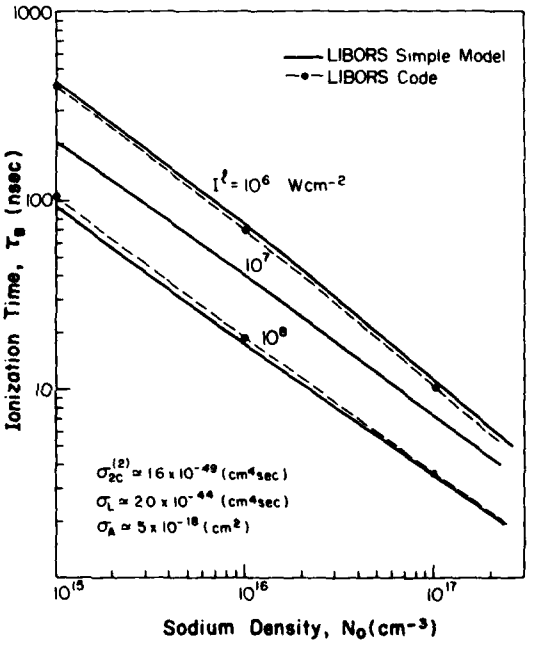

FIG. 7. A comparison of the ionization burnout time (≈95%) variation with density as predicted by the LIBORS simple model and the full computer code for sodium. Radiation trapping assumed for both with scale length of 0.1 cm.

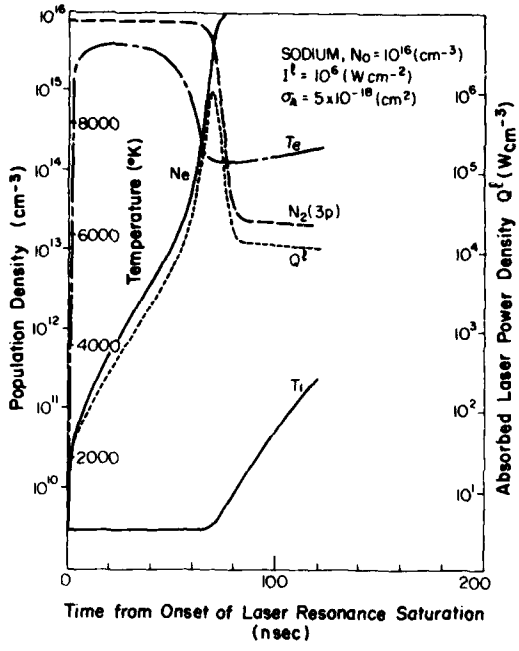

FIG. 8. Time histories of N_e, T_e, N_2, Q^t and T_i as predicted by the full LIBORS computer code (Refs. 15 to 18) for sodium with an original density of 10^{16} cm^{-3} and a laser irradiance I^t 10^6 W cm^{-2}.

the ionization time are reasonable. Not shown, but in fact observed in our LIBORS code results is the proportionality of the intermediate-state population densities and the electron density over much of the ionization period—corresponding to Eq. (18).

CONCLUSIONS

We have developed a relatively simple model of laser ionization based on resonance saturation. This model includes essentially all of the important collisional and radiative interactions that come into play when an alkali metal vapor (density range 10^{15} to 10^{17} cm^{-3}) is subject to a sudden pulse of intense laser radiation that is tuned to one of the resonance transitions of the alkali atom. This model reveals that once laser saturation of the relevant resonance transition has been achieved, ionization proceeds in three stages: First, seed ionization (including associative, laser-induced Penning and multiphoton ionization) creates an initial pool of seed electrons. Subsequently, in the intermediate ionization phase these free electrons are heated through superelastic collisions and then populate intermediate energy states which in turn are photoionized by the laser radiation. Finally, runaway ionization, through direct electron-impact ionization of the intermediate-level population, leads to a very rapid and near complete ionization burnout of the laser-irradiated species.

We have also been able to show that this model leads to two types of analytical solutions for the ionization time history of the irradiated vapor. Physical interpretation of the conditions that mediate which type of analytical solution characterizes the ionization time history is also provided. The ionization time for each of the alkali metals (Li through to Cs) has been evaluated under a wide range of conditions: initial number densities 10^{15} to 10^{17} cm^{-3} and laser irradiances from 10^5 to 10^8 W cm^{-2}. Although to date there has been very limited experimental work on this new class of dense plasma production, where results have been available they are consistent with our predictions. We have also been able to show that the predicted ionization times of this model are in excellent agreement with the results of our comprehensive LIBORS computer code, over a wide range of densities and laser irradiances, in the case of sodium. In general, the predictions of our simple LIBORS model should only be regarded as a guide to the expected time to achieve ionization burnout since the spatial and temporal characteristics of the laser beam will not in reality be rectangular and because many of the cross sections used are not known with great precision. Furthermore, our neglect of continuity is not valid for electron densities $\cdot 10^{\%}$, and this leads to an underestimate of the full ($\sim 95\%$) ionization time by about 25% for all but S3 solutions. A more detailed analysis of this will shortly be published by us.[35]

ACKNOWLEDGMENTS

Work supported by the Air Force Office of Scientific Research (AFOSR) (under Grant No. 76-2902C) and the Natural Science and Energy Research Council of Canada. Scholarship support for P. G. Cardinal was provided by the Natural Science and Engineering Research Council of Canada.

[1]T. B. Lucatorto and T. J. McIlrath, Phys. Rev. Lett. 37, 428 (1976).
[2]T. J. McIlrath and T. B. Lucatorto, Phys. Rev. Lett. 38, 1390 (1977).
[3]C. H. Skinner, J. Phys. B 13, 55 (1980).
[4]W. A. Young, M. Y. Mirza, and W. W. Duley, Opt. Commun. 31, 157 (1979).
[5]S. G. Leslie, J. T. Verdeyen, and W. S. Millar, J. Appl.

Phys. 48, 4444 (1977).
[6]A. C. Tam and W. Happer, Opt. Commun. 21, 403 (1977).
[7]G. H. Bearman and J. J. Leventhal, Phys. Rev. Lett. 41, 1227 (1978).
[8]M. Allegrini, G. Alzetta, A. Kopystynska, L. Moi, and G. Orriols, Opt. Commun. 22, 329 (1977).
[9]S. Geltman, J. Phys. B 10, 3057 (1977).
[10]R. M. Measures, J. Quant. Spectrosc. Radiat. Transfer 10, 107 (1970).
[11]R. M. Measures, J. Appl. Phys. 48, 2673 (1977).
[12]A. de Jong and F. van der Valk, J. Phys. B 12, L561 (1979).
[13]E. F. Worden, J. A. Paisner, and J. G. Conway, Opt. Lett. 3, 156 (1978).
[14]A. Klucharev, V. Sepman, and V. Vujnovic, J. Phys. B. 10, 715 (1977).
[15]P. G. Cardinal, UTIAS M.A.Sc. thesis, 1979 (unpublished).
[16]N. Drewell, UTIAS Report No. 229, 1979.
[17]R. M. Measures, N. Drewell, and P. Cardinal, J. Appl. Phys. 50, 2662 (1979).
[18]R. M. Measures, N. Drewell, and P. Cardinal, Appl. Opt. 18, 1824 (1979).
[19]R. M. Measures, P. L. Wizinowich, and P. G. Cardinal, J. Appl. Phys. 51, 3622 (1980).
[20]D. P. Burgess and M. J. Eckart, J. Phys. B 9, L519 (1976).
[21]B. L. Sharp and A. Goldwasser, Spectrochim. Acta, Part B 31, 431 (1976).
[22]J. M. Salter, J. Phys. B 12, L763 (1979).
[23]R. M. Measures, J. Appl. Phys. 39, 5232 (1968).
[24]J. M. Salter, D. D. Burgess, and N. A. Ebrahim, J. Phys. B 12, L759 (1979).
[25]A. B. Rodrigo and R. M. Measures, IEEE J. Quantum. Electron. QE-9, 972 (1973).
[26]J. W. Daily, Appl. Opt. 17, 225 (1978).
[27]G. S. Hurst, M. G. Payne, S. D. Kramer, and J. P. Young, Rev. Mod. Phys. 51, 767 (1979).
[28]T. J. McIlrath and J. L. Carlsten, Phys. Rev. A 6, 1091 (1972).
[29]Although the normal electron-electron relaxation time would suggest that at early time, deviations from a Maxwellian distribution might be appreciable, the very short time associated with inelastic collisional processes at the high density of atoms could well justify the assumption of a Maxwellian velocity distribution for times where $N_e > N_e^*$. For times less than this, the intermediate ionization (which is T_e dependent) is not regarded as important.
[30]G. V. Marr, *Photoionization Processes in Gases* (Academic, New York, 1967).
[31]M. J. Seaton, *Atomic and Molecular Processes*, edited by D. R. Bates (Academic, New York, 1962).
[32]T. Holstein, Phys. Rev. 83, 1159 (1951).
[33]R. E. Olson, J. Phys. B 12, L109 (1979).
[34]A. N. Klyucharev, A. V. Lazarenko, and V. A. Sheverev, Opt. Spektrosk. 46, 1157 (1979) [Opt. Spectrosc. (USSR) 46, 653 (1979)].
[35]R. M. Measures, P. G. Cardinal, and G. W. Schinn, J. Appl. Phys. (to be published).

Appendix C

A theoretical model of laser ionization of alkali vapors based on resonance saturation

R. M. Measures[a], P. G. Cardinal, and G. W. Schinn
Institute for Aerospace Studies, University of Toronto, 4925 Dufferin Street, Downsview, Ontario, Canada

(Received 30 June 1980; accepted for publication 1 December 1980)

We have developed a theoretical model of the ionization that results from extended laser saturation of an atomic resonance transition within a dense alkali vapor. Although this model includes all of the essential collisional-radiative interactions, nevertheless, it leads to relatively simple analytical relations that predict the ionization time history to within 20% of that calculated by our extensive laser ionization based on resonance saturation (LIBORS) computer code in the case of sodium. When allowance is made for the temporal and spatial nature of a realistic laser pulse, the apparent ionization time has been shown to be approximately double that of the value predicted on the basis of a steplike, flat laser pulse.

PACS numbers: 52.50.Jm, 34.80.Dp, 32.80.Kf, 32.80.Fb

INTRODUCTION

The concept of locking the population of two atomic levels in the ratio of their degeneracies by an intense pulse of laser radiation for both diagnostic and atomic measurement applications was first suggested by Measures.[1-3] Since then the field of *laser saturation spectroscopy*, as it has become known in the literature, has become firmly established and its range of applications has expanded to include (i) atomic lifetime measurements,[4-6] (ii) trace element analysis,[7,8] (iii) laser isotope spearation,[9] (iv) single atom detection,[10] (v) combustion studies,[11,12] (vi) flame measurements,[13] (vii) neutral hydrogen density measurements in Tokamaks,[14,15] and (viii) fusion plasma impurity diagnostics.[16]

In some experiments[17-19] the *laser intensified spontaneous emission* (referred to as *laser induced fluorescence* in much of the literature) was not observed to saturate even for values of laser spectral irradiance that far exceed the *saturated spectral irradiance*. Recent interferometric measurements,[20] however, have revealed that even in situations where the intensified emission does not appear to saturate, the atomic level populations are close to the infinite temperature distribution associated with a population ratio equal to the degeneracy ratio. Rodrigo and Measures[21] offered one possible explanation of this paradox in terms of the laser beam's radial profile and the observed spatially averaged emission signal. Recently, Salter[22] has proposed that radiation trapping could account for the apparent lack of saturation. Some combination of these mechanisms might, in fact, be needed to adequately account for these anomalous observations.

In another group of laser saturating experiments performed at relatively high atom densities ($> 10^{15}$ cm^{-3}) substantial ionization has been observed[23-26] when the laser pulse is tuned to a resonance transition and its duration is much greater than the resonance state lifetime. Measures[27] was the first to recognize that such extended laser saturation of a resonance transition represents a very effective means of coupling laser energy into a gaseous medium. In essence the dense population of resonance state atoms serve to funnel laser energy directly to the free electrons through superelastic collisions. These superelastically heated electrons can then readily excite and ionize resonance state atoms since, in effect, these atoms have their ionization energy reduced by the laser photon energy.[27,28] These same processes have recently been shown[29] to account for the fluorescence observed from levels that lie well above the laser pumped level in another series of experiments.[30-32]

The initial pool of free electrons in all of these experiments is expected to be created by the various laser induced collisional processes summarized by Geltman.[33]

We have developed a fairly comprehensive code for studying *laser ionizaton based on resonance saturation* (LIBORS). This LIBORS code treats the laser excited atom as a 20-energy level system and solves the subsequent set of energy and population rate equations by a fourth-order Runge-Kutta technique. A detailed description of the code is presented elsewhere[34-36] and will not be repeated here. It will suffice to mention that the code evaluates the temporal behavior of (i) each of the 20-atomic level populations, (ii) the free-electron density, (iii) the free-electron temperature, (iv) the ion temperature, (v) the laser power absorbed per unit volume, and (vi) the power radiated per second per unit volume as a result of radiative recombination to the resonance level, assuming a steplike laser pulse.

The results of our computer simulations for sodium are consistent with the experimental observations of Lucatorto and McIlrath[23] and suggest that LIBORS might be ideal for creating the plasma guide channels that are deemed to be necessary for transportation of electron or ion beams to the fuel pellet of future particle beam fusion reactors.[34] We have also shown that the concept of *superelastic laser energy conversion* (SELEC) could, under certain conditions, have several advantages over inverse bremsstrahlung as a means of coupling laser energy into a plasma or an un-ionized gaseous medium. In the event that SELEC is applied to a strong transition within a suitable ionic species, extremely rapid rates of plasma heating can be achieved[37]—a feature that is quite conducive to the development of short wavelength la-

[a]Professor of Applied Science and Engineering, University of Toronto.

 0021-8979/81/1269-09$01.10

sers. Indeed, in the case of a boron III plasma, we predict[37] that a heating rate in excess of 10^{13} °K s^{-1} could be attained with a laser irradiance of close to 10^8 W cm^{-2}.

In the present paper we have developed a more accurate theoretical model than has been previously published[38] and have shown that it can be used to predict the ionization time history for alkali vapors exposed to a realistic laser pulse, where allowance has to be made for both the spatial and temporal characteristics of the laser pulse.

LIBORS SIMPLE MODEL FORMULATION

We shall consider the case of a homogeneous, single constituent, atomic gaseous medium suddenly irradiated with an intense pulse of laser radiation that is tuned to one of the electronic resonance transitions. Although the interaction of this radiation field with the atoms is most accurately treated through use of the density matrix aproach, a rate equation analysis is reasonably reliable[39] if the bandwidth of the laser radiation is large compared to the Rabi frequency, and the collisional dephasing time is short compared to the times of interest.[40] For the typical conditions found in LIBORS work a rate equation analysis should be quite accurate.

The model we shall develop is particularly appropriate to atoms with low-lying resonance states, such as the alkali metals. For this class of atoms: $2E_{21} < E_{c1} \lesssim 3E_{21}$, where E_{21} ($= h\nu$, the laser photon energy) represents the energy difference between the ground and the laser excited resonance state and E_{c1} represents the ionization energy of the ground state. If the laser radiation is assumed to be suddenly applied at $t = 0$, then the subsequent chain of events can be viewed as proceeding in the four stages indicated in Fig. 1.

According to Measures[1] the resonance to ground-state population densities are locked in the ratio of their degeneracies, viz., $N_2/N_1 \approx g_2/g_1 \equiv g$; in a characteristic time, $\tau_R \approx [(1+g)R_{21}]^{-1}$, provided $I^l(\nu) \gg I_s(\nu)$ in the case of broadband laser radiation.

$$R_{21}\left(\equiv B_{21}\int I^l(\nu)\mathscr{L}(\nu)\frac{d\nu}{4\pi}\right)$$

represents the stimulated emission rate coefficient for the resonance transition. B_{21} represents the appropriate Milne coefficient and $\mathscr{L}(\nu)$ the corresponding line profile function. $I^l(\nu)$ represents the laser spectral irradiance and $I_s(\nu)$ is the *saturated spectral irradiance*, given by

$$I_s(\nu) = [8\pi h\nu^3/c^2(1+g)]\tau_2^{RAD}/\tau_2,$$

where $\tau_2^{RAD}(\equiv A_{21}^{-1})$, and τ_2 is the resonance state lifetime. A_{21} is the resonance transition Einstein probability. Invariably, τ_R is very short (much less than 1 ns for the typical laser fields under consideration) compared to any other process and we assign laser saturation to Stage 1.

Once the large pool of resonance state atoms is created, several kinds of interactions give rise to a linear growth of the free-electron density associated with Stage 2. The most important of these are *two-photon ionization of the resonance level, laser induced Penning ionization*, and *associated ionization*. In the case of the alkali metals, Geltman,[33] de Jong and van der Valk,[41] and Klucharev[42] have provided an estimate of the magnitude of the relevant cross sections. The appropriate rate of ionization during Stage 2 can be expressed in the form

$$\left.\frac{dN_e}{dt}\right|_{Stage2} \approx N_2\sigma_{2c}^{(2)}F^2 + \tfrac{1}{2}N_2^2(\sigma_L v F + \sigma_A v), \qquad (1)$$

where $\sigma_{2c}^{(2)}$ (cm^4 s) is the two-photon resonance state ionization rate coefficient, σ_L (cm^4 s) is the laser induced Penning ionization rate coefficient, v (cm s^{-1}) is the mean atom velocity, F (photons cm^{-2} s^{-1}) represents the laser photon flux density, i.e., $F = \int I^l(\nu)d\nu/h\nu$, and σ_A (cm^2) is the appropriate associative ionization cross section.

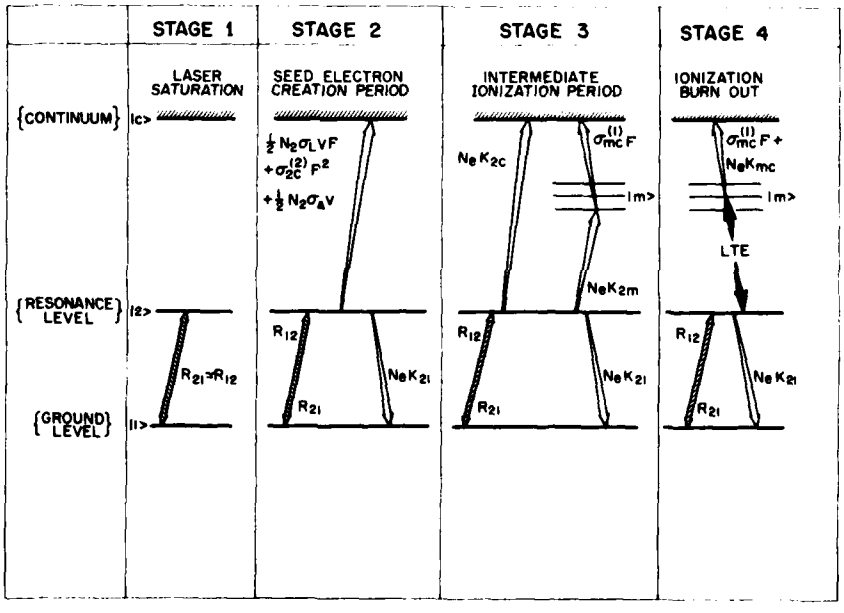

FIG. 1. Four stages of laser ionization based on resonance saturation. STAGE 1. Laser rapidly locks ground and resonance level populations in ratio of dengeracies. STAGE 2. (i) Rapid growth of free electrons due to two-photon ionization of resonance level and laser-induced Penning ionization. Associative ionization is important for some elements. (ii) Free electrons rapidly gain energy through *superelastic collisions*. STAGE 3. (i) Direct electron impact ionization of resonance level and single-photon ionization of collisionally populated upper levels dominate the rate of ionization. (ii) Electron temperature stabilizes as the rate of superelastic heating balances rate of collisional cooling through excitation. STAGE 4. (i) Runaway collisional ionization of upper levels occurs once a critical electron density achieved. (ii) Superelastic heating can no longer balance collisional cooling and electron temperature falls.

The electrons created by these initial processes rapidly gain energy through *superelastic collision quenching* of the laser sustained resonance state population, as first suggested by Measures.[27]

In Stage 3, the free-electron temperature is viewed as stabilizing as a result of a balance between the rate of superelastic heating and excitation cooling. This will be considered in more detail later. These electrons now give rise to an exponential growth in the free-electron density due to both direct collisional ionization of the resonance level and single-photon laser ionization of the collisionally populated intermediate levels.

Finally, in Stage 4, *runaway collisional ionization* of the intermediate levels occurs once a critical electron density is achieved. This process leads to the *ionization burnout* that results in almost complete ionization of the laser pumped species. Our full LIBORS computer code[34-36] indicates that during this rapid burnout phase, superelastic heating is unable to maintain the free-electron temperature and a sudden drop in the temperature is expected.

In order to obtain an analytical solution for the ionization time history from our LIBORS simple model we shall assume that the free-electron temperature stabilizes and remains constant throughout both Stages 3 and 4. Some justification for this assumption can be found in the following argument. During the linear growth period (Stage 2) the dominant ionization processes are independent of the free-electron temperature. This is fortunate because it is questionable whether the electron energy distribution could be characterized by a temperature during this period. During Stage 3, the free-electron energy equation can be reasonably well expressed in the form

$$\frac{d}{dt}\tfrac{3}{2}kT_e \approx N_2K_{21}E_{21} - N_1K_{12}E_{21} - N_2\sum_{m>2}K_{2m}E_{m2}, \quad (2)$$

where T_e is the free-electron temperature, K_{nm} is the appropriate electron collision rate coefficient, and E_{m2} the energy separation between the intermediate state $|m>$ and the resonance state $|2>$. The first term on the right-hand side represents the superelastic heating rate per electron while the subsequent terms represent the cooling rate per electron associated with the dominant collisional excitation processes. The sum over m in the last term extends over the group of intermediate levels that are rapidly populated by *hot* electrons and depopulated by single-photon laser ionization. Electron heating arising from the seed ionization processes is assumed to be of secondary importance during Stage 3 and 4. Also the gain in energy due to single-photon ionization and the loss in energy from direct impact ionization of the resonance level are assumed negligible in comparison to the superelastic heating and excitation cooling terms in Eq. (2).

Using electron collision rate coefficients that are based upon Seaton cross sections,[43] Eq. (2) yields under conditions of laser saturation a transcendental equation for the *steady-state superelastic temperature*

$$T_e^s \approx \frac{E_{32}/k}{\ln\left[\exp(-\epsilon_1/kT_e^s) + \dfrac{g}{\langle f_{12}\rangle}\sum_{m>3}\langle f_{2m}\rangle\exp(-\epsilon_m/kT_e^s)\right]}, \quad (3)$$

where $\epsilon_m \equiv E_{m2} - E_{32}$ and $\langle f_{im}\rangle \equiv f_{im}\langle\bar{G}\rangle_{im}\cdot f_{im}$ represents the absorption oscillator strength for the im transition and $\langle\bar{G}\rangle_{im}$ the relevant Gaunt factor averaged over a Maxwellian velocity distribution. This equation can be solved by an iterative procedure, or in light of the logarithmic nature of the denominator and the fact that $E_{m2} \approx E_{32}$ (in the model), it can be approximated by the expression

$$T_e^s \approx \frac{E_{32}/k}{\ln\left(1 + g\sum_{m>3} f_{2m}/f_{12}\right)}. \quad (4)$$

The ionization equation appropriate to this model takes the form

$$\frac{dN_e}{dt} = N_2\left[\sigma_{2c}^{(2)}F^2 + \tfrac{1}{2}N_2v(\sigma_LF + \sigma_A) + N_eK_{2c}\right] + \sum_{m>3}N_m(\sigma_{mc}^{(1)}F + N_eK_{mc}), \quad (5)$$

where $N_mN_eK_{mc}$ represents the volume rate of direct collisional ionization of the $|m>$ state, $N_m\sigma_{mc}^{(1)}F$ represents the volume rate of single-photon laser ionization of the $|m>$ state, K_{mc} is the appropriate electron collisional ionization rate coefficient of $|m>$ state, and $\sigma_{mc}^{(1)}$ is the single-photon ionization cross section[44] for the $|m>$ state.

The relevant intermediate level population rate equation can be expressed in the form

$$\frac{dN_m}{dt} = N_2N_eK_{2m} - N_m(\sigma_{mc}^{(1)}F + A_{m2}^{\dagger} + N_eC_m), \quad (6)$$

where $A_{m2}^{\dagger} = A_{m2}\gamma_{m2}$ represents the radiation-trapped Einstein transition probability for the $m2$ transition, γ_{m2} is the Holstein escape factor,[45] and

$$C_m \equiv K_{mc} + \sum_{n\neq m}K_{mn}. \quad (7)$$

If we introduce

$$P_m = \sigma_{mc}^{(1)}F, \quad (8)$$

and set

$$\rho_m = P_m + A_{m2}^{\dagger}, \quad (9)$$

then over a significant fraction of the time to ionize

$$\rho_m \gg N_eC_m, \quad (10)$$

as at low densities and weak fields $A_{m2}^{\dagger} \gg N_eC_m$ until burnout phase, while under intense illumination $P_m \gg N_eC_m$. Under these circumstances Eq. (6) has a solution

$$N_m(t) = N_2K_{2m}\exp(-\rho_mt)\int_0^t N_e(t^*)\exp(\rho_mt^*)dt^*, \quad (11)$$

if the vapor is assumed to be unexcited prior to laser irradiation, i.e., $N_m(0) = 0$. F, N_2, and K_{2m} are also taken to be constant over the period of interest.

The constancy of N_2 over an appreciable fraction of the time to ionize is quite reasonable on the grounds that the upper levels ($m>3$) only become significantly populated just prior to ionization burnout (Stage 4). In fact, if we use the saturation condition we can write $N_2 \approx GN_0$, where $G = g(1+g)^{-1}$ and N_0 represents the initial atom density. The time independence of K_{2m} is based upon our previous assumption of a stabilized temperature during the intermediate phase (Stage 3) and F has been set to be constant by our assertion of a steplike laser pulse. The viability of these assumptions is apparent from our LIBORS computer code results.[38]

Since the ionization burnout phase under the conditions of interest is short compared to the time to attain ionization burnout we can deduce that the solution prior to burnout will take the form

$$N_e(t) \approx N_e^* [\exp(\beta t) - 1]. \tag{12}$$

This gives a linear growth for $\beta t \ll 1$ corresponding to the *seed ionization phase* and an exponential growth for $\beta t > 1$ which takes account of the influence of the intermediate processes, i.e., Stage 3. N_e^* can be taken to be the seed electron density for which N_e departs significantly from a linear growth.

Substituting this form of solution, i.e., Eq. (12) in Eq. (11), yields an approximate relation for the intermediate level population

$$N_m(t) \approx N_2 K_{2m} N_e(t)/(\beta + \rho_m), \tag{13}$$

that is valid for $t > (1/\beta)\ln(1+\beta/\rho_m)$. This constraint is discussed elsewhere.[38] Equation (13) can be used in Eq. (5) to eliminate N_m and yield a simple form of ionization equation

$$\frac{dN_e}{dt} = S + IN_e + BN_e^2, \tag{14}$$

where we have introduced

$$S \equiv N_1[\sigma_{2c}^{(2)} F^2 + \tfrac{1}{2} N_2 \nu(\sigma_A + \sigma_L F)] \tag{15}$$

as the *seed ionization rate*,

$$I \equiv N_2\left(K_{2c} + \sum_{m>3} \frac{K_{2m} P_m}{\beta + \rho_m}\right) \tag{16}$$

as the *intermediate ionization rate coefficient*, and

$$B \equiv N_2 \sum_{m>3} \frac{K_{2m} K_{mc}}{\beta + \rho_m} \tag{17}$$

as the *burnout ionization rate coefficient*.

We see that we can now define

$$N_e^{**} \equiv I/B \tag{18}$$

as the critical electron density at which the burnout rate of ionization equals the intermediate rate of ionization. In a like manner we can define

$$N_e^* = S/I \tag{19}$$

as the characteristic electron density for which the intermediate ionization rate equals the seed ionization rate.

There are two forms of analytical solution for Eq. (14) depending on the relative values of S, I, and B. If $I^2 < 4SB$, then this is equivalent to $N_e^{**} < 4N_e^*$ and so the ionization proceeds directly from Stage 2 to Stage 4. That is to say seed ionization leads directly to runaway ionization. The solution to Eq. (14) under these circumstances takes the form

$$t = \frac{2}{a}\left(\tan^{-1}\frac{2BN_e + I}{a} - \tan^{-1}\frac{I}{a}\right), \tag{20}$$

where

$$a = (4SB - I^2)^{1/2}. \tag{21}$$

This class of solutions is in general indicative of a high rate of *seed ionization*.

If $I^2 > 4SB$, then $N_e^{**} > 4N_e^*$ and Stage 3 ionization will play some role in separating Stage 2 from Stage 4. The solution to Eq. (14) under these circumstances takes the form

$$t = \frac{1}{A}\ln\left(\frac{(N_e + R_1)}{(N_e + R_2)}\frac{R_2}{R_1}\right), \tag{22}$$

where

$$A = (I^2 - 4SB)^{1/2}, \tag{23}$$

$$R_1 = (I - A)/2B, \tag{24}$$

and

$$R_2 = (I + A)/2B. \tag{25}$$

From Eq. (14) it is apparent that I is associated with the exponential growth phase and we therefore identify β with I. Under these circumstances Eq. (16) represents a transcendental equation for I. We have found that I can be determined to about 1% accuracy by setting ρ_m equal to the maximum value of ρ_m in Eq. (16), then solving the resulting quadratic equation for I and using this approximate value of I in the denominators of the sum on the right-hand side of Eq. (16). The more accurate value of I is then substituted for β in Eq. (17) to ascertain B.

A pair of representative solutions for sodium and potassium are presented (broken curves) in Fig. 2. Although the ionization time histories and burnout times predicted from this analysis are expected to provide a reasonable compari-

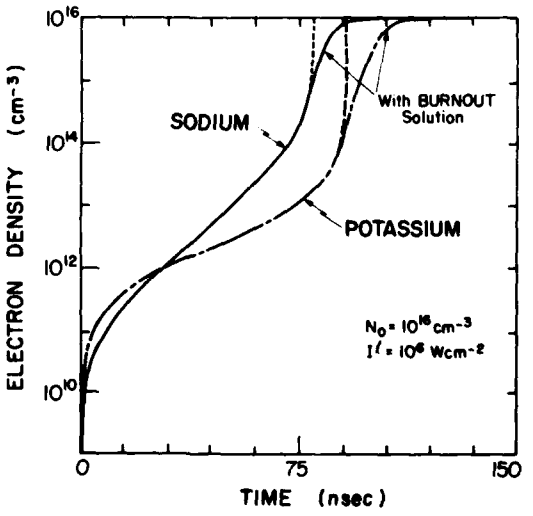

FIG. 2. Representative ionization time histories with and without the *burnout solution* for sodium and potassium with initial atom density $N_0 = 10^{16}$ cm^{-3} and a steplike laser irradiance, $I' = 10^6$ W cm^{-2}.

son between the elements and to indicate the dependence of these features on the laser irradiance and initial atom density—the form of the ionization equation (14) has one drawback. It does not take into account continuity and therefore predicts runaway ionization leading to a singularity in N_e. In reality this is not too serious as the *burnout phase* is very rapid, in all cases, so that the loss in accuracy in predicting the ionization burnout time from Eqs. (20) or (22) by setting $N_e^{\max} = N_0$, the initial atom density, is minimal.

A more reliable total solution can be obtained by treating the burnout phase separately. In essence the burnout phase can be regarded to arise when either $N_e \approx I/B$ (for $I^2 > 4SB$) or $N_e \approx (S/B)^{1/2}$ (for $I^2 < 4SB$). At these high electron densities, the rate of ionization is dominated by electron collision ionization and single-photon ionization of the intermediate level populations. In some cases electron collisional ionization of the resonance level may also be significant. Thus the *burnout ionization equation* can be expressed in the form

$$\frac{dN_e}{dt} = N_2 N_e K_{2c} + \sum_{m>3} N_m (N_e K_{mc} + \sigma_{mc}^{(1)} F). \tag{26}$$

In the burnout phase electron collisions will tend to bring the intermediate level populations into *local thermodynamic equilibrium* (LTE) with the resonance level population. Hence we can write for the intermediate level population

$$N_m = N_2 (g_m/g_2) \exp(-E_{m2}/kT_e). \tag{27}$$

Continuity can be taken into account by assuming that

$$N_e + N_2 + N_1 + \sum_{m>3} N_m = N_0 \tag{28}$$

applies in the burnout phase. If we also assume laser saturation of the resonance transition, then the continuity relation can be rewritten in the form

$$N_2 = \gamma (N_0 - N_e), \tag{29}$$

where

$$\gamma \equiv \frac{G}{1 + \sum_{m>3} (g_m/g_2) \exp(-E_{m2}/kT_e)}. \tag{30}$$

If Eq. (29) is used with Eq. (27) in Eq. (26), the *burnout phase ionization equation* can be written

$$\frac{dN_e}{dt} = (N_0 - N_e)(N_e \kappa + H), \tag{31}$$

where

$$\kappa \equiv \gamma \left(K_{2c} + \sum_{m>3} \frac{g_m}{g_2} K_{mc} \exp \frac{-E_{m2}}{kT} \right) \tag{32}$$

and

$$H \equiv \gamma \sum_{m>3} \frac{g_m}{g_2} \sigma_{mc}^{(1)} F \exp \frac{-E_{m2}}{kT}. \tag{33}$$

Equation (31) has a simple solution of the form

$$t = t_i + \left(\frac{1}{(\kappa N_0 + H)} \ln \frac{\kappa N_e + H}{N_0 - N_e} \right)_{N_e'}^{N_e}, \tag{34}$$

where t_i is the time at which the electron density reaches the

TABLE I: Basic parameters and 95% ionization times calculated from LIBORS model for several alkali metal vapors.

		Li	Na	K	Rb
E_{21}	(eV)	1.85	2.10	1.62	1.58
T_e^*	(°K)	11442	8433	7757	8036
σ_A	(cm^2)				
(at $N_0 = 10^{16}$)		0	3.26×10^{-18}	1.27×10^{-17}	1.22×10^{-17}
σ_L	(cm^4 s)	9.1×10^{-44}	2.0×10^{-44}	1.2×10^{-43}	9.6×10^{-43}
$\sigma_{2c}^{(2)}$	(cm^4 s)	2.2×10^{-48}	1.7×10^{-49}	2.9×10^{-49}	7.7×10^{-48}
$\sigma_{max}^{(1)}$	(cm^2)	1.0×10^{-17}	2.9×10^{-18}	2.3×10^{-18}	8.2×10^{-19}
$\langle A_{m2} \rangle$ [a]	(s^{-1})	3.5×10^{7}	2.4×10^{7}	2.9×10^{7}	9.8×10^{6}
$\langle K_{mc} \rangle$ [b]	($cm^3 s^{-1}$)	2.5×10^{-7}	1.78×10^{-7}	1.5×10^{-7}	1.6×10^{-7}
$\langle K_{2m} \rangle$	($cm^3 s^{-1}$)	1.73×10^{-8}	3.62×10^{-8}	8.3×10^{-8}	1.26×10^{-7}
N_0 (cm^{-3})	I' (Wcm^{-2})		95% Ionization Time (ns)		
10^{15}	10^5	1120	972	1200	1140
10^{15}	10^6	521	539	1080	914
10^{15}	10^7	264	262	707	343
10^{15}	10^8	125	102	169	84.4
10^{16}	10^5	188	140	113	104
10^{16}	10^6	90.9	93.8	112	98.0
10^{16}	10^7	42.3	51.7	100	60.2
10^{16}	10^8	20.0	22.8	44.3	20.2
10^{17}	10^5	24.2	15.7	10.6	9.28
10^{17}	10^6	14.3	13.4	10.6	8.98
10^{17}	10^7	7.00	8.98	9.88	7.14
10^{17}	10^8	3.26	4.65	6.68	3.46

[a] The results presented in this table assume radiation trappping with a scale length of 0.1 cm.
[b] The *intermediate levels* chosen for these calculations correspond to the next four levels that are optically connected to the resonance level.

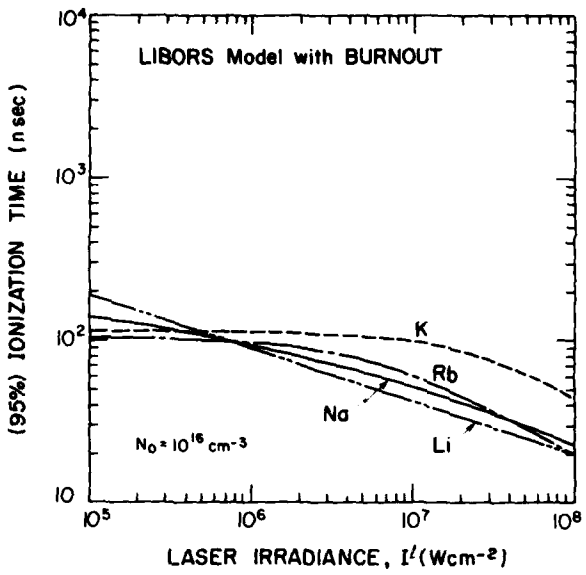

FIG. 3. Variation of the 95% *ionization time* with laser irradiance for lithium, sodium, potassium, and rubidium assuming a steplike laser pulse of extended duration.

critical value N_e^l for switching solutions. N_e^l is chosen to be the electron density at which the slope of $N_e(t)$, corresponding to Eq. (14), becomes steeper than the slope corresponding to Eq. (31). This procedure results in a smooth transition as seen by reference to Fig. 2 where two representative electron density time histories are presented, with and without *burnout solutions*, for both sodium and potassium. Similar curves have been obtained for lithium and rubidium under the same conditions of density and laser irradiance.

The basic parameters and the time to achieve 95% ionization, evaluated from the above analysis is displayed in Table I for lithium, sodium, potassium, and rubidium. As might be expected, these 95% ionization times are somewhat longer than the ionization times evaluated[38] solely on the basis of Eq. (14), but for the most part the difference is within 30%. The variation in the 95% ionization time as a function of laser irradiance at an initial atom density of 10^{16} cm^{-3} is presented in Fig. 3 for Li, Na, K, and Rb. In the case of cesium, the combination of a predicted low electron temperature and a large associative ionization cross section leads to a situation where the slopes cross at an electron density that is too small to justify the use of the burnout solution.

SIMPLE MODEL COMPARISON WITH LIBORS COMPUTER CODE RESULTS FOR SODIUM

In order to test the accuracy of our simple model of LIBORS we have made a direct comparison between the electron density time histories predicted by our LIBORS computer code[34-36] and that predicted by the model described herein. This comparison has, at the moment, been restricted to sodium due to the cost and time involved in running the full code for a different alkali. The results for $N_0 = 10^{15}$ and 10^{16} cm^{-3} and $I^l = 10^6$ and 10^8 W cm^{-2} are presented in Fig. 4. Both linear and logarithmic plots are used in order to display the degree of agreement over a range of electron density spanning six orders of magnitude.

It is clear that the simple LIBORS model gives excellent agreement with the full LIBORS computer code over a wide range of conditions. The differences in the 95% ionization times are, in general, within 20%, while the times to achieve only 10% ionization are much closer. What is particularly worthy of note is the close overlap of the ionization histories over six orders of magnitude variation in the electron density. Clearly the LIBORS simple model can be viewed as containing the essence of the complex array of collisional-radiative processes.

ALLOWANCE FOR SPATIAL AND TEMPORAL CHARACTERISTICS OF THE LASER PULSE

In order to be able to make a comparison between the simple model description of LIBORS and experimental observations, it is immediately apparent that we have to take account of both the radial profile of the laser pulse and its temporal history.

The above analysis has been predicated on the basis of a step function form of laser pulse, that is to say the laser irradiance was assumed to be instantly switched to its maximum value and remain at that value indefinitely. In reality we have found in a preliminary experiment[46] that a typical flashlamp dye laser pulse can be well represented by the expression

$$I^l(t) \approx 1.1 \times 10^7 E^l (t/\tau_3)(1 - t/\tau_1)\exp(-t/\tau_2), \quad (35)$$

where $I^l(t)$ represents the laser irradiance in W cm^{-2} and E^l the total energy in the laser pulse in J. τ_3 (≈ 160 ns), τ_1 (≈ 1154 ns), and τ_2 (≈ 810 ns) represent the three characteristic times needed to define the shape of the pulse.

The temporal variation of the free-electron density corresponding to the laser pulse described by Eq. (35) can be evaluated by replacing this laser pulse by a series of representative rectangular pulses and integrating the appropriate ionization equation over each time interval. The lower limit for the electron density in each step is set equal to the maximum value achieved in the previous integration interval. The initial time for the integration is obtained by displacing the time origin by an amount equal to the difference in the time required to reach the starting electron density along the ionization curve corresponding to the previous value and the new value of laser irradiance.

In order to predict the temporal variation of the radiative recombination emission the *free-electron line density*,

$$N_e^l(t) = \int_0^R N_e(r,t)2\pi r dr, \quad (36)$$

within the effective field of view of our photodetection system[46] (radius R) has to be evaluated as a function of time. This is accomplished by using cylindrical geometry and dividing the observed alkali vapor column segment into a series of equal-area annular zones colinear with the laser beam axis. Each zone is assumed to be exposed to a laser pulse having a temporal variation given by Eq. (35). The laser pulse is also assumed to have a Gaussian radial profile of the form

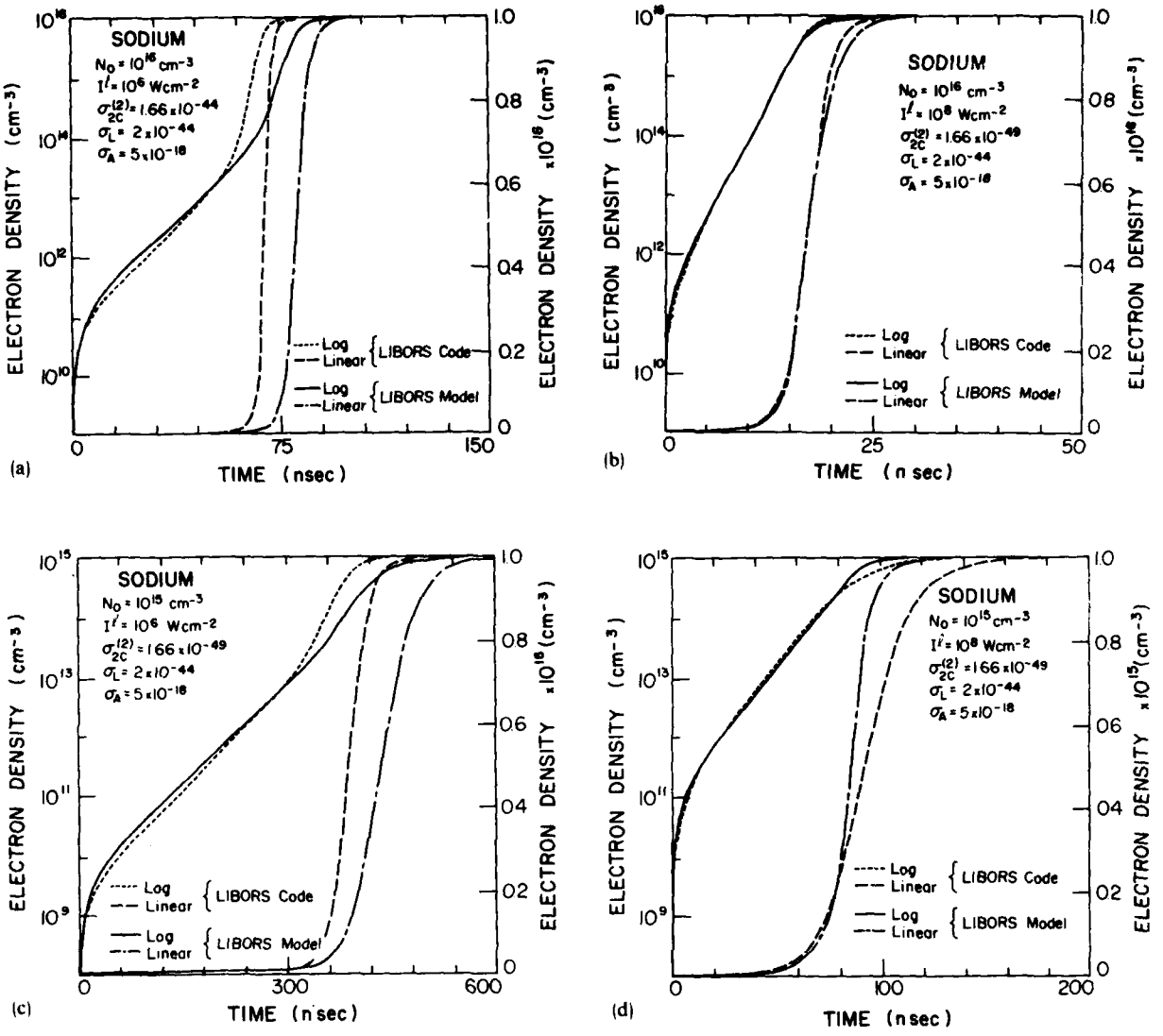

FIG. 4. Comparison of the ionization time histories (on both linear and logarithmic scales) as calculated from the simple LIBORS model and as evaluated from the full LIBORS code for a range of conditions in the case of sodium.

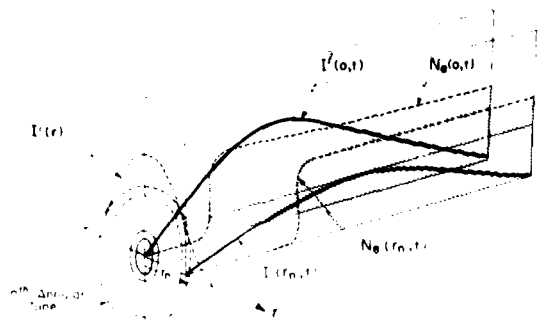

FIG. 5. Schematic representation of the ionization in both space and time indicating both the temporal and spatial nature of the laser pulse

$$I^l(r,t) = I^l(t)\exp[-(r/r_0)^2], \tag{37}$$

where $I^l(t)$ is given by Eq. (35) and r_0 represents the exponential radius for the laser pulse. Equation (36) is evaluated using a Simpson's integration technique where $I^l(r,t)$ and $N_e(r,t)$ are determined at the mean radius and at the two boundary radii of each annular zone. In order to facilitate computation we assumed that the electron density froze at either the *burnout* value or the value that caused breakdown of the laser saturation condition. A schematic representation of the variation of ionization in both space and time allowing for the spatial and temporal nature of the laser pulse is presented in Fig. 5.

In Fig. 6, we present a comparison between the temporal variation of the free-electron line density, I, (evaluated to a radius of 0.6 cm) for the three cases (i) a steplike laser

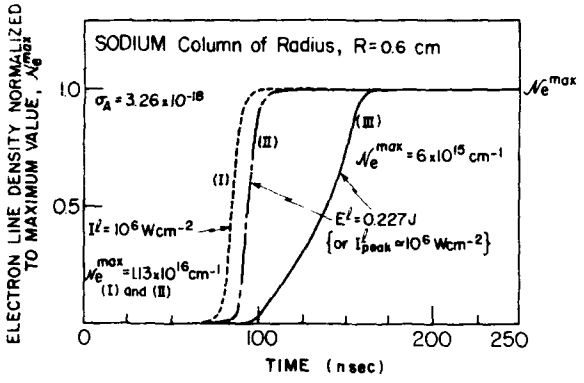

FIG. 6. Comparison of the temporal variation of the *free electron line density*, N_e, in a sodium column evaluated to a radius of 0.6 cm for the three cases. (i) Steplike, flat laser pulse for $I^l = 10^6$ W cm^{-2}. (ii) Laser pulse is assumed to have realistic temporal variation, Eq. (35) of text, but uniform radial distribution. Energy in the pulse is set to be 0.227 J corresponding to a peak irradiance of 10^6 W cm^{-2}. (iii) Laser pulse is assumed to have both a realistic temporal variation and a Gaussian radial distribution with an energy of 0.227 J.

pulse that also has a flat radial distribution so that $I^l = 10^6$ W cm^{-2} for $t \geq 0$ and $0 < r \leq 0.6$ cm. (ii) A laser pulse having a realistic time history, given by Eq. (35), but a flat radial distribution. The energy of the laser pulse is assumed to be 0.227 J which corresponds to a peak laser irradiance of 10^6 W cm^{-2}. (iii) A realistic laser pulse having a time history, given by Eq. (35), and a Gaussian radial distribution, given by Eq. (37), with an exponential radius of 0.2 cm. The energy of the laser pulse is again assumed to be 0.227 J.

The maximum *free-electron line density*, N_e^{max} and corresponding maximum free-electron density, averaged over the column radius, $\langle N_e \rangle^{max}$ appropriate to each of these three cases is presented in Table II.

It is clear from Fig. 6 that in an experiment the apparent time to achieve 95% ionization would be about double that predicted on the basis of our simple model.

CONCLUSIONS

We have developed a theoretical model of the ionization that arises when an alkali metal vapor is suddenly irradiated by an intense pulse of laser radiation that is tuned to one of the alkali resonance transitions. This model includes essentially all of the important collisional and radiative interactions. Once saturation of the resonance transition is achieved ionization is assumed to proceed in three stages: (i) *seed ionization* creates an initial pool of free electrons that are free to gain energy through *superelastic collisions*, (ii) these *hot* electrons are then capable of directly *ionizing the resonance level atoms* and populating the intermediate atomic levels, which are subsequently *photoionized*, and (iii) direct *electron impact ionization* of the intermediate level population subsequently leads to a very rapid and near complete *ionization burnout* of the laser irradiated species.

Analytical solutions for the ionization, derived from this relatively simple model, are found to lead to free-electron density time histories that are in very close agreement

TABLE II. Sodium $N_0 = 10^{16}$ cm^{-3}.

Case	I_e^{max} (cm^{-1})	$\langle N_e \rangle^{max}$ (cm^{-3})
(I)	1.13×10^{16}	10^{16}
(II)	1.13×10^{16}	10^{16}
(III)	6×10^{15}	5.3×10^{15}

with those obtained on the basis of our detailed LIBORS computer code in the case of sodium. The model has also been applied to other alkali metal vapors and the predicted time to achieve 95% ionization has been tabulated over a wide range of conditions.

In an experiment, the laser pulse will not necessarily have a steplike time history and a flat spatial distribution, as assumed in the simple LIBORS model. We have shown that the *apparent time* to achieve 95% ionization may be nearly twice that predicted by our simple model, if allowance is made for the temporal and radial nature of an experimental laser pulse.

ACKNOWLEDGMENTS

This work was supported by USAF AFOSR (under Grant No. 76-2902C) and the Natural Science and Engineering Research Council of Canada.

[1] R. M. Measures, J. Appl. Phys. **39**, 5232 (1968).
[2] R. M. Measures, Phys. Fluids **13**, 1889 (1970).
[3] R. M. Measures and A. B. Rodrigo, Appl. Phys. Lett. **20**, 102 (1972).
[4] R. M. Measures, N. Drewell, and H. S. Kwong, Phys. Rev. A **16**, 1093 (1977).
[5] H. S. Kwong and R. M. Measures, Appl. Opt. **19**, 1025 (1980).
[6] W. Gornik, D. Kaiser, W. Lange, H. H. Radloff, and H. Schulz, Appl. Phys. **1**, 285 (1973).
[7] R. M. Measures and H. S. Kwong, Appl. Opt. **18**, 281 (1979).
[8] H. S. Kwong and R. M. Measures, Anal. Chem. **51**, 428 (1979).
[9] G. S. Jones, I. Itzkan, C. T. Pike, R. H. Levy, and L. Levin, J. Quant. Elect. **QE-12**, 111 (1976).
[10] V. I. Balykin, V. S. Letokhov, V. I. Mishin, and V. A. Semchishen, JETP Lett. **26**, 359 (1977).
[11] J. W. Daily, Appl. Opt. **16**, 568 (1977).
[12] R. P. Lucht and N. M. Lauendeau, Appl. Opt. **18**, 856 (1979).
[13] J. W. Hosch and E. H. Piepmeier, Appl. Spectrosc. **32**, 444 (1978).
[14] D. W. Koopman, T. J. McIlrath, and V. P. Myerscough, J. Quant. Spectrosc. Radiat. Transfer **19**, 555 (1978).
[15] R. Hess and F. Burrell, J. Quant. Spectrosc. Radiat. Transfer **21**, 23 (1979).
[16] K. G. Muller and M. Stania, J. Appl. Phys. **49**, 5801 (1978).
[17] B. L. Sharp and A. Goldwasser, Spectrochim. Acta Part B. **31**, 431 (1976).
[18] D. D. Burgess and M. J. Eckart, J. Phys. B **9**, L519 (1976).
[19] R. D. Driver and J. L. Snider, J. Phys. B **10**, 595 (1976).
[20] J. M. Salter, D. D. Burgess, and N. A. Ebrahim, J. Phys. B **12**, L759 (1979).
[21] A. B. Rodrigo and R. M. Measures, IEEE J. Quant. Electron. **QE-9**, 972 (1973).
[22] J. M. Salter, J. Phys. B **12**, L763 (1979).
[23] T. B. Lucatorto and T. J. McIlrath, Phys. Rev. Lett. **37**, 428 (1976).
[24] T. J. McIlrath and T. B. Lucatorto, Phys. Rev. Lett. **38**, 1390 (1977).
[25] C. H. Skinner, J. Phys. B **13**, 55 (1980).
[26] W. A. Young, M. Y. Mirza, and W. W. Duley, Optics Commun. **31**, 157 (1979).
[27] R. M. Measures, J. Quant. Spectrosc. Radiat. Transfer **10**, 107 (1970).

[28]R. M. Measures, J. Appl. Phys. **48**, 2673 (1977).
[29]J. Krasinsky, T. Stacewicz, and C. R. Stroud, Jr., Optics Commun. **33**, 158 (1980).
[30]M. Allegrini, G. Alzetta, A. Kopystynska, L. Moi, and G. Orriols, Opt Commun. **22**, 329 (1977).
[31]S. G. Leslie, J. T. Verdeyen, and W. S. Millar, J. Appl. Phys. **48**, 4444 (1977).
[32]G. H. Bearman and J. J. Leventhal, Phys. Rev. Lett. **41**, 1227 (1978).
[33]S. Geltman, J. Phys. B **10**, 3057 (1977).
[34]R. M. Measures, N. Drewell, and P. Cardinal, J. Appl. Phys. **50**, 2662 (1979).
[35]R. M. Measures, N. Drewell, and P. Cardinal, Appl. Opt. **18**, 1824 (1979).
[36]N. Drewell, UTIAS Report No. 229, 1979 (unpublished).
[37]R. M. Measures, P. L. Wizinowich, and P. G. Cardinal, J. Appl. Phys. **51**, 3622 (1980).
[38]R. M. Measures and P. G. Cardinal, Phys. Rev. A **23**, 804 (1981).
[39]G. S. Hurst, M. G. Payne, S. D. Kramer, and J. P. Young, Rev. Mod. Phys. **51**, 767 (1979).
[40]T. J. McIlrath and J. L. Carlsten, Phys. Rev. A **6**, 1091 (1972).
[41]A. de Jong and F. van der Valk, J. Phys. B **12**, L561 (1979).
[42]A. Klucharev, V. Sepman, and V. Vujnovic, J. Phys. B **10**, 715 (1977).
[43]M. J. Seaton, in *Atomic and Molecular Processes*, edited by D. R. Bates (Academic, New York, 1962).
[44]G. V. Marr, *Photoionization Processes in Gases* (Academic, New York, 1967).
[45]T. Holstein, Phys. Rev. **83**, 1159 (1951).
[46]P. G. Cardinal, P. L. Wizinowich, and R. M. Measures, J. Quant. Spectrosc. Radiat. Transfer (in press).

japia,81100j1156,e11002

Erratum: Theoretical model of laser ionization of alkali vapors based on resonance saturation [J. Appl. Phys. 52, 1296 (1981)]

R. M. Measures, P. G. Cardinal, and G. W. Schinn
Institute for Aerospace Studies, University of Toronto, 4925 Dufferin Street, Downsview, Ontario, Canada

PACS numbers: 52.50.Jm, 34.80.Dp, 32.80.Kf, 32.80.Fb, 99.10. + g

In the above paper, Fig. 6 and Table II were incorrect. The correct Fig. 6 and Table II are provided herein. A small section of the text relating to Fig. 6 and Table II was also incorrect. The correction reads:

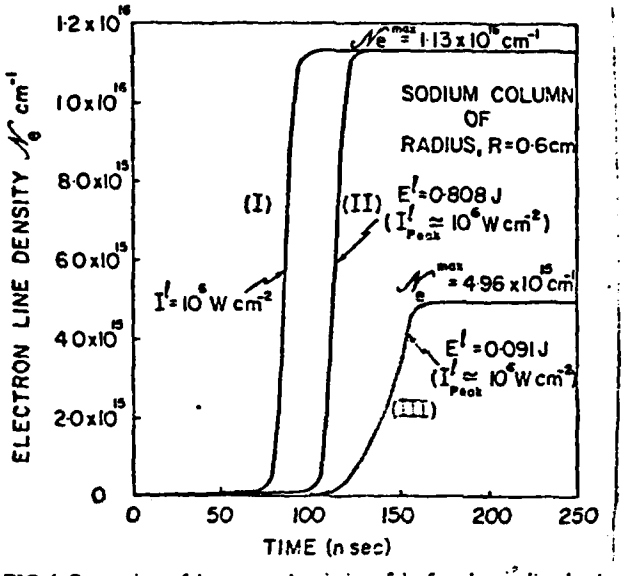

FIG. 6. Comparison of the temporal variation of the *free electron line density*, $\mathcal{N}_e$, in a sodium column evaluated to a radius of 0.6 cm for the three cases. (I) Steplike, flat laser pulse for $I^I = 10^6$ W cm^{-2}. (II) Laser pulse is assumed to have realistic temporal variation, Eq. (35) of text, but uniform radial distribution out to 0.6 cm. Energy of the pulse is set to be 0.808 J corresponding to a peak irradiance of 10^6 W cm^{-2}. (III) Laser pulse is assumed to have both a realistic temporal variation, Eq. (35), and a Gaussian radial distribution with an exponential radius of 0.20cm and an energy of 0.091 J, giving a peak irradiance of 10^6 W cm^{-2}.

TABLE II. Sodium $N_0 = 10^{16}$ cm^{-3}.

Case	$\mathcal{N}_e^{max}$(cm^{-1})	$\langle N_e \rangle^{max}$(cm^{-3})
(I)	1.13×10^{16}	10^{16}
(II)	1.13×10^{16}	10^{16}
(III)	4.96×10^{15}	4.39×10^{15}

In Fig. 6, we present a comparison between the temporal variation of the free-electron line density, $\mathcal{N}_e$ (evaluated to a radius of 0.6 cm) for the three cases: (I) A steplike laser pulse that also has a flat radial distribution, so that $I^I = 10^6$ W cm^{-2} for $t>0$ and $0<r<0.6$ cm. (II) A laser pulse having a realistic time history, given by Eq. (35), but a flat radial distribution out to 0.6 cm. The energy pulse of the laser is assumed to be 0.808 J, which corresponds to a peak laser irradiance of 10^6 W cm^{-2}. (III) A realistic laser pulse having a time history, given by Eq. (35), and a Gaussian radial distribution, given by Eq. (37), with an exponential radius of 0.2 cm. The energy of the laser pulse is assumed to be 0.091 J.

It might be pointed out that these errors do not in any way modify our conclusions as the change in the effective ionization time for the case of the realistic laser pulse is still close to double that obtained with a steplike pulse.

Appendix E

THE INFLUENCE OF MOLECULAR NITROGEN UPON PLASMA CHANNEL FORMATION BY LASER RESONANCE SATURATION*

R. M. Measures, S. K. Wong and P. G. Cardinal

Institute for Aerospace Studies
University of Toronto
4925 Dufferin Street
Downsview, Ontario, Canada
M3H 5T6

Abstract

Laser resonance saturation of alkali vapours represents a very attractive method of creating the extended plasma channels of interest in light ion beam fusion. We have undertaken a preliminary study of the influence of molecular nitrogen upon this laser ionization technique. Our results indicate that the electron cooling, resonance quenching and the increase in the laser energy requirement are acceptable, providing that the alkali seeding exceeds 0.5%.

*Work supported by the U.S. Sandia National Laboratory under Contract No. 49-2859A and a grant from the Natural Science and Engineering Research Council of Canada.

1. INTRODUCTION

A fusion reactor based upon *multiple light ion beam drivers* promises to be less expensive and more efficient than other inertial confinement reactor schemes. The light ion beam approach to fusion also lends itself to methods of minimizing the wall loading of such a reactor by employing a large reactor cavity and using an atmosphere that will absorb most of the energy liberated (other than that released in the form of fast neutrons) when the fuel pellet undergoes fusion. A *stand off* distance of several meters may be required in order to protect the array of ion diodes from the microexplosion and this will necessitate the development of an efficient mode of ion beam transport across the reactor chamber.

There is a reasonable body of experience that has demonstrated that light ion beams can be efficiently transported for distances of at least one meter by means of current carrying plasma channels.[1-3] These plasma channels provide both charge and beam current neutralization and sufficient azimuthal magnetic field to confine and guide the ions. Recent experiments have also shown that these discharge channels can be initiated and guided by laser heating of a molecular gas.[4,5] In this work a CO_2 laser is used to vibrationally excite ammonia molecules thereby creating a low density, very weakly ionized channel for guiding the discharge. Although this approach may be adequate for testing the concept it is unlikely to be a candidate for a fusion power reactor where the ambient temperature could be in excess of 1000°K.

We have proposed[6] that saturating a strong transition within one of the gaseous constituents (such as lithium vapour) of a fusion reactor with an appropriately tuned laser represents an almost ideal method of creating the multiple electrical discharge guide paths. In regard to this task the advantages inherent in our proposed *laser ionization based on resonance saturation* - LIBORS technique are:

(1) *High Efficiency* due to the large cross sections involved in directly converting the laser energy into ionization and electron energy.
(2) *Complete Ionization* (> 95%) of laser pumped species along the path of the laser beam, even for relatively modest values of laser irradiance.
(3) *Uniform Plasma Channels* should be formed due to the linear rate of energy deposition along the path of the laser beam.
(4) *Superelastic Heating* of the free electrons to provide high conductivity channels.

(5) *Rapid Formation* of the plasma channels through exponential growth of ionization.
(6) *Minimum Pellet Preheat* by the laser radiation due to the modest demand of laser energy.
(7) *Compatibility of the constituent* (such as lithium vapour), that is amenable to LIBORS, with the proposed operating conditions within a fusion reactor.
(8) *Resonance Line Lasers* currently under development[7] could lead to a simplification of the design and operation of the lasers required for LIBORS.

In our initial study[6] we have shown that a laser pulse of less than 1 joule would be required to create a plasma channel with an electron density of close to 10^{15} cm^{-3} over a 5m path in the case of a 0.1 torr sodium atmosphere. Furthermore, we can say, based on our recent development of a simple model of LIBORS,[8,9] that this estimate would also apply to a similar lithium atmosphere. This can be seen by reference to figure 1 where the variation in the 95% ionization burnout time with laser irradiance is presented for lithium, sodium, potassium and rubidium. Although these ionization times were estimated on the basis of a spatially uniform, step-like laser pulse, we have recently shown[9] that in the case of sodium, allowance for a realistic laser pulse (both spatially and temporally) should only lead to a doubling of the *observed* ionization time. By way of illustration, in figure 2, we present the time history of the growth in the *free electron line density*, $\mathcal{N}_e(t)$ for three kinds of laser pulse.

An analysis[10] of the radiant heat pulse, from the fusion created fireball within the atmosphere of a light ion beam reactor, has suggested that it might lead to excessive loading of the reactor walls. A more recent analysis[11] has found that seeding this argon atmosphere with as little as 0.2% of sodium vapour could degrade this heat pulse to a more satisfactory level. Thus it would appear that the alkali vapour could serve two useful purposes within the reactor. The possibility of using a molecular gas as the main constituent of the reactor cavity atmosphere has also been suggested.[11]

In this paper we report on an initial study of the influence of molecular gas upon the plasma channel formation potential of LIBORS. Nitrogen was chosen as a representative molecular gas with no obvious disadvantage. In particular, we set out to see if laser resonance saturation of sodium vapour could still

lead to the formation of a plasma channel, with an electron density of close to 10^{15} cm^{-3}, in a time of less than 1 μsec in the presence of molecular nitrogen at a density of at least 2×10^{17} cm^{-3}. In addition we have evaluated the *increase in the minimum laser energy required for the creation of such channels* by this background gas. Where possible we have made simplifying assumptions that are strongly conservative and we therefore expect that our results will, if anything, probably overpredict the laser energy required to create these plasma channels. Even so, our analysis is encouraging for it appears that LIBORS still represents an efficient and low energy method of producing the discharge guide path necessary for ion beam transport.

2. LASER IONIZATION WITH NITROGEN BACKGROUND GAS

The presence of an appreciable background density of a molecular gas such as nitrogen will invariably have a detrimental effect on the laser ionization process. Clearly the large number of internal energy states associated with a molecule will represent an effective *sink* for the energy of both the free electrons and the laser excited species. The most serious of these are considered below:

Potential Influence of Nitrogen

(i) *Free electron cooling through excitation, dissociation and ionization of the nitrogen molecules, viz.,*

$e^- + N_2 \rightarrow N_2^+ + 2e^- - (15.58\ \text{eV})$ *Ionization*

$e^- + N_2 \rightarrow N^+ + N + 2e^- - (14.54\ \text{eV})$ *Dissociative Ionization*

$e^- + N_2 \rightarrow N + N + e^- - (9.76\ \text{eV})$ *Dissociation*

The group of interactions shown above are all expected to be unimportant due to the relatively low electron temperature found in LIBORS of the alkali metal vapours (typically ≤ 1 eV). In the case of

$e^- + N_2 \rightarrow N_2^* + e^- - (\geq 6.2\ \text{eV})$ *Electronic Excitation*

the energy spacing between the ground state ($X^1\Sigma_g^+$) of N_2 and its first excited electronic state ($A^3\Sigma_g^+$) is about 6.2 eV and so electronic excitation of N_2 should also be relatively unimportant unless the alkali seeding drops below 0.1%.

$e^- + N_2 \rightarrow N_2 + e^- - (\approx 0.01\ \text{eV})$ *Rotational Excitation*

has also been neglected in the present analysis due to the small cross section and small amount of energy exchanged in this interaction. Thus the primary cooling mechanism for the free electrons has been assumed to result from:

$e^- + N_2(w) \rightarrow N_2(u) + e^- - (\epsilon_u - \epsilon_w)$ *Vibrational Excitation*

of the nitrogen molecules, where $\Delta\epsilon_{uw} = \epsilon_u - \epsilon_w = (u - w) \times 0.29$ (eV). ϵ_v represents the energy of vibrational state described by the v-vibrational quantum number and $u > w$.

(ii) Quenching of the laser excited resonance state through vibrational excitation of nitrogen molecules

$Na(3p) + N_2(w) \rightarrow Na(3s) + N_2(u) + [E_{21} - \Delta\epsilon_{uw}]$

where E_{21} represents the sodium resonance energy (equal to the laser photon energy).

We see that for each resonance state atom quenched by collision with a nitrogen molecule, the excess energy between the resonance energy and that required to vibrationally excite the molecule from w to u, goes into translational energy of the colliding species, thereby heating the gaseous mixture. (13)

(iii) Depletion of the alkali seed atoms through the formation of nitrides has been assumed to be negligible due to the low decomposition temperature of these compounds (e.g., NaN_3 decomposes for $T > 300$ K).

(iv) Removal of low energy electrons through the formation of N_2^- appears to be negligible due to the negative electron affinity of N_2. (14)

It is apparent that the two most important interactions to be considered are, *electron cooling* and direct *resonance level quenching* through vibrational excitation of the nitrogen molecules. We shall now consider each in turn.

Electron Cooling Through Vibrational Excitation of Nitrogen

The total electron-nitrogen scattering cross section is found to peak just in the energy range of interest. (15) The magnitude and structure of this cross section is associated with a resonance interaction that leads to the vibrational excitation of N_2 through the momentary formation of N_2^- according to Herzenberg (16) and Birtwistle and Herzenberg. (17) The absence of an electric dipole moment for N_2 ensures that the probability of direct vibrational excitation is small. (15)

The LIBORS energy equation (8) for the free electrons in the presence of nitrogen molecules can be written in the form

$$\frac{d}{dt}(N_e\epsilon_e) = N_2N_eK_{21}E_{21} + (2E_{21} - E_{c2})N_2\sigma_{2c}^{(2)}F^2 + \frac{1}{2}(2E_{21} - E_A)N_2^2\sigma_A v$$
$$+ \frac{1}{2}(3E_{21} - E_{c1})N_2^2\sigma_L F v + \sum_{n>2}(E_{21} - E_{cn})N_n\sigma_{nc}^{(1)}F$$
$$- N_e\sum_{n>1}N_nK_{nc}E_{cn} - N_eC - N_e^2H_{ei} - N_eNH_{ea}$$
$$+ N_e^3\sum_{n>1}K_{cn}E_{cn} - N_e^2\epsilon_e\sum_{n>1}\beta(n) + N_e\sum_{u>w}\sum\langle\sigma v\rangle_{uw}^{e}n_u\Delta\epsilon_{uw}$$
$$- N_e\sum_{u>w}\sum\langle\sigma v\rangle_{wu}^{e}n_w\Delta\epsilon_{uw} \qquad (1)$$

where ϵ_e (J) represents the mean translation energy and N_e the density of the free electron. Note N_2 in this equation represents the sodium resonance state population density and N_n (cm^{-3}) represents the population density of the n level in sodium. n_u and n_w represent the respective nitrogen population densities in the u and w vibrational states of the ground electronic state.

The first term on the RHS of equation (1) represents the superelastic heating term for the free electrons arising from electron collision quenching of the laser sustained resonance level population. E_{mn} (J) represents the energy separation between levels m and n of the *laser pumped species*, LPS. E_{cn} represents the ionization energy of level n of LPS and K_{cn} represents the three-body recombination rate coefficient for level n. The next three terms of equation (1) represent the contribution to the free electron energy from the three most likely electron seed creation processes. In the case of sodium:

(i) Resonance State Two-Photon Ionization
$Na(3p) + 2h\nu \rightarrow Na^+ + e^- + KE$ (≈ 1.17 eV)

(ii) Associative Ionization
$Na(3p) + Na(3p) \rightarrow Na_2^+ + e^- + KE$ (≈ 0.04 eV)

(iii) Laser-Induced Penning Ionization
$Na(3p) + Na(3p) + h\nu \rightarrow Na^+ + Na(3s) + e^- + KE$ (≈ 1.17 eV)

Na(3p) and Na(3s) represent a resonance and ground state atom, respectively. $h\nu$ represents the laser photon energy and corresponds to the energy difference between the resonance and ground states, E_{21}. $\sigma_{2c}^{(2)}$ (cm^4 sec) represents the two-photon ionization rate coefficient (sometimes referred to as the generalized cross section) for the resonance level, σ_A and E_A represent, respectively, the cross section and ionization energy corresponding to associative ionization, σ_L represents the cross section for laser-induced Penning ionization, v represents the mean velocity of the LPS.

$\sigma_{nc}^{(1)}$ (cm^2) represents the single photon ionization cross section for level n, and the sum extends over all levels $n > 2$ for which ionization by a single laser photon can be achieved, F (photons cm^{-2} sec^{-1}) represents the appropriate photon flux per unit area of the laser beam, i.e.,

$$h\nu F = \int I^{\lambda}(\nu)d\nu.$$

C represents the loss of energy per electron due to the net collisionally induced upward movement of bound electrons (exclusive of the resonance

superelastic term) and is given by

$$C = \sum_{n=1}\sum_{m>n}(N_mK_{mn} - N_nK_{nm})E_{mn} + N_2K_{21}E_{21}$$

where $N_2K_{21}E_{21}$ represents the laser-induced superelastic heating term for the free electrons. H_{ei} represents the rate of elastic energy transfer to ions through Coulomb scattering collisions and if the electrons and ions have Maxwellian velocity distributions H_{ei} takes the form (18)

$$H_{ei} = \frac{e^4}{m_i}\left(\frac{8m_e}{\pi kT_e}\right)^{1/2}\left(\frac{T_e - T_i}{T_e}\right)\ln\left(\frac{9(kT_e)^3}{8\pi m_e e^6}\right)$$

where T_e (°K) and T_i (°K) represent the respective electron and ion temperatures (viz., $\epsilon_e = \frac{3}{2}kT_e$) and m_e (g) and m_i (g) their respective masses. e is the electronic charge (esu). N (cm^{-3}) represents the total neutral atom density, and H_{ea} represents the rate of elastic energy coupling between the free electrons and the neutral atoms. We can approximate H_{ea} by

$$H_{ea} \approx \left(\frac{8\epsilon_e}{\pi_e}\right)^{1/2}(T_e - T_a)\sigma_{ea}\frac{4m_e}{m_a}$$

where σ_{ea} represents the electron atom elastic scattering cross section. $\beta(n)$ represents the radiative recombination rate coefficient for level n of the LPS.

The last two terms of equation (1) take account of the energy gained and lost to the free electrons through vibrational de-excitation and excitation respectively. $\langle\sigma v\rangle_{wu}^{e}$ represents the electron collisional excitation rate coefficient for excitation from w to u.

The electron energy equation can be divided into two equations - one taking account of the rate of change of the electron density and the other gives the rate of change of the mean electron translational energy. If we assume that the free electrons are described by a Maxwellian velocity distribution corresponding to an electron temperature T_e, then we can write, for $\epsilon_e = \frac{3}{2}kT_e$,

$$\frac{3}{2}k\frac{dT_e}{dt} = \text{LIBORS terms} + \sum_{u>w}\sum\langle\sigma v\rangle_{uw}^{e}n_u\Delta\epsilon_{uw} - \sum_{u>w}\sum\langle\sigma v\rangle_{wu}^{e}n_w\Delta\epsilon_{uw} \qquad (2)$$

and

$$\frac{dN_e}{dt} = \text{LIBORS terms} \qquad (3)$$

We see that the influence of the nitrogen molecules is felt through their effect on T_e, and subsequently on the various electron collisional rate coefficients. In order to determine the extent of this influence we need to solve not only the atomic population rate equations and the energy equations, but also the appropriate set of nitrogen vibrational state population rate equations,

$$\frac{dn_u}{dt} = N_e\left\{\sum_{w\neq u}n_w\langle\sigma v\rangle_{wu}^{e} - n_u\sum_{w\neq u}\langle\sigma v\rangle_{uw}^{e}\right\}$$
$$+ \langle\sigma v\rangle^{E}\left[\sum_{w\neq u}(n_un_{u+1}P(u+1, u, w, w+1) + n_wn_{u-1}P(u-1, u, w, w-1)\right.$$
$$\left. - n_{w+1}n_uP(u, u+1, w+1, w) - n_{w-1}n_uP(u, u-1, w-1, w))\right] \qquad (4)$$

The first two summation terms in equation (4) take account of the electron induced rates of excitation and de-excitation of the ground electronic state having a vibrational quantum number "u". The subsequent four summation terms are concerned with the rate of creation and the rate of destruction of the population in this u-vibrational state through vibration-vibration energy exchange collisions between nitrogen molecules. Thus $\langle\sigma v\rangle^{E}$ represents the elastic (gas kinetic) collision rate coefficient between nitrogen molecules. P(u+1, u, w, w+1) represents the probability that in a collision between two nitrogen molecules there will be a vibrational exchange of energy equal to one quanta of vibration energy, i.e. the molecule that was in state-(u+1), drops to u, while the molecule that was in state-w is raised to w+1.

For a harmonic oscillator it can be shown that (19)

$$P(u+1, u, w, w+1) = P(u, u+1, w+1, w) = (u+1)(w+1)P(1, 0, 0, 1) \qquad (5)$$

and

$$P(u, u-1, w-1, w) = P(u-1, u, w, w-1) = uwP(1, 0, 0, 1) \qquad (6)$$

If we further introduce the total nitrogen density,

$$n_T = \sum_u n_u \tag{7}$$

and the average vibrational quanta,

$$\bar{v} = \sum_v v n_v / n_T \tag{8}$$

then we can write

$$\frac{dn_u}{dt} = N_e \left\{ \sum_{w \neq u} n_w \langle \sigma v \rangle^e_{wu} - n_u \sum_{w \neq u} \langle \sigma v \rangle^e_{uw} \right\} + \frac{1}{\tau^V} \left[(u+1)(\bar{v}+1) n_{u+1} - \{u + (2u+1)\bar{v}\} n_u + u\bar{v} n_{u-1} \right] \tag{9}$$

where

$$\tau^V = [\langle \sigma v \rangle^E n_T P(1, 0, 0, 1)]^{-1} \tag{10}$$

represents the effective relaxation time for vibrational exchange.

A set of equations of the form given by equation (9) need to be solved in conjunction with the normal set of LIBORS equations and the amended electron energy equation - equation (2). In general the rate of electron excitation from the lowest vibrational state is larger, or of the same order of magnitude, as that from any of the higher vibrational states. In addition a molecule in an excited vibrational state can be collisionally de-excited and heat the free electrons. Consequently, if we assume that essentially all of the nitrogen molecules are in their lowest vibrational state, the rate of electron cooling will be as large as possible and invariably we will underestimate T_e. This in turn will lead to a *conservative* estimate of the lengthening of the ionization time associated with the molecular background gas. With the assumption that all the nitrogen molecules are in the lowest vibrational state we avoid having to solve the set of vibrational rate equations and can write for the electron energy equation:

$$\frac{3}{2} k \frac{dT_e}{dt} = \text{LIBORS terms} - n_o \sum_{w>o} \langle \sigma v \rangle^e_{ow} \Delta\epsilon_{wo} \tag{11}$$

where n_o is set equal to the total nitrogen density.

It should also be noted that $\langle \sigma v \rangle^e_{ow}$ decreases as w increases and so in our preliminary work we have summed to $w = 4$ in equation (11). These rates were numerically evaluated from the cross-sectional data available in the literature.[20] The subsequent vibrational cooling term in equation (11) is dependent upon the electron temperature and is fitted by an expression of the form

$n_o A T_e^B \exp(CT_e)$ in our LIBORS code, where $A = 1.315 \times 10^{-35}$, $B = 7.341$ and $C = -7.32 \times 10^{-4}$ and T_e is in K.

Resonance Quenching Through Vibrational Excitation of Nitrogen

In addition to cooling the electrons the nitrogen molecules will also quench the resonance state sodium atoms through the following interaction

$$Na(3p) + N_2(w) \rightarrow Na(3s) + N_2(u) + (E_{21} - \Delta\epsilon_{uw})$$

Here again $N_2(w)$ and $N_2(u)$ represent nitrogen molecules in the w and u vibrational states, respectively. In such a quenching collision the vibration energy of the nitrogen molecule is increased and the difference between the atom resonance energy and the gain in vibrational energy will appear in the form of increased translational energy of the collision partners. This form of heating will be considered later.

Each time a sodium resonance atom is returned to its ground level by a quenching collision an additional laser photon is required to elevate the atom back to its resonance state. In effect this raises the value of the *saturated spectral irradiance*, $I_s(\nu)$. As was first shown by the author,[21] the resonance and ground level populations of the laser excited atoms are only locked in the ratio of their degeneracies, g, if $I^\ell(\nu) \gg I_s(\nu)$, where $I^\ell(\nu)$ is the laser spectral irradiance (assumed broadband compared to the atomic linewidth). *The saturated spectral irradiance*

$$I_s(\nu) = \frac{8\pi h\nu^3}{c^2(1+g)} \left\{ \frac{\tau^{RAD}}{\tau} \right\} \tag{12}$$

where $h\nu$ is the laser photon energy, c is the velocity of light, ν is the frequency of the laser radiation, τ^{RAD} is the radiative lifetime of resonance level and τ is the actual lifetime in the presence of quenching collisions.

In the case of the sodium resonance transition,

$$I_s(\nu) = 6.07 \times 10^{-10} \text{ Wcm}^{-2} \text{ Hz}^{-1}$$

in the absence of collisional quenching. If the laser bandwidth is about 0.1 nm (or 86 GHz) this corresponds to stating that for saturation

$$I^\ell \gg 52 \text{ Wcm}^{-2}$$

In general we can write

$$\frac{1}{\tau} = A_{21} + N_e \left\{ K_{21} + K_{12} + \sum_{n>2} K_{2n} \right\} + \sum_u n_u \sum_w \langle \sigma v \rangle^Q_{uw} \tag{13}$$

where $\langle \sigma v \rangle^Q_{uw}$ is the nitrogen collision quenching rate involving vibrational transitions from u to w and A_{21} represents the Einstein spontaneous transition probability for the resonance to ground transition. If we assume as before that the majority of the nitrogen molecules are in the lowest vibrational level of ground electronic state then we can write

$$\frac{1}{\tau} = A_{21} + N_e \left\{ K_{21} + K_{12} + \sum_{n>2} K_{2n} \right\} + C^Q_{21} \tag{14}$$

where

$$C^Q_{21} = n_o v^Q \sum_w \sigma^Q_{ow} \tag{15}$$

and

σ^Q_{ow} is the effective cross section for vibrational excitation from o to w through quenching with Na(3p),

$v^Q = \left\{ \frac{8kT}{\pi\mu} \right\}^{1/2}$

T is the gas temperature, and

μ is the reduced mass for the sodium-nitrogen collision.

In table 1 we present estimates[22,23] of the Na(3p)-N_2 quenching cross sections and the corresponding energy defects, $E_{21} - \Delta\epsilon_{ow}$. In the absence of nitrogen the electron superelastic quenching leads to a minimum resonance state lifetime of about 12.5 nsec (compared to $\tau^{RAD} = 15.9$ nsec) for a sodium atom density of 10^{15} cm^{-3}, corresponding to a vapour temperature of 613 K.[24]

The presence of 2×10^{17} cm^{-3} of nitrogen molecules further reduces this lifetime to about 7.6 nsec which in turn increases the requirement for laser saturation, from equation (12)

$$I^\ell \gg 109 \text{ Wcm}^{-2}$$

This poses no problem as the values of laser irradiance throughout our analysis considerably exceeds this value.

The power extracted per unit volume from the laser field resulting from these nitrogen quenching collisions can be expressed in the form

$$Q^\ell_{n_o} = n_o N_2 v^Q E_{21} \sum_w \sigma^Q_{ow} \tag{16}$$

and is included in the LIBORS code to allow for the additional laser power density absorbed in the presence of nitrogen. N_2 is again the sodium resonance state density.

For times somewhat less than the ionization time we can approximate equation (16) by the form

$$Q^\ell_{n_o} = G n_o N_o v^Q E_{21} \sum_w \sigma^Q_{ow} \tag{17}$$

where we have assumed laser saturation which gives[21]

$$N_2 = GN_o \tag{18}$$

with

$$G = \frac{g}{1+g} \tag{19}$$

For $N_o = 10^{15}$ cm^{-3}, $n_o = 2 \times 10^{17}$ cm^{-3} we have $Q^\ell_{n_o} = 1.3 \times 10^4$ Wcm^{-3} using the values of σ^Q_{ow} given in table 1. This represents a fairly large rate of laser energy deposition into the nitrogen gas. Indeed, the rate of translationally heating the nitrogen molecules (ϵ_{n_o} is mean thermal energy of a nitrogen molecule) is given by the expression

$$\frac{d\epsilon_{n_o}}{dt} = GN_o v^Q \sum_w \sigma^Q_{ow} (E_{21} - \Delta\epsilon_{ow}). \tag{20}$$

At $N_o = 10^{15}$ cm^{-3} and $n_o = 2 \times 10^{17}$ cm^{-3} equation (20) gives

$$\frac{d\epsilon}{dt} n_o = 1.35 \times 10^5 \text{ eV sec}^{-1} \text{ molecule}^{-1}.$$

and leads to an increase in temperature of 157 K for each 100 nsec of laser irradiation (until appreciable ionization occurs).

This gas heating would invariably lead to thermal depopulation of the vibrational ground state and as indicated earlier would reduce the electron cooling rate. This would mean that τ_e would be higher and the ionization time reduced. This is consistent with our statement that our calculations would be conservative. That is to say our estimate of the increase in laser energy required in the presence of N_2 will be larger than required in reality.

We have also omitted the ion-nitrogen translation energy exchange terms from the ion energy equation. Such a term would, in effect, tend to prevent the ion temperature from rapidly rising towards the electron temperature and thereby mean that the electron-ion energy loss term ($N_e^2 H_{ei}$ of equation 1) would remain large for a longer period. This should not affect the ionization time and in order to test this we ran one case where the ion temperature was forced to stay at room temperature (an extreme example). The results of this run confirmed our justification for avoiding the complexity of including the ion-nitrogen energy exchange terms.

LIBORS Computer Code Results With and Without Nitrogen

In order to see which of the *seed ionization processes* is likely to dominate at any given value of laser irradiance we have evaluated the ionization rate for each as a function of I^ℓ assuming a $N_o = 10^{15}$ cm^{-3}. The results (for the cross sections used in most of our code runs) are presented as the full lines in figure 3. It is evident that associative ionization will dominate for $I^\ell \leq 2 \times 10^7$ Wcm^{-2}, while two photon ionization of the resonance level will be the primary seed ionization process for higher values of laser irradiance.

Recent experiments[25] have suggested that the laser induced Penning cross section, σ_L, could be as large as 5.6×10^{-41} cm^4 sec and so we have added this result (broken curve) to figure 3. Clearly, if this is correct laser induced penning ionization is likely to be the dominant seed electron creation process over the I^ℓ range of interest. Nevertheless, most of our LIBORS code runs used the smaller value of 2×10^{-44} cm^4 sec for σ_L. It is evident that if we had used the larger value of σ_L the ionization time would have been somewhat shorter and this would have the effect of reducing the amount of laser energy required to form a plasma channel of a given length. We have proved this to be the case for one set of conditions where the ionization burnout time was indeed reduced by about a factor of 3.

This reaffirms our assertion that our predictions will be conservative.

In table 2 we present the results of a broad series of LIBORS code runs used to gauge the likely conditions of interest. These runs were also used to ascertain the degree of ionization achievable within 1 μsec at a laser irradiance of 1 MWcm^{-2}. The results are presented in figure 4 and from these we can see that in order to obtain an appreciable degree of ionization (i.e., $\alpha > 50\%$), the sodium doping density $N_o \geq 5 \times 10^{15}$ cm^{-3} for a nitrogen density $n_o \simeq 3 \times 10^{18}$ cm^{-3}.

Since the presence of nitrogen leads primarily to a cooling of the electrons we decided to check the variation of this cooling with sodium density for a given laser irradiance and nitrogen density. The results are presented in figure 5 where it is evident that both the plateau and minimum values of the electron temperature decrease with decreasing sodium density for a given nitrogen density. The corresponding variation in ionization burnout time can be seen by reference to figure 6. Clearly, the ionization time increases and the final electron density achieved decreases with decreasing N_o. It is evident from these results that plasma channel formation with an electron density of about 10^{15} cm^{-3} should be attainable within 1 μsec provided $N_o \geq 10^{15}$ cm^{-3}, $I^\ell \geq 10^6$ Wcm^{-2} and $n_o \leq 2 \times 10^{17}$ cm^{-3}. The value of 2×10^{17} cm^{-3} for the nitrogen density is in keeping with current thinking about the likely atmospheric conditions within a light ion beam fusion reactor.[12]

We can gauge directly from the influence of a nitrogen atmosphere of about 13 torr upon the maximum electron density, peak electron temperature and ionization burnout time attained with $I^\ell = 10^6$ Wcm^{-2}, for $N_o = 10^{15}$ cm^{-3} by reference to figure 7. The full lines correspond to laser ionization in the absence of nitrogen, while the broken curves refer to the case where $n_o = 2 \times 10^{17}$ cm^{-3}. It can be seen that the presence of the nitrogen reduces both the peak and the final electron temperature by about a third and this, in effect, doubles the ionization time and prevents full ionization (84% as opposed to 99.9% for $n_o = 0$) from being attained.

The difference in the power density extracted from the laser field Q^ℓ, under these same conditions, can also be seen from figure 8, where the temporal variation in Q^ℓ is presented with that of both the resonance state N_2 and electron densities, N_e. Clearly, although Q^ℓ reaches a peak where the product $N_2 N_e$ is a maximum for both $n_o = 0$ and $n_o = 2 \times 10^{17}$ cm^{-3}, implying that electron superelastic quenching always dominates the peak absorption. It is quite apparent that the presence of the nitrogen significantly increases the laser power density required prior to this peak. We shall return to this point in the next section.

In figure 9, we present the variation of the 75% ionization time, τ_B,

where Q^ℓ_{max} is taken to be the peak value of Q^ℓ corresponding to the $I^\ell = 10^8$ Wcm^{-2} runs, i.e.,

$$Q^\ell_{max} = Q^\ell_{max}(N_o, n_o, I^\ell = 10^8) \qquad (25)$$

The *ionization burnout time*, from equation (21), becomes

$$\tau_B^\ell(N_o, n_o, I_o^\ell, L) = \left[a(N_o, n_o) + b(N_o, n_o)(I_o^\ell - Q^\ell_{max} L)^{x(N_o, n_o)} \right]^{-1} \qquad (26)$$

and from equation (22)

$$E_o^\ell(N_o, n_o, I_o^\ell, L) = \frac{I_o^\ell}{a(N_o, n_o) + b(N_o, n_o)(I_o^\ell - Q^\ell_{max} L)^{x(N_o, n_o)}} \qquad (27)$$

The values of a, b and x were obtained for the two sets of runs shown in figure 9, and

$$Q^\ell_{max} = \begin{cases} 1.50 \times 10^4 \text{ Wcm}^{-3} \text{ for } n_o = 0 \\ 2.04 \times 10^4 \text{ Wcm}^{-3} \text{ for } n_o = 2 \times 10^{17} \text{ cm}^{-3} \end{cases}$$

Equations (26) and (27) were used to show the variation of the laser energy with laser pulse length (chosen to achieve at least 75% ionization along a 5m long channel of 1 cm^2 cross sectional area, see figure 11. The full curve assumes $N_o = 10^{15}$ cm^{-3} and $n_o = 0$, while the broken curve assumes $N_o = 10^{15}$ cm^{-3} and $n_o = 2 \times 10^{17}$ cm^{-3}. Clearly the former situation leads to a minimum laser energy density, $E^\ell_{min} = 3.2$ J cm^{-2}, a corresponding laser pulse duration $\tau^\ell = 300$ nsec and $I^\ell_o = 1.07 \times 10^7$ Wcm^{-2}, while the latter case gives $E^\ell_{min} = 9.1$ J cm^{-2}, $\tau^\ell = 650$ nsec and $I^\ell_o = 1.4 \times 10^7$ Wcm^{-2}.

We see that although the presence of 13 torr of nitrogen increases the minimum laser energy density required for creating a 5m plasma channel from 3.2 Jcm^{-2} to 9.1 Jcm^{-2}, this is not excessive. Furthermore the actual laser energy required to create such a channel can still be less than 1J if a 0.1 cm^2 channel cross sectional area is acceptable and consistent with laser beam divergence and beam shaping optics. It should also be noted that the increase in the laser pulse duration (300 nsec to 650 nsec) is also reasonable as it would lead to an ionization time that is within the time required to avoid turbulent break-up of the channel (> 1 μsec).

with laser irradiance for $N_o = 10^{15}$ cm^{-3}, $n_o = 0$ (●-points) and $n_o = 2 \times 10^{17}$ cm^{-3} (○-points). The full and broken curves are respective fits to these data by a relation of the form:

$$\tau_B = \frac{1}{a + b(I^\ell)^x} \qquad (21)$$

We can see from figure 9 that for values of laser irradiance ranging from 10^6 to 10^8 Wcm^{-2}, the sodium vapour ionization time is roughly doubled in the presence of 13 torr of nitrogen as a result of electron cooling.

Nitrogen Effects on Laser Requirements for Plasma Channel Creation

We shall now proceed to estimate the energy density of the laser pulse needed to create a plasma channel of length L in sodium vapour of initial atom density, $N_o = 10^{15}$ cm^{-3} in the absence of any nitrogen background gas. We shall then recalculate the energy density required in the presence of 13 torr of nitrogen (i.e., $n_o = 2 \times 10^{17}$ cm^{-3}). As previously shown[6] the ionization time increases with depth for as the laser pulse burns its way through the sodium vapour its irradiance decreases. This will mean that even if the original laser pulse were step-like its temporal nature will change with penetration into the vapour column. Although we are currently working on this complex problem the analysis included in this report assumes that we are always dealing with a step-like laser pulse. We therefore assume that the laser energy density required to create a plasma channel can be written in the form

$$E_o^\ell \simeq I_o^\ell \tau_B^f \qquad (22)$$

where I_o^ℓ (Wcm^{-2}) represents the incident laser irradiance and τ_B^f (sec) represents the 75% ionization time after a penetration depth L (cm). Under condition of laser saturation it has been shown[6] that the laser irradiance at the end of the channel length

$$I_f^\ell = I_o^\ell - Q^\ell L \qquad (23)$$

This relation assumes that the laser power density absorbed is independent of the laser irradiance (and therefore position). This is not strictly true for $I^\ell \geq 10^7$ Wcm^{-2}, as can be seen from figure 10. The deviation from constant Q^ℓ is due primarily to the growing importance of single photon ionization at the higher values of laser irradiance. Thus to be conservative we shall in fact write

$$I_f^\ell = I_o^\ell - Q^\ell_{max} L \qquad (24)$$

In figure 12 we have evaluated the variation in the *minimum laser energy density* with length required to achieve at least 75% *ionization* in pure sodium vapour at about 60m torr ($N_o = 10^{15}$ cm^{-3}) and in the presence of about 13 torr ($n_o = 2 \times 10^{17}$ cm^{-3}) of nitrogen.

3. CONCLUSIONS

An inertial confinement fusion reactor based upon light ion beam drivers will require an efficient means of transporting the ion beams across the reactor to the fuel pellet. It appears that multiple plasma discharge channels could accomplish this task. One of the most attractive methods of ensuring that these discharge channels are straight, well defined and brought to a common focus is to create a system of well ionized plasma channels prior to striking the dischargea. *Laser ionization based on resonance saturation* of an alkali vapour has been proposed as ideal for the task of forming such highly ionized plasma channels very rapidly with a relatively low energy laser.

The purpose of the present study was to evaluate whether the presence of an appreciable background of molecular nitrogen was likely to effectively degrade this means of creating the discharge guide channels or to increase the laser energy requirement to the point where it might become impractical. In an attempt to compensate for the many poorly known cross sections used in our analysis we have been conservative wherever possible. Thus, although the accuracy of our analysis may not be better than a factor of two we feel that our conclusions will be reliable.

Our conclusions are:

(i) The primary effects of the nitrogen background gas upon LIBORS are to cool the free electrons, thereby increasing the ionisation time, and to increase the laser energy requirement.

(ii) Near to fully (> 90%) ionized channels can be rapidly created within a sodium (or lithium) seeded nitrogen atmosphere providing the alkali is present at a concentration of greater than 0.5%.

(iii) If the nitrogen density within a reactor is expected to be about 2×10^{17} cm^{-3}, then an electron density of close to 10^{15} cm^{-3} can be created over a 5m path with a sodium density of 10^{15} cm^{-3}, provided the laser energy density is at least 9.1 Jcm^{-2} and the pulse duration is about 650 nsec.

(iv) The ionization time could be reduced significantly, but only at the cost of much higher laser energy density. For example, full ionization could be achieved within 300 nsec along a channel of 5m length if a laser with an output energy density of 23 Jcm^{-2} were to be used.

(v) The presence of nitrogen not only cools the free electrons but in quenching the laser pumped species is itself directly heated. This could further improve the channel capabilities of LIBORS through the creation of a low density core to the channel.

In light of our encouraging theoretical results we would recommend that an extensive experimental program be undertaken to test our conclusions and to see if plasma channels created through laser resonance saturation offer any advantages over other approaches towards the formation of discharge guide channels. In particular, it would be worth comparing LIBORS with direct photoionization (either single or two photon) techniques. The latter only provides energy to the free electrons on their creation while in LIBORS the laser continues to provide energy through superelastic energy conversion. This could be important when an electron cooling background gas, such as nitrogen, is present. Another important difference expected between direct photoionization and LIBORS is the predicted gas heating associated with the latter. This leads to the formation of a hot, low density core to the channel.

It is expected that the choice between the competing laser techniques for creating the discharge guide channel will probably be made on the basis of which technique can create a channel that is of high enough quality to ensure very high transport efficiency for the ion beams at a laser energy that is small enough to avoid appreciable pellet preheat. We feel that LIBORS will prove to be the most suitable technique when all factors are taken into consideration.

Table I. Sodium/nitrogen resonance quenching cross sections and energy defects.

Vibrational Excitation	Q_{ov} ($\AA^2$)	$E_{21}-\Delta\epsilon_{ov}$ (eV)
0 → 3	3.74	1.23
0 → 4	5.86	0.94
0 → 5	7.81	0.65
0 → 6	6.23	0.36
0 → 7	1.9	0.07

Table II. LIBORS code results with and without nitrogen.

$I^{\ell} = 10^{6}$ Wcm^{-2} $\qquad \sigma_L = 2 \times 10^{-44}$ cm^{4}sec

$\sigma_{2c}^{(2)} = 1.66 \times 10^{-49}$ cm^{4}sec $\qquad \sigma_A = 5 \times 10^{-18}$ cm^2

Sodium Density N_o (cm^{-3})	Nitrogen Density n_o (cm^{-3})	Computer Run Time (nsec)	Electron Density Achieved N_e^{max} (cm^{-3})	Electron Temperature At end of Run T_e (K)
1×10^{15}	0	606	9.988×10^{14}	6275
5×10^{15}	0	220	4.982×10^{15}	6889
1×10^{16}	0	120	9.957×10^{15}	7581
1×10^{15}	2×10^{17}	1015	8.397×10^{14}	3935
5×10^{15}	2×10^{17}	412	4.702×10^{15}	4554
1×10^{16}	2×10^{17}	177	9.518×10^{15}	5090
1×10^{15}	3×10^{18}	1004	5.744×10^{11}	3288
5×10^{15}	3×10^{18}	825	3.439×10^{15}	3615
1×10^{16}	3×10^{18}	337	7.480×10^{15}	4006

REFERENCES

1. J. N. Olsen, D. J. Johnson, R. J. Leeper, Appl. Phys. Lett., 36, 808-810, 1980.
2. S. L. Bennett, S. C. Young, S. J. Stephanakis, F. W. Oliphant, G. Cooperstein, S. Goldstein, D. Mosher, Bull. of Am. Phys. Soc., 24, 1031, 1979.
3. R. J. Freeman, L. Baker, P. A. Miller, L. P. Mix, J. N. Olsen, J. W. Poukey, T. P. Wright, "Electron and Ion Beam Transport to Fusion Targets", Sand. 79-0734C, Sandia Laboratories, 1979.
4. J. N. Olsen and L. Baker, "Laser-Initiated Discharge Channels for Ion Beam Transport", Paper 4P4-APS Meeting, San Diego, Nov. 1980 (Bulletin of Am. Phys. Soc., 25, 899, 1980).
5. J. N. Olsen and R. J. Leeper, "Propagation of Ion Beams in Laser-Initiated Discharge Channels", Paper 2C1, 1981 IEEE International Conference on Plasma Science, Santa Fe, New Mexico, 18-20 May 1981.
6. R. M. Measures, N. Drewell and P. Cardinal, J. Appl. Phys., 50, 2662-2669, 1979.
7. D. J. Ehrlich and R. M. Osgood, Jr., Appl. Phys. Lett., 34, 655-658, 1979.
8. R. M. Measures and P. G. Cardinal, Phys. Rev. A23, 804-815, 1981.
9. R. M. Measures, P. G. Cardinal and G. Schinn, J. Appl. Phys., 52, 1269-1277, 1981.
10. G. A. Moses and R. R. Peterson, Nuclear Fusion 20, 849-857, 1980.
11. R. R. Peterson, G. W. Cooper and G. A. Moses, "Cavity Gas Analysis for Light Ion Beam Fusion Reactors", University of Wisconsin Report No. 371, 1980.
12. J. N. Olsen (private communication).
13. A. V. Eremin, A. A. Kulikovskii and I. M. Naboko, Opt. Spectrosc. 49, 9-13, 1980.
14. J. C. Y. Chen, J. Chem. Phys. 40, 3513, 1964 (see also Ref. 23).
15. S. C. Brown, "Electron-Molecule Scattering" (Wiley Interscience).
16. A. Herzenberg, J. Phys., B1, 548, 1968.
17. D. T. Birtwistle and A. Herzenberg, J. Phys., B4, 53, 1971.
18. H. Petschek and S. Byron, Ann. Phys. 1, 270, 1957.

19. J. F. Clarke and M. McChesney, "Dynamics of Relaxing Gases", Butterworth Inc., Boston, 1976.
20. J. Y. Chen, J. Chem. Phys. 41, 3863, 1964.
21. R. M. Measures, J. Appl. Phys., 39, 5232-5245, 1968.
22. E. Bauer, E. R. Fisher and F. R. Gilmore, J. Chem. Phys. 51, 4173-4181, 1969.
23. H. F. Krause, J. Fricke and W. L. Fite, J. Chem. Phys. 56, 4593-4605, 1972.
24. A. N. Nesmeyanov, "Vapour Pressure of the Elements", p. 443, Translator, J. I. Carasso.
25. J. Weiner and P. Polak-Dingels, J. Chem. Phys. 74, 508-511, 1981.

FIGURE CAPTIONS

1. Variation of 95% ionization burnout times, τ_B, with laser irradiance I^{ℓ} as predicted by simple model for lithium, sodium, potassium and rubidium, corresponding to initial density $N_o = 10^{15}$ cm^{-3}.
2. Comparison of the temporal variation of the *free electron line density* $\mathcal{N}_e$ of a sodium column evaluated to a *radius of 0.6 cm for the three cases:* (i) Steplike, flat laser pulse for $I^{\ell} = 10^{6}$ W cm^{-2}. (ii) Laser pulse is assumed to have realistic temporal variation but uniform radial distribution out to 0.6 cm. Energy in the pulse is set to be 0.808 J corresponding to a peak irradiance of 10^{6} W cm^{-2}. (iii) Laser pulse is assumed to have both a realistic temporal variation and a Gaussian radial distribution with an exponential radius of 0.20 cm and an energy of 0.091 J, giving a peak irradiance of 10^{6} W cm^{-2}.
3. Variation of three primary seed ionization rates with laser irradiance for sodium at 10^{15} cm^{-3}.

   $\left.\frac{dN_e}{dt}\right|_A$ - associative ionization rate, $\left.\frac{dN_e}{dt}\right|_L$ - laser induced penning ionization rate and $\left.\frac{dN_e}{dt}\right|_T$ - two photon resonance state ionization.
4. Percentage degree of ionization achieved within one microsecond for several sodium/nitrogen atmospheres assuming a laser irradiance of 10^{6} Wcm^{-2}.
5. Dependence of electron and ion temperature time histories on sodium density assuming 10^{6} Wcm^{-2} laser irradiance and a nitrogen density of 2×10^{17} cm^{-3}.
6. Dependence of electron density time histories on sodium density assuming a laser irradiance of 10^{6} Wcm^{-2} and a nitrogen density of 2×10^{17} cm^{-3}.
7. A comparison of the temporal variation in electron density N_e, electron temperature T_e and ion temperature, T_i, with (2×10^{17} cm^{-3}) and without nitrogen, assuming a laser irradiance of 10^{6} Wcm^{-2} and a sodium density of 10^{15} cm^{-3}.

8. A comparison of the temporal variation in the electron density, the resonance state density and the absorbed laser power density, q^{ℓ} (Wcm^{-3}), with (2×10^{17} cm^{-3}) and without nitrogen assuming a laser irradiance of 10^{6} Wcm^{-2} and a sodium density of 10^{15} cm^{-3}.

9. Variation of the 75% ionization time with laser irradiance for sodium density 10^{15} cm^{-3} assuming a zero and 2×10^{17} cm^{-3} density of nitrogen. LIBORS code points, (•) for $n_o = 0$ and (o) for $n_o = 2 \times 10^{17}$ cm^{-3}. Curves are analytical fits to the points of the form $\tau_{\beta} = [a+b(I^{\ell})^{x}]^{-1}$.

10. Dependence of laser absorbed power density q^{ℓ} time history upon laser irradiance for sodium density of 10^{15} cm^{-3} assuming zero (*full curves*) and 2×10^{17} cm^{-3} nitrogen (broken curves).

11. Variation of laser energy density, E^{ℓ} (Jcm^{-2}) with laser pulse duration necessary to achieve 75% ionization at the end of a 5m channel in sodium vapour at 10^{15} cm^{-3} and in sodium/nitrogen (10^{15} cm^{-3}/ 2×10^{17} cm^{-3}) atmosphere.

12. Dependence of the minimum laser energy density, E^{ℓ}_{min} (Jcm^{-2}), necessary to achieve 75% ionization burnout at the end of channel - upon the channel length, assuming sodium/nitrogen atmospheres of (10^{15} cm^{-3}/zero) and (10^{15} cm^{-3}/2×10^{17} cm^{-3}).

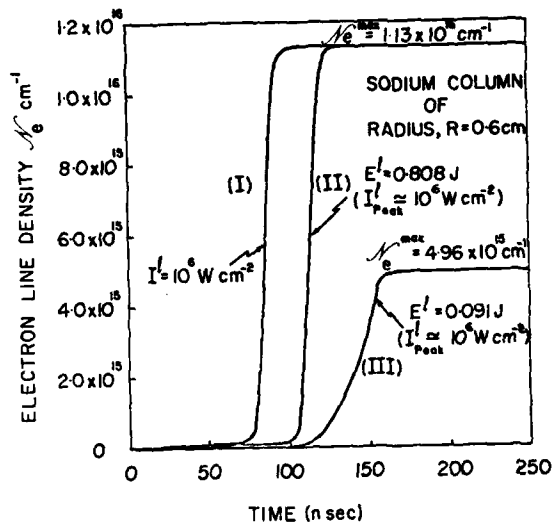

Fig. 2

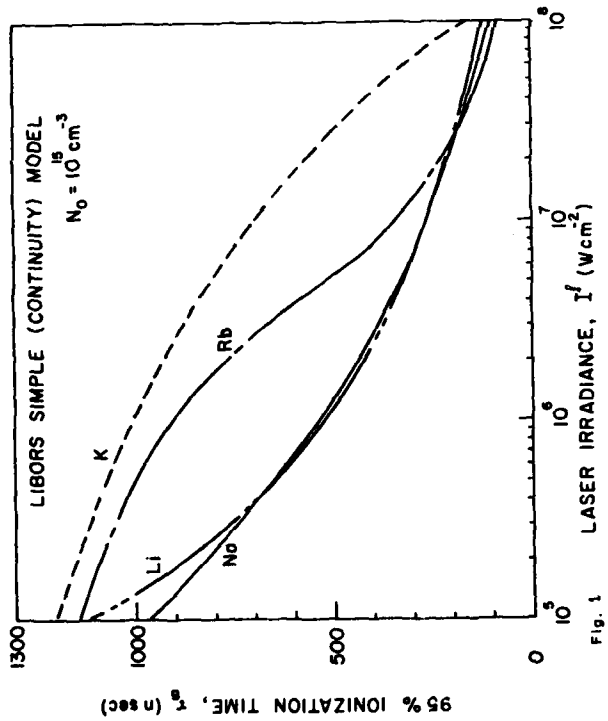

Fig. 1

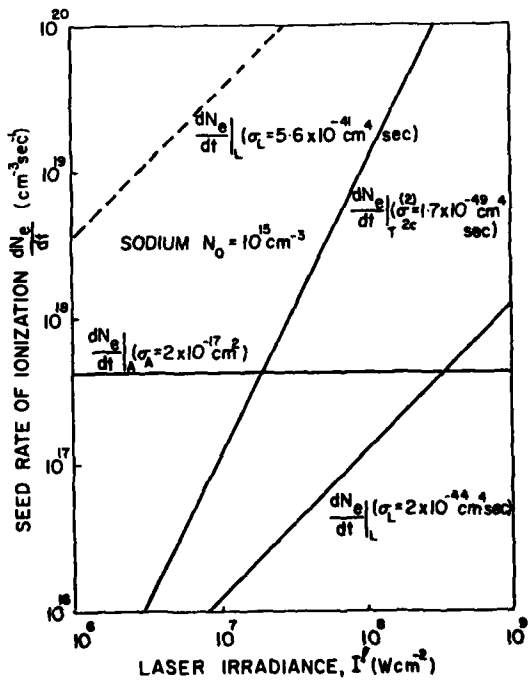

Fig. 3

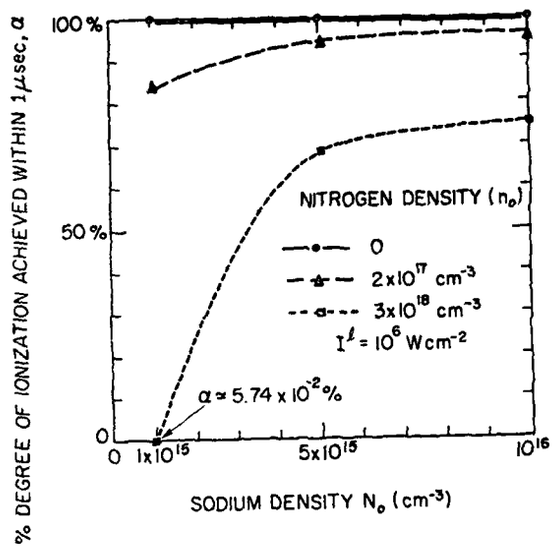

Fig. 4

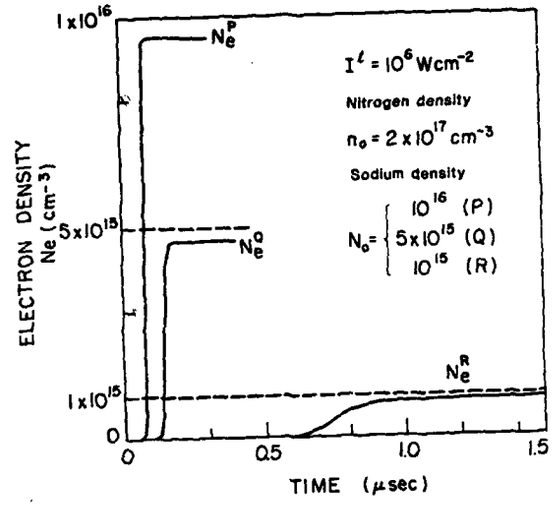

Fig. 6

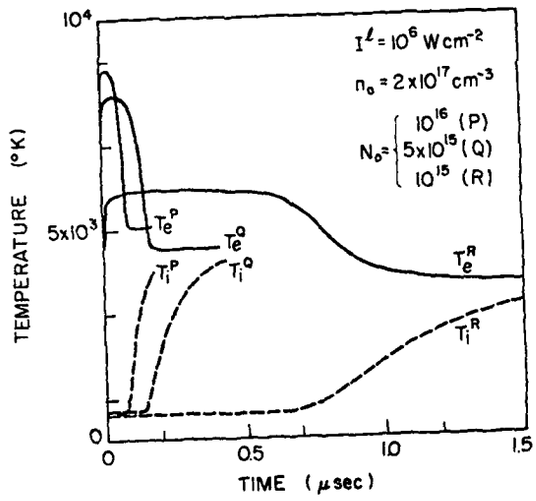

Fig. 5

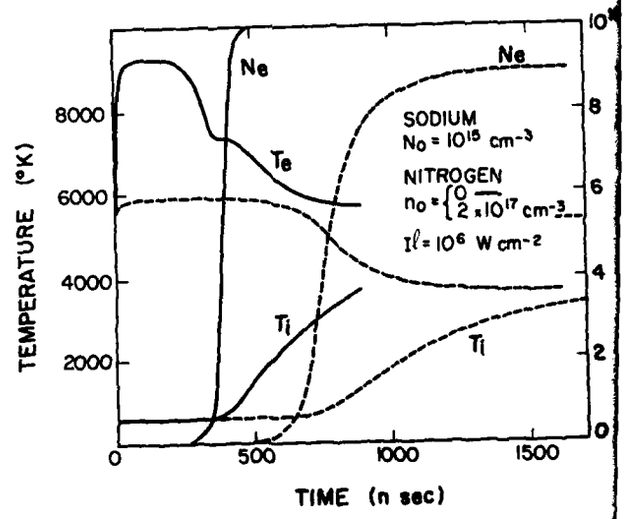

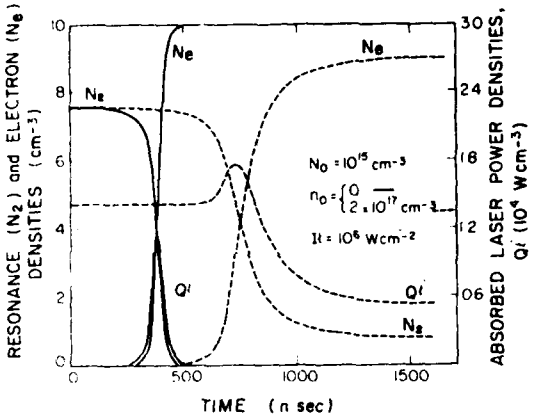

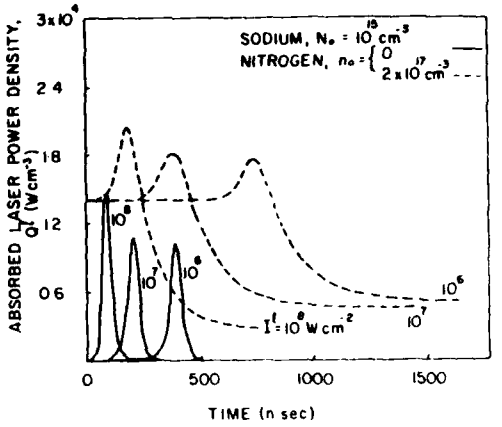

Fig 10

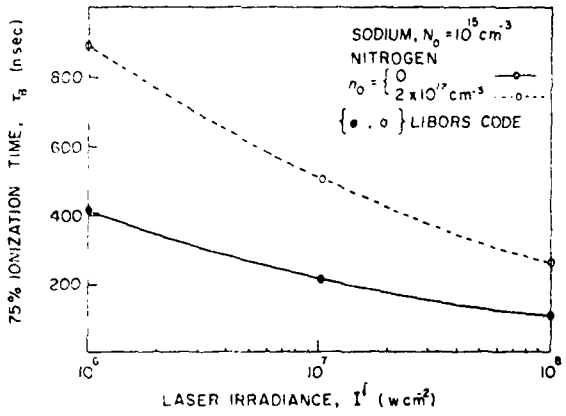

Fig 9

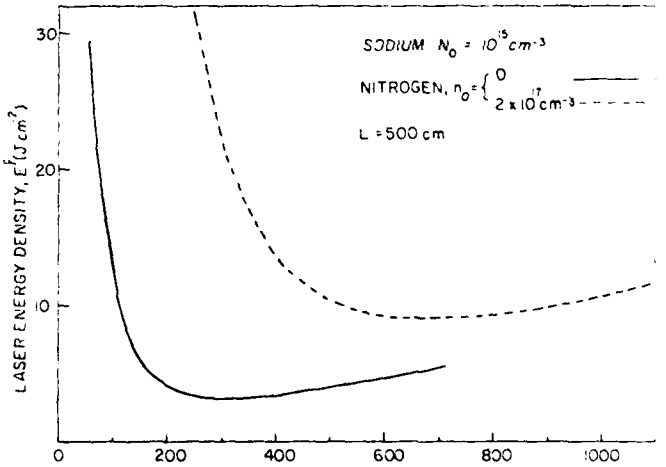

Fig 11

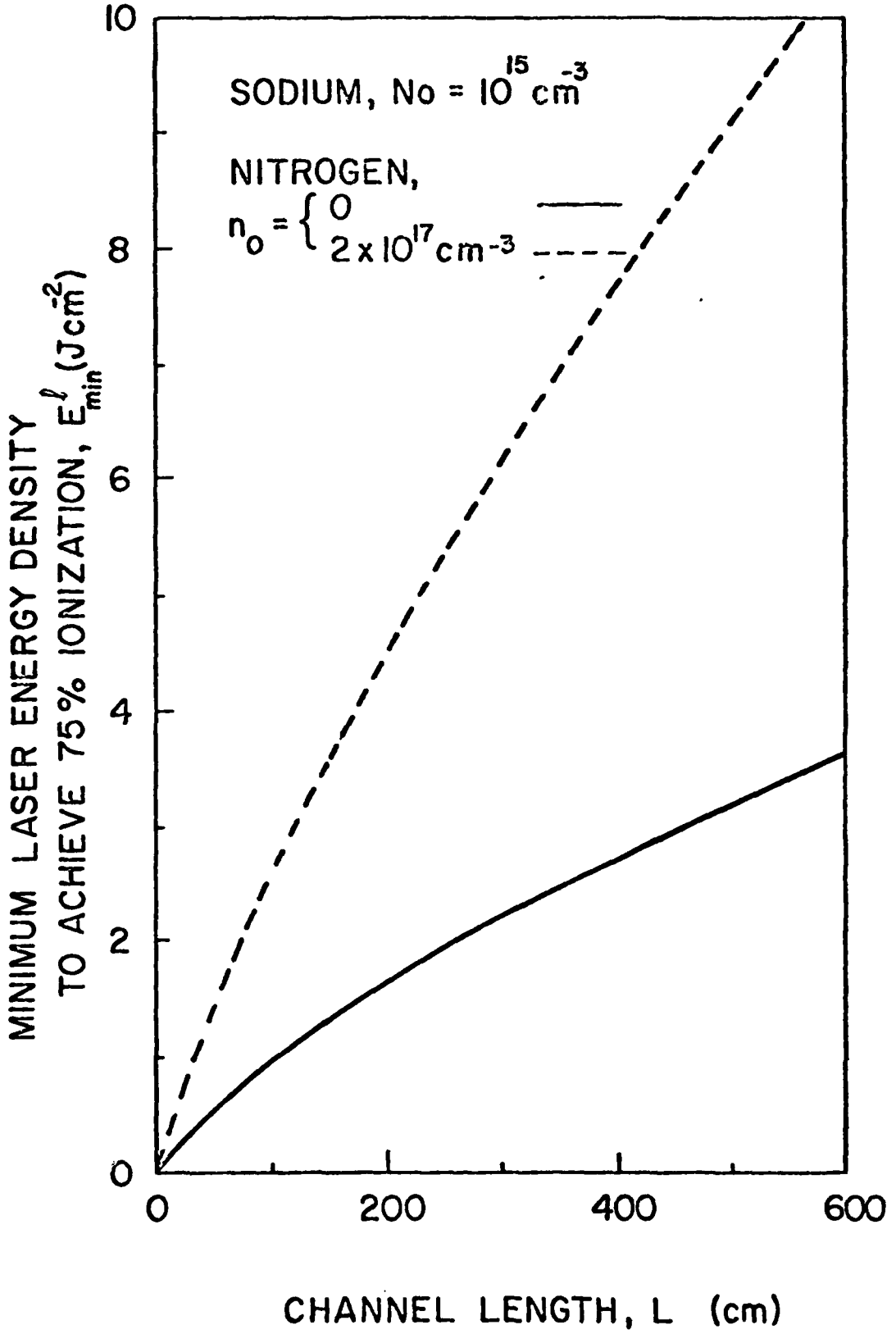
SODIUM, No = 10^{15} cm^{-3}
NITROGEN,
n_o = { 0
2×10^{17} cm^{-3}
MINIMUM LASER ENERGY DENSITY
TO ACHIEVE 75% IONIZATION, E^{ℓ}_{min} (Jcm^{-2})
0
2
4
6
8
10
0
200
400
600
CHANNEL LENGTH, L (cm)

Fig. 12

UNCLASSIFIED

SECURITY CLASSIFICATION OF THIS PAGE (When Data Entered)

REPORT DOCUMENTATION PAGE		READ INSTRUCTIONS BEFORE COMPLETING FORM
1. REPORT NUMBER	2. GOVT ACCESSION NO.	3. RECIPIENT'S CATALOG NUMBER
4. TITLE (and Subtitle) THE INFLUENCE OF MOLECULAR NITROGEN UPON PLASMA CHANNEL FORMATION BY LASER RESONANCE SATURATION		5. TYPE OF REPORT & PERIOD COVE 6. PERFORMING ORG. REPORT NUMBE
7. AUTHOR(s) R. M. Measures, S. K. Wong and P. G. Cardinal		8. CONTRACT OR GRANT NUMBER(s) AFOSR 80-0057A
9. PERFORMING ORGANIZATION NAME AND ADDRESS University of Toronto, Institute for Aerospace Studies, 4925 Dufferin St., Downsview, Ontario, Canada, M3H 5T6		10. PROGRAM ELEMENT, PROJECT, TA AREA & WORK UNIT NUMBERS
11. CONTROLLING OFFICE NAME AND ADDRESS Air Force Office of Scientific Research, Bldg. 410, Bolling Air Force Base, D.C. 23032 U.S.A.		12. REPORT DATE 13. NUMBER OF PAGES
14. MONITORING AGENCY NAME & ADDRESS(if different from Controlling Office)		15. SECURITY CLASS. (of this report) Unclassified 15a. DECLASSIFICATION/ DOWNGRADI SCHEDULE

16. DISTRIBUTION STATEMENT (of this Report)

Approved for public release; distribution unlimited.

17. DISTRIBUTION STATEMENT (of the abstract entered in Block 20, if different from Report)

18. SUPPLEMENTARY NOTES

To be published in J. of Appl. Phys. 1982

19. KEY WORDS (Continue on reverse side if necessary and identify by block number)

Laser Resonance Saturation, Laser Ionization, Laser Heating, Plasma Channel Formation, Molecular Quenching, Electron Laser Heating, Ion Beam Fusion, Gas Breakdown, Alkali Metal Plasmas

20. ABSTRACT (Continue on reverse side if necessary and identify by block number)

Laser resonance saturation of alkali vapours represents a very attractive method of creating the extended plasma channels of interest in light ion be fusion. We have undertaken a preliminary study of the influence of molecul nitrogen upon this laser ionization technique. Our results indicate that t electron cooling, resonance quenching and the increase in the laser energy requirement are acceptable, providing that the alkali seeding exceeds 0.5%.

DD FORM 1 JAN 73 1473

UNCLASSIFIED

SECURITY CLASSIFICATION OF THIS PAGE (When D

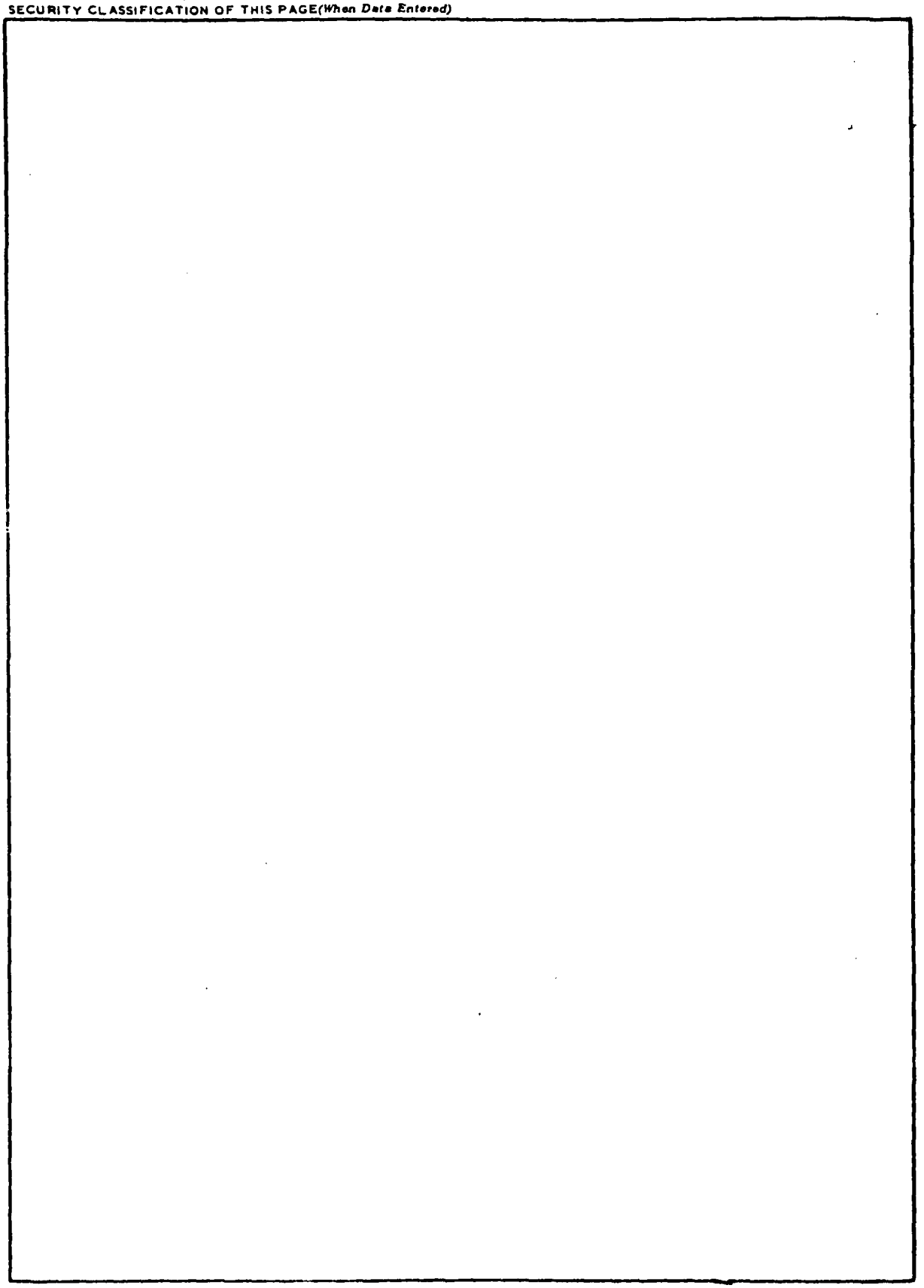

Appendix F

J. Quant. Spectrosc. Radiat. Transfer Vol. 25, pp. 537–545, 1981
Printed in Great Britain

0022-4073/81/060537-09$02.00/0
Pergamon Press Ltd

ANOMALOUS LASER ENERGY ABSORPTION ASSOCIATED WITH RESONANCE SATURATION

P. G. CARDINAL, P. L. WIZINOWICH, and R. M. MEASURES
Institute for Aerospace Studies, University of Toronto, 4925 Dufferin Street, Downsview, Ontario, Canada M3H 5T6

(*Received* 29 *September* 1980)

Abstract—Laser energy absorption measurements have been undertaken in an experiment involving the transmission of a pulse of laser radiation through sodium vapour. The wavelength of the laser was tuned to overlap the 589 nm resonance transition of the sodium atoms. Although simple radiation transport appears to account for the attenuation of the laser beam at low values of incident laser irradiance, anomalously large absorption has been observed at high values of incident laser energy. We suggest that this *anomalous absorption of laser energy* can be regarded as evidence of superelastic electron heating and subsequent ionization.

INTRODUCTION

In recent years several experiments have provided evidence of anomalous behaviour associated with the interaction of intense laser radiation tuned to saturate a resonance transition within a metal vapour. Measures[1] was the first to suggest the concept of laser selective saturation of atomic transitions for the purpose of undertaking both plasma diagnostics and the measurements of atomic parameters.

However, several attempts (Sharp and Goldwasser,[2] Burgess and Eckart,[3] Driver and Snider[4]) at observing saturation of laser-induced fluorescence failed. Salter[5] has attributed this failure to radiation trapping, while Rodrigo and Measures[6] and Daily[7] proposed an alternative explanation in terms of the laser beam spatial profile and spatial averaging of the observed signal. Recently, Salter *et al.*[8] also failed to observe saturation of the laser-induced emission but they were able to confirm, using an interferometric technique, that the laser locked the atomic level populations in the ratio of their respective degeneracies, as predicted by Measures.[1]

In another group of experiments involving laser saturation of metal-vapour resonance transitions, Lucatorto and McIlrath,[9] McIlrath and Lucatorto,[10] Skinner,[11] and Young *et al.*[12] observed substantial ionization, while Leslie *et al.*,[13] Allegrini *et al.*,[14] and Bearman and Leventhal[15] recorded strong emissions from levels that were well above the laser-pumped transition. These results can be understood in terms of the superelastic heating and reduced ionization potential ideas enunciated by Measures.[16,17] The initial pool of free electrons necessary for these interactions could easily be created by the various collision-radiative processes discussed by Geltman.[18] Further theoretical work on laser ionization based on resonance saturation (LIBORS) has been recently undertaken by Measures *et al.*[19,20] and Measures and Cardinal.[21]

In this paper, we present the results of an experiment in which the attenuation of a laser pulse, tuned to the 589 nm resonance transition of sodium, was measured as a function of atom density and laser energy. We compare these results with the attenuation predicted on the basis of simple radiation transport theory.

EXPERIMENTAL FACILITY AND RESULTS

Our experimental facility includes a Phase-R Model DL-2100A flashlamp pumped dye laser, a specially designed and built crossed heat pipe (Heat-cross), an energy meter, two photodiodes, two cameras and two Heath monochromators with accompanying photomultipliers. A schematic of the experimental arrangement is presented as Fig. 1. The Heat-cross oven used to contain the sodium vapour is shown in Fig. 2 and has four windows. These provided access for the laser beam and enabled us to evaluate the absorption of the laser pulse after transmission through the column of sodium vapour, the length of which was about 40 cm and was determined by the position of the water cooling coils and the argon buffer gas pressure (see Refs. 22 and 23).

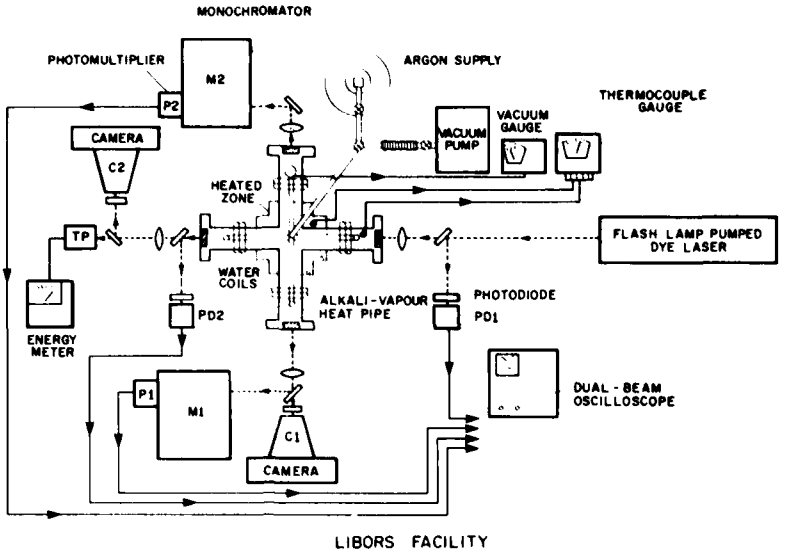

Fig. 1. Schematic representation of the laser ionization based on resonance saturation (LIBORS) facility.

Fig. 2. Heat-cross sodium oven showing heaters and water cooling coils.

Observations of any laser-induced emission or laser-scattered radiation can be made through the other pair of windows.

Rhodamine 6G in ethanol was used in the dye laser to provide energy output pulses that ranged between 100 and 400 mJ. Tuning of the output to the 589.0 nm D resonance line of sodium was accomplished through use of a 316 line/mm grating that was blazed at 63°35′. The spectral width of the dye laser output was further narrowed to about 0.06 nm by the inclusion of a one to two intracavity beam expander.[24]

The pair of photodiodes was calibrated against the energy meter so that the shape and energy of both the incident and transmitted laser pulses could be monitored. Figure 3 presents a

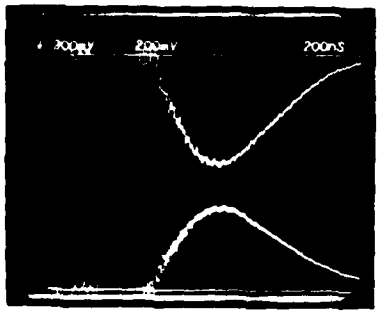

Fig. 3.

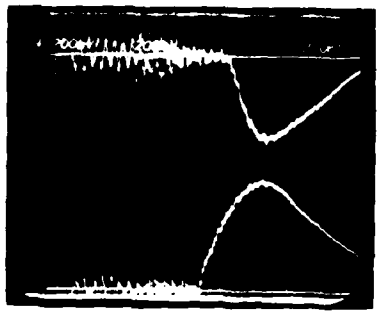

Fig. 4.

Fig. 3. Photodiode signals: the lower trace corresponds to an incident laser pulse of about 300 mJ, while the upper displays the inverted signal for the same laser pulse after transmission through the heat-cross in the absence of sodium vapour.

Fig. 4. Photodiode signals: the lower trace corresponds to an incident laser pulse of about 400 mJ, while the upper trace displays the inverted singal corresponding to the distorted laser pulse after transmission through a 40 cm column vapour at a density of about 2.9×10^{15} cm $^{-3}$.

representative pair of photodiode signals corresponding to an absence of sodium vapour within the Heat-cross. The lower trace corresponds to an incident laser pulse of about 300 mJ, while the upper trace displays the inverted signal that corresponds to the transmitted laser pulse. The FWHM can be seen to be about 700 nsec. The distortion in the laser pulse shape arising from transmission through 40 cm of sodium at about 2.9×10^{15} cm $^{-3}$ can be seen by reference to Fig. 4. When the sodium vapour pressure is increased to correspond to a density of about 1.5×10^{16} cm $^{-3}$, almost complete absorption of the laser pulse is observed (see Fig. 5). The variation in the amount of laser energy absorbed as a function of incident laser energy for three values of sodium atom density (2.9×10^{15}, 6.3×10^{15}, and 1.5×10^{16} cm $^{-3}$) is presented as Fig. 6.

The incident dye laser pulse temporal history can be reasonably well fitted by the expression $I^{l}(t) = I_0(t/\tau_3)[1 - (t/\tau_1)]\exp(-t/\tau_2)$, where we have found that $\tau_3 \approx 160$, $\tau_1 = 1154$, and $\tau_2 = 810$ nsec. Also $I_0 = 1.1 \times 10^{7} E^{l}$, where I^{l} and I_0 are in Wcm $^{-2}$ if E^{l} is in joules. In Fig. 7 we present a representative comparison of the incident laser time history curve, as given by the above analytical expression, and the experimentally observed points taken from one of our laser pulse oscillograms. The laser beam has been assumed to have a gaussian radial profile with an exponential radius of 0.2 cm.

THEORETICAL ANALYSIS

In an attempt to account theoretically for the observed absorption of laser energy, we shall represent the sodium atom by the ground state $|1\rangle$, the resonance state $|2\rangle$, and the continuum $|c\rangle$. We shall consider a one-dimensional situation and assume that a rate-equation analysis is

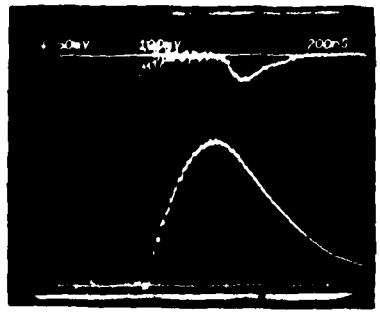

Fig. 5. Photodiode signals: the lower trace corresponds to an incident laser pulse of about 270 mJ, while the upper trace displays the inverted signal corresponding to the residue of laser energy detected after transmission through a 40 cm column of sodium vapour at a density of about 1.5×10^{16} cm $^{-3}$.

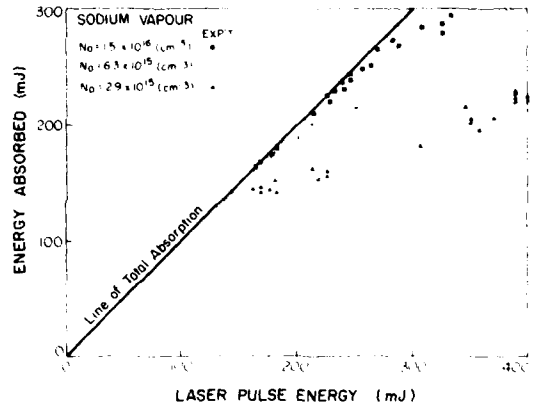

Fig. 6. Experimentally observed variation of absorbed laser energy with incident laser pulse energy for three values of sodium atom density.

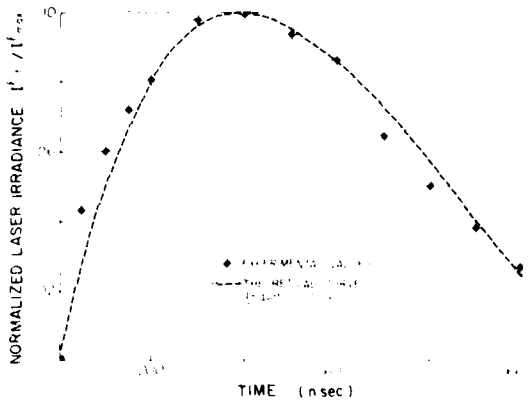

Fig. 7. Comparison of the laser pulse temporal history with the theoretical profile given by Eq. (20). Both curves are normalized by their respective maximum values.

justified because of the broad bandwidth of the laser and the fast dephasing time associated with the densities of interest. Under these circumstances, the appropriate population rate equation for the resonance state can be written in the form

$$\frac{\partial}{\partial t}N_2(z,t) = N_1(z,t)R_{12}(z,t) - N_2(z,t)\{R_{21}(z,t) + A_{21}^{+} + R_{2i}(z,t) + \frac{1}{2}N_2(z,t)[R_A + R_I(z,t)]\}, \quad (1)$$

where $N_1(z,t)$ and $N_2(z,t)$ represent the ground and resonance state population densities, respectively, at a distance z from the boundary of the sodium vapour and at a time t after the laser pulse is switched on. Also, $A_{21}^{+}[\equiv \gamma_{21}A_{21}]$ represents the radiation trapped spontaneous emission probability; γ_{21} is the relevant photon escape factor and A_{21} is the Einstein transition probability; $R_{2i}(z,t)[=\sigma_{2i}^{(2)}F^2(z,t)]$ represents the two photon ionization rate for the resonance state; $\sigma_{2i}^{(2)}$ is the appropriate two photon ionization rate coefficient and $F(z,t)$ corresponds to the laser photon flux density at (z,t), i.e. $F(z,t) = I^{l}(z,t)/h\nu$; $I^{l}(z,t)$ represents the laser irradiance and $h\nu(=E_{21})$ the laser photon energy; $R_A(=\langle\sigma v\rangle_A)$ represents the effective collision rate coefficient for associative ionization of two resonance state atoms; $R_I(z,t)[=\langle\sigma v\rangle_I F(z,t)]$ represents the laser induced Penning ionization rate coefficient for two resonant state atoms; $R_{21}(z,t)[=B_{21}\int I^{l}(\nu,z,t)f_{21}(\nu)\,d\nu/4\pi]$ represents the stimulated emission rate, where B_{21} is the Milne stimulated emission coefficient, $I^{l}(\nu,z,t)$ represents the spectral laser irradiance, and $f_{21}(\nu)$ represents the resonance to ground state line profile function; $R_{12}(z,t)[=gR_{21}(z,t)]$ represents the absorption rate; $g = g_2/g_1$ is the ratio of degeneracies for the resonance and ground levels, respectively.

If we invoke continuity,

$$N_1(z, t) + N_2(z, t) = N_0, \tag{2}$$

where N_0 represents the original atom density (all atoms are assumed to be in the ground state prior to laser irradiation). If we also assume that the laser spectral width $\Delta\nu^l$ is very much greater than the line width of the atomic transition, then

$$R_{21}(z, t) \approx \frac{B_{21} I^l(z, t)}{4\pi\Delta\nu^l} = \sigma_{21}^l F(z, t), \tag{3}$$

where

$$\sigma_{21}^l \equiv h\nu B_{21}/4\pi\Delta\nu^l. \tag{4}$$

If we use Eqs. (2) and (3) in Eq. (1), we can write

$$\frac{\partial}{\partial t} N_2(z, t) = gN_0\sigma_{21}^l F(z, t) - N_2(z, t)\Big\{(1+g)\sigma_{21}^l F(z, t) + A_{21}^\dagger + \sigma_{2c}^{(2)} F^2(z, t) + \frac{1}{2} N_2(z, t)[\langle\sigma v\rangle_A + \langle\sigma v\rangle_L F(z, t)]\Big\}. \tag{5}$$

The corresponding one-dimensional radiative transfer equation can be expressed in the form

$$\frac{\partial}{\partial t}\{F(z, t)/c\} + \frac{\partial}{\partial z} F(z, t) = \{N_2(z, t) - gN_1(z, t)\}\sigma_{21}^l F(z, t) - 2N_2(z, t)\sigma_{2c}^{(2)} F^2(z, t) - \frac{1}{2} N_2^2(z, t)\langle\sigma v\rangle_L F(z, t). \tag{6}$$

For the conditions of our experiment, the speed of light may be regarded as infinite. Under these circumstances, the pair of coupled partial differential equations (5) and (6) can be nondimensionalized and expressed in the form

$$\frac{\partial}{\partial\tau} n(x, \tau) = \phi(x, \tau) - n(x, \tau)\{1 + \phi(x, \tau) + \omega\phi^2(x, \tau) + n(x, \tau)[a + p\phi(x, \tau)]\}, \tag{7}$$

$$\frac{\partial}{\partial x}\phi(x, \tau) = \{n(x, \tau)[1 - b\phi(x, \tau) - n(x, \tau)p] - 1\}\phi(x, \tau), \tag{8}$$

where $\tau \equiv A_{21}^\dagger t$ and $x \equiv GN_0\sigma^l z$ are the nondimensional time and space variables; $G \equiv g/(1+g)$ and $\sigma^l \equiv \sigma_{21}^l(1+g)$. The nondimensional excited atom density and photon flux density are, respectively, $n \equiv N_2/GN_0$ and $\phi \equiv F/F_s$. The saturated photon flux density is

$$F_s \equiv A_{21}^\dagger/\sigma^l \quad \text{while} \quad \omega \equiv \sigma_{2c}^{(2)} F_s^2/A_{21}^\dagger,$$

$$b \equiv 2\sigma_{2c}^{(2)} F_s/\sigma^l, \quad a \equiv \frac{1}{2} GN_0\langle\sigma v\rangle_A/A_{21}^\dagger, \quad \text{and} \quad p \equiv \frac{1}{2} GN_0\langle\sigma v\rangle_L/\sigma^l.$$

Equations (7) and (8) do not lend themselves to analytical solution and would have to be solved by numerical techniques. For the conditions that apply to our experimental work, we can make a number of simplifying assumptions that are reasonably well justified. In Table 1, we have listed the values of the parameters that correspond to our experimental conditions. If we

Table 1. The sodium parameters corresponding to experimental conditions.

$A_{21}^\dagger = 6.29 \times 10^7\ \gamma_{21}\ \text{sec}^{-1}$; $\sigma^l = 8.0 \times 10^{-11}\ \text{cm}^2$; $\sigma_{2c}^{(2)} = 1.67 \times 10^{-40}\ \text{cm}^4\ \text{sec}$; $\langle\sigma v\rangle_A = 2.4 \times 10^{-11}\ \text{cm}^3\ \text{sec}^{-1}$; $\langle\sigma v\rangle_L = 1.6 \times 10^{-19}\ \text{cm}^3$; $G = 0.75$; $F_s = 7.9 \times 10^{19}\ \gamma_{21}$ photons $\text{cm}^{-2}\ \text{sec}^{-1}$; $\omega = 1.66 \times 10^{-17}\ \gamma_{21}$; $b = 3.3 \times 10^{-17}\ \gamma_{21}$; $F_{\max}$ (corresponding to 400 mJ) $\approx 1.8 \times 10^{24}$ photons $\text{cm}^{-2}\ \text{sec}^{-1}$; $\phi_{\max} \approx 1.79 \times 10^5/\gamma_{21}$; $N_0^{\max} = 1.5 \times 10^{16}\ \text{cm}^{-3}$.

set $\phi = \phi_{max}$, $N_0 = N_0^{max}$ and evaluate each of the terms within the braces on the r.h.s. of Eq. (7), we have

$$\left\{1 + \frac{1}{\gamma_{21}}[1.79 \times 10^5 + 5.33 \times 10^{-7} + n(x, \tau)(2.15 \times 10^{-5} + 2.02 \times 10^{-6})]\right\}.$$

Since $n(x, \tau) \leq 1.0$, it is clear that, for the conditions that prevail in our experiment, we can neglect the last three terms on the r.h.s. of Eq. (7) and write

$$\frac{\partial}{\partial \tau} n(x, \tau) \approx \phi(x, \tau) - n(x, \tau)[1 + \phi(x, \tau)]. \tag{9}$$

In a like manner, it can be easily demonstrated that the second and third terms on the r.h.s. of Eq. (8) are unimportant for our experiment and, consequently,

$$\frac{\partial}{\partial x} \phi(x, \tau) \approx [n(x, \tau) - 1]\phi(x, \tau). \tag{10}$$

If we further assume that the laser irradiance changes slowly during the times of interest, then we can approximately set $(\partial/\partial\tau)n(x, \tau) = 0$, which leads to a pseudo-steady-state nondimensional resonance level density given by

$$n(x, \tau) \approx \frac{\phi(x, \tau)}{1 + \phi(x, \tau)}. \tag{11}$$

Under saturation conditions, $\phi(x, \tau) \gg 1$ and $n(x, \tau) = 1$, i.e. $N_2 = GN_0$. If Eq. (11) is used with the nondimensionalized radiative transfer equation, we can write

$$\frac{\partial}{\partial x} \phi(x, \tau) = -\frac{\phi(x, \tau)}{1 + \phi(x, \tau)}, \tag{12}$$

which has the solution

$$\phi(x, \tau) + \ln\{\phi(x, \tau)\} = \phi(0, \tau) + \ln\{\phi(0, \tau)\} - x. \tag{13}$$

Although, Eq. (13) is a transcendental equation and has to be solved iteratively, there exists two limiting analytical forms of solution to Eq. (12). Under saturating conditions, $\phi(x, \tau) \gg 1$ and Eq. (12) yields the linear attenuation equation

$$\phi(x, \tau) = \phi(0, \tau) - x \tag{14}$$

first proposed by Measures.[16] Alternatively, if $\phi(x, \tau) \ll 1$, Eq. (12) yields the Beer–Lambert exponential attentuation equation

$$\phi(x, \tau) = \phi(0, \tau) \exp(-x). \tag{15}$$

Using our earlier definitions, we may write for the saturation photon flux density

$$F_s = \frac{8\pi c \Delta\lambda' \gamma_{21}}{\lambda^4 (1 + g)} \tag{16}$$

and for the nondimensional scale length (corresponding to the length of the sodium vapour column, L)

$$x_L = GN_0 \lambda^4 A_{21}(1 + g)L/8\pi c \Delta\lambda', \tag{17}$$

where λ is the laser wavelength and $\Delta\lambda'$ corresponds to the laser line-width.

The energy in the transmitted laser pulse is given by the relation

$$E_T = h\nu F_s \int_0^{\tau_1} \phi(x_L, \tau)\, d\tau. \tag{18}$$

The laser energy absorbed in transmission through the vapour is

$$E_A = E^I - E_T. \tag{19}$$

COMPARISON BETWEEN THEORY AND EXPERIMENT

In order to determine theoretically both the energy absorbed and the distortion in the laser pulse time history after transmission through the 40 cm column of sodium vapour within the Heat-cross, Eq. (13) is solved iteratively for $x = x_L$ and the resulting solutions are then numerically integrated, as indicated in Eq. (18). In order to solve Eq. (13), the nondimensional incident photon flux density, $\phi(0, \tau)$, has to be ascertained. This can be achieved by employing the analytical approximation to the incident laser-pulse time history described in the experimental section, viz.

$$\phi(0, \tau) = \frac{4.14 \times 10^5 E^I}{\gamma_{21}} \left(\frac{\tau}{10\gamma_{21}}\right) \left\{1 - \frac{\tau}{72.6\gamma_{21}}\right\} \exp\left(-\frac{\tau}{51\gamma_{21}}\right), \tag{20}$$

where E^I represents the total energy (J) in the incident laser-pulse. The radiation trapping factor, γ_{21}, is treated as a fitting parameter. In general the value of γ_{21} was selected such that the theoretically predicted value of the laser energy absorbed, E_A, closely approximated the observed value.

A representative example of our results is presented in Fig. 8, where the theoretical laser-pulse shapes, before and after transmission through the sodium column ($N_0 = 2.9 \times 10^{15}$ cm^{-3}), are compared with the corresponding experimentally determined laser-pulse shapes. The incident laser energy for Fig. 8 is 400 mJ and the values of E_A are 225 mJ (experimental value) and 227 mJ (theoretical value corresponding to $\gamma_{21} = 0.97$). Although some aspects of this comparison look reasonable, it is clear that our theoretical analysis leads to too small a degree of absorption with regard to the leading edge of the laser pulse and tends to overestimate the amount of absorption in the tail of the laser pulse. The degree of overprediction is made even worse when allowance is made for the overprediction of the laser irradiance available in the tail of the incident laser pulse, as described by Eq. (20).

We interpret the difference between our theoretical predictions and the experimental results (as illustrated in Fig. 8) as evidence of anomalous absorption of laser energy by the sodium vapour. Even stronger evidence of this anomalous absorption is provided in Fig. 9, where the

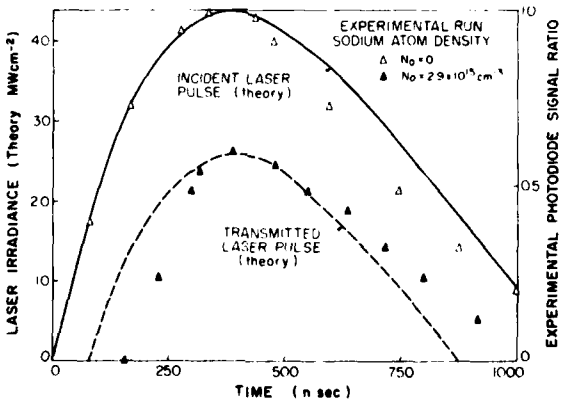

Fig. 8. Comparison of the laser pulse temporal histories (for both incident and transmitted laser pulses) with the corresponding theoretical profiles.

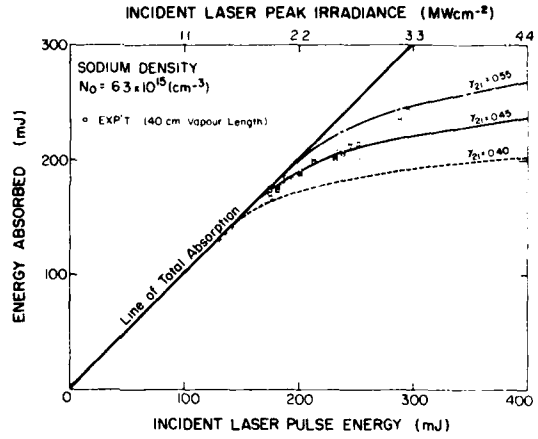

Fig. 9. Comparison of theoretical and experimental variations of the absorbed laser energy with the incident laser pulse energy for a sodium atom density of about 2.9×10^{15} cm $^{-3}$, using the photon escape factor γ_{21} as a fitting parameter.

laser energy absorbed by the sodium vapour is plotted as a function of the incident laser energy for an atom density of about $6.3 \times 10^{15}\,\mathrm{cm}^{-3}$. Several theoretical curves are shown corresponding to values for γ_{21} of 0.40, 0.45 and 0.55. It is clear that a choice of $\gamma_{21} \approx 0.45$ gives a reasonable fit to the absorbed energy for incident laser energy values up to about 250 mJ. However, for larger values of incident laser energy the theoretical curve underpredicts the observed absorption.

A similar result is found at other sodium vapour pressures. At each atom density, it is possible to find a value of γ_{21} which provides a reasonable fit of the theoretically predicted energy loss with incident laser energy at low values of laser irradiance but fails to account for the degree of absorption at high values of incident laser energy. This can be seen by reference to Fig. 10. The values of γ_{21} that allow a theoretical fit to the observed absorption data appear to be somewhat larger than would be estimated using the radiation trapping theory of Holstein.[25] This result is not surprising in light of the strong radial distribution of excited states created by the laser beam.

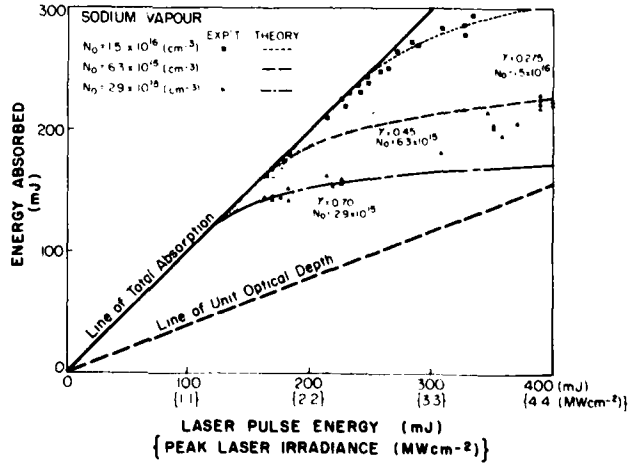

Fig. 10. Comparison of theoretical and experimental variations of absorbed laser energy with the incident laser pulse energy for three sodium atom densities: 2.9×10^{15}, 6.3×10^{15}, and 1.5×10^{16} cm $^{-3}$. The appropriate value of the photon escape factor γ_{21} was determined by requiring a best fit to the experimental data at the low end of the incident laser pulse energy range.

DISCUSSION AND CONCLUSIONS

We have been able to demonstrate that the energy absorbed from a laser-pulse, tuned to one of the resonance transitions of the attenuating medium, can be understood in terms of simple radiation transport for low values of laser irradiance. However, anomalous absorption is observed to arise for increasing values of incident laser energy. This additional absorption of energy does not have its origin in either two-photon ionization or laser-induced Penning ionization of the large population of resonance state atoms.

We believe that this anomalous absorption of laser energy results from the development of an appreciable density of free electrons, which are then able to extract a significant amount of energy from the laser beam through superelastic collision quenching of the laser maintained resonance state population. This interaction, in effect, heats the free electrons and enables them to produce further ionization and excitation.[16,19–21] The initial pool of free electrons necessary for this mode of energy extraction is expected to be produced by associative ionization, two-photon resonance ionization, and laser-induced Penning ionization. Preliminary measurements on the lifetimes of line and continuum emission from the Heat cross substantiates this possibility. This radiation is found to persist for several microseconds beyond the laser pulse, a time consistent with a decaying dense plasma.

If appreciable ionization does occur, then the theoretical underprediction of transmitted laser irradiance in the tail of the laser-pulse (see Fig. 8) can be understood in terms of a reduced neutral atom density along the path of the laser beam.

Acknowledgements—Work supported by USAF/AFOSR (under Grant No. 80-0057) and the Natural Science and Engineering Research Council of Canada. Scholarship support for P. G. Cardinal was provided by the Natural Science and Engineering Research Council of Canada.

REFERENCES

1. R. M. Measures, *J. Appl. Phys.* **39**, 5232 (1968).
2. B. L. Sharp and A. Goldwasser, *Spectrochim. Acta* **31B**, 431 (1976).
3. D. D. Burgess and M. Eckart, *J. Phys. B: Atom. Molec. Phys.* **9**, L519 (1976).
4. R. D. Driver and J. L. Snider, *J. Phys. B: Atom. Molec. Phys.* **10**, 595 (1977).
5. J. M. Salter, *J. Phys. B: Atom. Molec. Phys.* **12**, L763 (1979).
6. A. B. Rodrigo and R. M. Measures, *IEEE J. Quant. Elect.* **QE-9**, 972 (1973).
7. J. W. Daily, *Appl. Opt.* **17**, 225 (1978).
8. J. M. Salter, D. D. Burgess, and N. A. Ebrahim, *J. Phys. B: Atom. Molec. Phys.* **12**, L759 (1979).
9. T. B. Lucatorto and T. J. McIlrath, *Phys. Rev. Lett.* **37**, 428 (1976).
10. T. J. McIlrath and T. B. Lucatorto, *Phys. Rev. Lett.* **38**, 1390 (1977).
11. C. H. Skinner, *J. Phys. B: Atom. Molec. Phys.* **13**, 55 (1980).
12. W. A. Young, M. Y. Mirza and W. W. Duley, *Opt. Commun.* **31**, 157 (1979).
13. S. G. Leslie, J. T. Verdeyen and W. S. Millar, *J. Appl. Phys.* **48**, 4444 (1978).
14. M. Allegrini, G. Alzetta, A. Kopystynska, L. Moi, and G. Orriols, *Opt. Commun.* **22**, 329 (1977).
15. G. H. Bearman and J. J. Leventhal, *Phys. Rev. Lett.* **41**, 1227 (1978).
16. R. M. Measures, *JQSRT* **10**, 107 (1970).
17. R. M. Measures, *J. Appl. Phys.* **48**, 2673 (1977).
18. S. Geltman, *J. Phys. B: Atom. Molec. Phys.* **10**, 3057 (1977).
19. R. M. Measures, N. Drewell, and P. Cardinal, *J. Appl. Phys.* **50**, 2662 (1979).
20. R. M. Measures, N. Drewell, and P. G. Cardinal, *Appl. Opt.* **18**, 1824 (1979).
21. R. M. Measures and P. G. Cardinal, "Laser Ionization Based on Resonance Saturation—A Simple Model Description" (Feb. issue *Physical Rev. A*, 1981).
22. M. M. Hessel and P. Jankowski, *J. Appl. Phys.* **43**, 209 (1972).
23. M. M. Hessel, R. D. Drullinger and H. P. Broida, *J. Appl. Phys.* **46**, 2317 (1975).
24. T. W. Hänsch, *Appl. Opt.* **11**, 895 (1972).
25. T. Holstein, *Phys. Rev* **83**, 1159 (1951).


DAT
ILM